DISSERTATION

SINGLE HIGH DOSE IRRADIATION: APPLICABILITY OF CELL SURVIVAL CURVE MODELING AND IN VIVO EVALUATION OF TUMOR BIOLOGIC RESPONSE

Submitted by

Katy Lynn Swancutt

Department of Environmental and Radiological Health Sciences

In partial fulfillment of the requirements

For the Degree of Doctor of Philosophy

Colorado State University

Fort Collins, Colorado

Fall 2015

Doctoral Committee:

Advisor: Susan M. LaRue

James T. Custis
Howard L. Liber
Rodney L. Page

ABSTRACT

SINGLE HIGH DOSE IRRADIATION: APPLICABILITY OF CELL SURVIVAL CURVE MODELING AND IN VIVO EVALUATION OF TUMOR BIOLOGIC RESPONSE

The observed clinical success of stereotactic radiation therapy (SRT), in which radiation therapy treatment is delivered in one to five, high-dose fraction of ionizing radiation, has generated interest in the biologic mechanisms by which SRT achieves tumor control. Since the use of linear quadratic formalism to predict tumor cell kill and clinical tumor control has not been corroborated by clinical trial results, it has been proposed that alternative mechanistic responses occur in response to high dose irradiation in addition to mitotic cell death of tumor clonogens in direct response to radiation-induced DNA damage. One suggested mechanism based on observations of tumor endothelial cell apoptosis following doses above 8 to 10 Gy proposes that tumor vascular damage may increase cell killing of associated tumor parenchyma, thus explaining the clinical success of SRT. The work described herein sought to determine whether tumor cell killing behaved predictably at high doses based on established survival curve models using *in vitro* techniques and whether parameters to tumor vascular response *in vivo* were impacted differently at high doses versus low doses. In addition, the role of vascular dysfunction as a potentially impactful process in the tumor response to high dose, single fraction irradiation was investigated by measuring microenvironmental changes in the time period between irradiation and the expected peak of endothelial cell apoptotic events. For both *in vitro* and *in vivo* experiments, canine tumors were chosen as the optimal model for human cancers due to the

similarities between canine and human tumor size, cellular kinetics, and initiation from similar environmental exposures (among numerous other reasons).

Using the standard clonogenic assay, cell survival curves were constructed for eight different canine cancer cell lines and one normal canine endothelial cell line. Careful conduction of experiments allowed for collection of data at doses above 10 Gy (in many cases up to 14 or 15 Gy). Modeling of these data was conducted using the linear quadratic formula, the well-established single-hit multitarget model, the new Kavanagh-Newman universal survival curve, and a hypothetical model based on the linear quadratic model with an added component proportional to dose cubed. It was determined that no single model provided the best fit for all cell lines and the linear quadratic model failed to describe data in the high dose region in a majority of cell lines. Rank order analysis of cell lines showed consistency between measured surviving fractions in the low dose region (SF_2 versus SF_8), but extrapolation of measured high-dose data to calculate surviving fraction values at 24 Gy (SF_{24}) produced rank orders nearly opposite of those at low doses. The reversal of ranks indicated crossing of survival curves at some point beyond the limits of experimental measurement, suggesting that perhaps some unique mechanisms (in isolated tumor cells, in the absence of stromal components) occur at high doses that have not been observed. Extrapolated SF_{24} values, representing cell survival following a single fraction of 24 Gy, were compared to surviving fraction calculations for a dose fractionation schedule of three fractions of 8 Gy to total 24 Gy by calculating the cubed value of each cell line's SF_8. The *in vitro* studies indicated that a single fraction of 24 Gy resulted in several orders of magnitude more cell killing than three fractions of 8 Gy, leading to the prediction that a single 24 Gy treatment would be more clinically efficacious than a treatment

delivering 24 Gy divided among three equal fractions. Such *in vitro* studies may be useful in guiding the design of dose fractionation protocols for SRT.

To investigate the role of tumor vasculature in tumor response to single fraction, high-dose irradiation, spontaneously occurring canine soft tissue sarcomas were treated with either 2, 8, or 24 Gy in a randomized clinical trial. Tumor microenvironmental factors related to vascular function were monitored before and after irradiation. These factors included tumor oxygenation, interstitial fluid pressure, and perfusion. Samples were taken for quantification of endothelial cell apoptosis, plasma nitrate and nitrite as long-lived indicators of nitric oxide, serum ASMase and oxidative stress. The timeline of events in which high dose, single fraction irradiation induced changes in the tumor microenvironment was of particular interest, and measurements were taken for three hours immediately after irradiation and again at twenty four and forty eight hours after irradiation. Interim analysis of the clinical trial following enrollment of nine dogs suggests that oxygenation following a single fraction of 2 Gy behaved consistently with expectations at twenty four and forty eight hours. Tumors treated with 24 Gy showed a trend of increasing oxygenation within one to two hours of irradiation, which decreased again by three hours. It was concluded that more dogs are needed to clarify any trends observed in this study, given the high degree of heterogeneity of tumor microenvironmental factors within a tumor and between individuals.

ACKNOWLDEGEMENTS

This work would not have been possible without the generous contributions of the Morris Animal Foundation, the family of "Baron" Porter, the Molly Silverman Foundation, the Center for Companion Animal Studies, and funding from the Colorado State University DVM/PhD Dual Degree Program. I would like to thank my advisor, Dr. LaRue, for taking me on as a student and guiding me throughout the PhD research as well as through veterinary school. I was very lucky to have a mentor with extensive experience as a scientist and veterinarian. Thank you to my excellent committee members: Dr. Custis who acted as the voice of reason and logic, Dr. Liber who graciously opened his lab to me, and Dr. Page who arranged for the funding that kept this project going. I am tremendously indebted to the Flint Animal Cancer Center family, a group of people who collaborate, teach, and work better than any facility I've ever known. In particular, I was extremely lucky to have the friendship and assistance of Laura Chubb, Ruth Rose, Sarah Gookin, and Danielle Roteliuk. I am grateful to the members of the Radiation Oncology clinical service, including technicians Sara Bruns and Anne Golden, and the residents, Drs. Griffin, Nolan, Yoshikawa, Pohlman, and Swift. This work could not have been conducted without the gracious assistance from the Flint Animal Cancer Center Clinical Trials group, the Radiology service, and the Analytical Toxicology Lab. I would like to thank the families of our clinical trial participants, as well as my own wonderful family and friends for their continuous support and encouragement.

DEDICATION

My work is dedicated to the memory of Laureen Jane Swancutt

June 21, 1954 - July 17, 2014

TABLE OF CONTENTS

CHAPTER 1

INTRODUCTION

STEREOTACTIC RADIATION THERAPY

Physicians experimented with application of ionizing radiation to treat cancer (among other maladies) almost immediately after Rontgen's discovery of X-rays in 1896.[1] For the sake of simplicity and in light of the complete absence of knowledge concerning biologic effects of X-ray exposure, dose was administered to some of the early clinical cases in a single treatment rather than multiple treatments or "fractions."[2] It was quickly discovered that delivering high doses in a single treatment caused severe, irreparable toxicities in tissues comprised of slowly-dividing cells ("late responding tissues"), such as the spinal cord or kidney, which could not be excluded from the irradiation field due to their proximity to the intended target. The morbidity of such toxicities, called "late effects," due to the delay between irradiation and clinical presentation, was determined to be unacceptable; the risk of such collateral damage in normal tissues has since limited the dose per fraction and total dose that can be delivered in pursuit of tumor control. Utilization of low doses in multiple fractions to treat tumors became routine following Coutard's popularization of fractionated dose delivery in the 1930's.[3,4] Administration of low doses (i.e. 2 Gy) on a daily basis over the course of several weeks, a standard regimen referred to herein as traditional or protracted fractionated radiation therapy, allows for the accumulation of radiation damage to tumor cell DNA, which is not typically repaired as effectively as radiation damage to the DNA of normal cells (although DNA damage affecting certain cell cycle checkpoint genes, for example, may negate this principle).[5] Fractionated

radiation therapy has been the primary radiation therapy modality for the greater part of the past century.[6]

However, substantial technological innovations have improved radiation oncologists' ability to minimize the dose absorbed by normal tissues while generating a steeply increasing dose gradient at the normal tissue-to-tumor interface, thus allowing for drastic escalation of dose per fraction to a tumor. The delivery of ultra-high doses per fraction, generally 10 to 20 Gy in each of one to five fractions, to extracranial tumors is a practice known as stereotactic radiation therapy (SRT).[7] Also called stereotactic body radiation therapy (SBRT) or stereotactic ablative radiotherapy (SABR), SRT originated from stereotactic radiosurgery (SRS) and requires the precise implementation of the following characteristics: 1) careful immobilization of targeted tissues to account for patient movement, inherent motion of internal organs (e.g. gating or dampening of breathing motion) and accurate repositioning, 2) verification of positioning using fiducial markers and/or image guided radiation therapy (IGRT), and 3) computer based planning of a highly conformal dose distribution that allows for 95% or more of the tumor volume to receive a very high prescription dose while the dose at the normal tissue-to-tumor interface decreases sharply to spare surrounding normal tissues (a feat that may be achieved using intensity modulated radiation therapy, GammaKnice, CyberKnife, or Tomotherapy, when available).[7]

SRT can be prescribed as a single fraction treatment or in the form of a highly hypofractionated (sometimes called "oligofractionated") protocol. The use of SRT is particularly valuable to veterinary radiation oncology, where patients are treated while under general anesthesia, because the overall treatment time is significantly abbreviated relative to traditional fractionated radiation therapy protocols. Given the desirability of achieving tumor control in a

short duration of time by non-invasive radiation therapy, a great deal of new interest has been generated in optimizing dose delivery protocols. Such protocols would ideally be informed by knowledge of the cellular mechanisms by which one to five dauntingly large doses achieve tumor control.

Since the development of SRT, which originated as stereotactic radiosurgery (SRS) in the form of GammaKnife technology for the treatment of brain tumors in 1951,[8] numerous clinical trials have attempted to evaluate the clinical efficacy of SRT in the treatment of a wide variety of tumor types. Clinical results concerning the use of SRT for extracranial lesions began to appear in the literature only a decade ago. One study reported that 80% of patients with liver, lung, or retroperitoneal masses treated with a SRT protocol of 7.7 to 30 Gy (total dose) given in one to four fractions had no progressive disease at follow-up evaluation (which was at least a month and a half and at most three years and two months) and half of the tumors treated either decreased in size or disappeared completely.[9] A study using a single fraction of 10 Gy to treat primary and metastatic lesions of the vertebral column in five patients, all of whom had failed previous treatment with traditional fractionated radiation therapy, succeeded in halting disease progression in all patients at a median follow-up of six months.[10] Numerous clinical reports testing SRT protocols to treat primary and metastatic disease of the lung and liver produced impressive results: extremely low frequency of local progression,[11-18] local tumor control rates as high as 98% at six months and actuarial local tumor control of 81% at eighteen months in liver tumors (given 14 to 26 Gy in one fraction),[12] cause-specific survival at three years as high as 88% in non-small-cell lung cancer patients,[13] and notable rarity of high grade side effects overall.[9-18] Since many clinical trials have yet to mature past the point of ten year patient follow-up, it cannot yet be determined with total confidence whether or not severe late toxicities will

occur from SRT. However, physicians continue to record surprisingly successful clinical outcomes with virtually no major complications using SRT to treat malignancies of the spine, lung, liver, kidney, and prostate.[9-25] One study evaluating 60 Gy (total dose) delivered in three fractions to thirty seven medically inoperable patients with non-small-cell lung cancer emphasized the fact that the maximum tolerated dose had not been reached, in spite of aggressive dose escalation, and a tumor response rate of 87% was achieved without approaching doses that risked unacceptable toxicity.[17] Results acquired to date have led radiation oncologists to question whether tumor response can be improved by further dose escalation or if there is a threshold beyond which additional dose provides no additional benefit. It is unknown how high a dose can be delivered before dose limiting toxicities emerge, given confident avoidance of normal tissues. Dose fractionation protocols are best designed based on knowledge of the cellular and tissue responses in tumor and in normal tissues, with the goal of exploiting any differences between them. However, from a mechanistic standpoint it is not known exactly how the types of large-dose, hypofractionated or single-fraction protocols delivered in SRT lead to the appreciable clinical outcome of tumor control.

In contrast, the biologic mechanisms by which traditional fractionated radiation therapy achieves tumor control are well characterized. When ionizing radiation deposits energy in a random distribution encompassing cells, multiple cellular components sustain damage either directly via ionization and excitation of molecular bonds, or indirectly via redox reactions of free radicals generated in the radiolytic degradation of water (particularly hydroxyl radicals and other reactive oxygen species).[5] Persistent damage incurred by DNA that is not successfully repaired by the cell leads to the accumulation of genetic instability and complications of the mitotic process that ultimately lead to cell death. While irradiated cells can sometimes undergo

apoptotic or necrotic death before their next division, they more frequently survive from a literal standpoint throughout a handful of mitotic cycles only to eventually fail completion of a mitotic event due to the accumulation of DNA damage (particularly double-strand breaks) leading to the formation of fatal dicentric, ring, or anaphase bridge-causing chromosomes or loss of function in vital genes.[5] The term "mitotic cell death," has been given to the process in which irradiated cells lose the capacity for indefinite proliferation. In the case of malignant cells, which characteristically have the capacity for unlimited reproduction,[26] mitotic cell death is considered as good an outcome as literal cell death.

The challenge of any cancer therapeutic lies in targeting neoplastic cells while sparing normal cells; fractionation of the total dose into multiple smaller doses achieved this for radiation therapy.[27] Ionizing radiation deposits energy indiscriminately (in fact, randomly) within a targeted volume but cancer cells are significantly less effective in repairing DNA single and double strand breaks than normal cells. Fractionating the total dose into small, daily doses introduces time gaps between fractions in which irradiated normal cells can repair any DNA damage incurred; as daily doses continue, DNA damage would accumulate to a much greater degree in tumor cells than in cells with normal DNA repair pathway components. Functional DNA repair mechanisms also contribute to the potential for normal cells to repopulate within irradiated tissues, although tumor cells also have repopulation capabilities which may be accelerated if time-dose fractionation protocols are excessively protracted. Since radiosensitivity is enhanced during certain phases of the replicative cell cycle (for example, cells irradiated during radioresistant S phase into radiosensitive G_2/M phase) as well as in conditions of higher oxygen concentrations, the time between fractions simultaneously allows for tumor cells to undergo redistribution (or "reassortment) into different cell cycle phases and reoxygenation

(taking advantage of acute fluctuations in tumor oxygenation). While repopulation, redistribution, and reoxygenation provide compelling reasons to treat with traditional, fractionated radiation therapy, differential repair capabilities between normal and neoplastic cells is the factor that best enhances the therapeutic ratio between tumor control and late effects.[28]

The response to radiation exposure on a cellular level has long been thought of as predictive of overall tumor response to radiation therapy; the radiosensitivity of a given human tumor cell line has been shown to reflect the clinical radioresponsiveness of the corresponding tumor type in numerous cases.[29] A vast majority of cell line irradiation experiments have been conducted with this principle in mind, resulting in an overwhelming focus on cellular response to low doses (particularly 2 Gy, as evidenced by the prevalence of reporting surviving fractions at 2 Gy, or "SF_2 values") to connect *in vitro* experiments directly to fractionated radiation therapy. Numerous models have been proposed to describe the effect of radiation dose on cell survival, including the simple exponential model (which is mainly applicable to non-mammalian cell responses and to high linear energy transfer (LET) radiations),[30] the single-hit multi-target model,[30] the lethal-potentially lethal model,[31] the repair-saturation model,[32] the universal survival curve and its variations,[33,34,35] and the most clinically impactful model to date: the linear quadratic model of cell survival. Multiple modifications can be made to the basic structure of the linear quadratic model to improve fitting of data,[36-40] but its simplest form has become all-pervading in modern radiation oncology. The linear quadratic model describes cell survival (S) in terms of "dual radiation action," or cell killing via two components, α and β, which are proportional to dose (D) and to the square of the dose, respectively,[41,42] according to the following expression:

$$S = e^{-(\alpha D + \beta D^2)} \qquad [1]$$

Equation 1 fits experimental cell survival data versus dose with a function that has both linear and quadratic components which are thought to correspond to the formation of two DNA double-strand breaks from a single radiation track (the linear response) and of two DNA double-strand breaks in close proximity from two separate radiation tracks (the quadratic response) based on early studies of radiation-induced chromosomal aberrations.[5] Linear quadratic modeling has become popular particularly due to its simplicity, having only two adjustable parameters, but mainly due to applications of those parameters in the form of a very important tool: the α/β ratio. The α/β ratio is equal to the dose where the linear component of the modeled data induces equivalent cell kill to the quadratic component.[5] The α/β ratio of late responding tissues such as the spinal cord, kidney, or bladder have been measured and were found to be low numbers (ranging from 1.0 to 7 Gy for the aforementioned tissues) while acutely responding tissues such as skin, jejunum, colon, or testis have higher α/β ratios (which range from 6 to 13 Gy).[5] Knowing the characteristic α/β ratio of a given cell type is valuable because it can be used to calculate change in the total dose necessary to achieve an equivalent tissue response when dose per fraction is varied. When the tissue response of interest is some quantity of log cell kill, the total dose required to reach it is termed the "biologically effective dose" (BED).[43, 44] If the α/β ratio of a cell type involved in the biologic effect of interest is known, then the following expression can be used to determine the relationship between some type of log cell kill effect (E), the number of fractions (n), and the dose per fraction (d):

$$E = n(\alpha d + \beta d^2) \quad [2]$$

This can be re-written in the following two equations:

$$E = (nd)(\alpha + \beta d) \quad [3]$$

$$E = \alpha(nd)(1 + {}^{d}/_{\alpha/\beta}) \quad [4]$$

The term *nd* (the product of the number of fractions and the dose per fraction) is equivalent to the total dose (D). The final part of Equation 4 is thought of as relative dose effectiveness, so dividing by α produces a relationship between BED (E/α), total dose (*nd*), and relative effectiveness:

$$E/\alpha = (nd)(1 + {}^{d}/_{\alpha/\beta}) \qquad [5]$$

Equation 5 can be used by physicians to compare the potential to cause acute and late effects or to cause tumor cell death responses among various dose fractionation protocols or how to make adjustments to a prescribed fractionation protocol so that the appropriate total dose may still be reached in the event that a patient has missed a treatment or was accidentally overdosed. Since its development thirty years ago, physicians' ability to prevent unacceptable late effects has been attributed to the concept of biologically effective doses in fractionated radiation therapy protocol design.[44,45] As seen in Equation 5, the α/β ratio obtained from experimental quantification of dose dependent cell survival is made crucial to fractionated radiation therapy protocol design by a simple set of equations that take information directly from the lab bench to a patient's bedside (or couch-side, in the case of radiation therapy).

Biologically effective dose takes into account the effect of DNA double-strand break repair by factoring in the α/β ratio of certain cell types. Double-strand breaks generated by a single track ("*intra*track" radiation action), which produces the α component of a cell survival curve, are more difficult to repair as they are lacking in a genetic template that is typically intact in one homolog of a chromosome containing the potentially off-set double-strand breaks characteristic of the β component ("*inter*track" radiation action) in linear quadratic formalism. The role of repair makes mechanistic sense when using the BED formula to condense or expand fractionated protocols, for example abbreviating a fractionation schedule originally calling for

thirty fractions of 2 Gy into a twenty fraction protocol would require a daily dose of 2.81 Gy in a tumor consisting of a cell type with an α/β ratio of 10 Gy. It is important to note that while acutely responding tissues have consistently high α/β ratios and late responding tissues are reliably low, tumors can have a much wider range of α/β ratio values (for example, the α/β ratio of prostate carcinomas is around 1 to 1.7 Gy,[46] while different types of fibrosarcomas can fall anywhere within the range of 5 to 30 Gy).[47] This begs the question of whether BED calculations are as accurate when the effect in question is tumor response as opposed to an effect in acute or late responding tissues. Particularly in the case of single high dose irradiation or SRT, in which there is no role of repair between fractions, the applicability of linear quadratic formalism and BED calculations is uncertain.

Proponents of linear quadratic formalism warned that use of single high dose irradiation to treat cancer was dangerous when physicians, encouraged by successful use of stereotactic radiosurgery to treat benign arteriovenous malformations, first began to turn their attention to malignant brain and extracranial tumors.[48] The idea that the benefits of tumor reoxygenation and normal tissue sparing would be lost with a single high dose treatment led many radiation oncologists to resist adoption of single fraction SRT, believing that preliminary clinical successes could have been further improved if the single dose had been divided among at least five or six fractions.[48] In response, it was suggested that the linear quadratic model of cell killing may not apply to high dose irradiations because the model 1) best describes the low dose, linear region of survival curves, and 2) predicts that survival curves continue to bend in the quadratic region, a phenomenon that contradicts experimental results and predicts a higher degree of cell killing than has been measured.[49,50] Counterargument stated that linear quadratic formalism should retain status as radiobiological dogma because it 1) is "the best model we have," 2) can be

made more accurate by adding multiple varieties of modifications at the expense of its simplicity, and 3) has a proven mechanistic basis, which other models lack.[51,52] However, accepting the mechanistic basis of linear quadratic cell kill "requires a very serious leap of faith," considering several mathematical inconsistencies exist between the model and observed radiobiological response, including the lack of predicted synergistic results when two doses (of the same or different types of radiation) are delivered simultaneously.[53] In addition, the original concept of intratrack and intertrack (supposedly the α and β components of cell kill, respectively) dual radiation action came from correlational explanations of the dose dependence of chromosomal aberration yield, rather than from experiments testing or observing direct, causal relationships.[53]

From a more empirical standpoint, the ability of the linear quadratic formula to fit high dose data has been determined to be poor.[33,36,54,55] Goodness-of-fit analyses of survival curves containing high dose data, which are extremely difficult to obtain experimentally, have determined that the linear quadratic formula best fits the middle dose region of survival curves, but fit worsens at very high doses.[54,55] Furthermore, linear quadratic fitting seems to heavily weight data in the low dose region, the inclusion of which strongly skews the corresponding α/β ratio such that influence of the high dose region is minimal, calling into question the usefulness of applying an α/β ratio to treatments in the high dose region.[55] Preliminary *in vitro* work comparing measured cell survival outcomes versus predicted cell kill based on BED calculations for various dose fractionation schedules (ranging from one fraction treatment to twenty fraction treatments to a murine mammary sarcoma cell line, EMT6) found that observed cell kill was significantly less than predicted, suggesting that linear quadratic modeling and BED calculations should not be used in the design of single fraction or hypofractionated protocols.[57] Analysis of a

in vivo study of survival of murine jejunal crypt clonogens after 14 Gy "split dose" irradiation, meaning dose delivered in two fractions, found that if the first dose was large (e.g. 10 Gy first followed four hours later by 4 Gy) then the calculated isoeffect dose using linear quadratic modeling was underestimated by approximately 8%, which would be a clinically significant error.[58]

With increasing reports of positive clinical outcomes following SRT for lung and liver tumors, some proponents of linear quadratic formalism have admitted that, at the very least, SRT carries the benefit of eliminating the risk of accelerated tumor repopulation due to the short duration in which dose is delivered.[54,59] A true paradigm shift away from linear quadratic formalism has yet to occur as it remains highly useful in traditional, fractionated radiation therapy and should remain in place since not all tumor types are prime targets for SRT. A more important lesson to take away from the argument against the use of linear quadratic and BED equations for single high dose irradiation is the suggestion that single high dose treatment may induce a biologic response that is mechanistically distinct from the well-established response observed following treatment with fractionated radiation therapy.

TUMOR VASCULAR ENDOTHELIUM AND SINGLE HIGH DOSE IRRADIATION

Alongside the proposition that the four R's of radiobiology do not apply to single fraction high-dose irradiation or SRT,[60,61] which has strong opposition and requires further study,[62,63,64] attention has been drawn to the potential biologic mechanisms that could explain the clinical success of SRT. Based on theoretical calculations (again, linear quadratic in origin) of hypofractionated dose schedules required to overcome tumor hypoxia to achieve desired levels

of cell kill, Brown *et al.* predicted that a treatment of 180 Gy delivered in three fractions at 60 Gy per fraction would barely be sufficient,[65] while Fowler *et al.* similarly predicted that at least 23 Gy per fraction delivered in three fractions (69 Gy total) would be required.[56] However, the reality is that tumor control is being reached by SRT in clinical trials using dose fractionation schedules that are much less aggressive than calculations have predicted.[9-25] Clearly another variable besides classical dual radiation action is involved in achieving tumor control where high dose irradiation is concerned.

While tumor control is typically considered to be an effect of direct cell killing by radiation, not all known radiation effects are mediated by direct cell killing. Secondary processes unrelated to direct cell killing occur in instances of nausea and vomiting following irradiation of the upper abdomen, acute edema and erythema following irradiation of the skin (an inflammatory response producing vascular leakage), fatigue experienced by patients receiving large volume irradiation (particularly within the abdomen), and in somnolence following cranial irradiation.[6] There is also a possibility that the immune system has some nebulous role in enhancing tumor cell kill following radiation therapy, although studies examining aspects of an immune response to single large-dose irradiation are uncommon.[66-72]

The culprit with the most potential for increasing tumor cell killing beyond expectations and above calculations is the basic component of tumor vasculature: the endothelial cell. As evidenced by the extensive amount of research pursuing anti-angiogenic therapeutic modalities, it has long been believed that tumor vascular endothelium is a prime secondary target for anti-cancer therapeutics due to the dependence of tumor parenchyma cell survival and proliferation on a (minimally) functional blood supply; treating both cancer cells and associated vascular stroma may be more effective than targeting cancer cells alone.[73] Tumor microvasculature is

drastically different in morphology and function relative to normal vasculature in that endothelial cells are assembled haphazardly from sprouting or intussusception of existing vessels at the borders or a developing neoplasm (angiogenesis) or from blood-borne endothelial progenitor cells (vasculogenesis). The result of hasty construction produces microvasculature that is highly disorganized, tortuous, sinusoidal, branched, has irregular diameters, and often forms dead ends. Tumor endothelial cells typically form single-layer, capillary-like vessels that are frequently devoid of innervation, basement membrane, pericytes, and smooth muscle cells and are often separated from each other, allowing for gaps that facilitate profound vascular leakage as well as the escape of potentially metastatic tumor cells.[74] The chaotic structure of tumor microvasculature directly dictates functionality, which explains several important characteristics of tumor microenvironment. Tumor perfusion is highly heterogenous (although usually within the range of sluggish to completely stopped) and prone to frequent, transient changes, matching the heterogeneity of tumor vascular distribution. As a result, tumor oxygenation is generally poor (i.e. much lower than the typical partial pressure of oxygen of around 40 mmHg in normal tissues). As previously discussed, such tumor hypoxia is a formidable challenge to radiation therapy due to the decreased abundance of oxygen from which reactive oxygen species may be generated (overall leading to less indirect DNA damage). Tumor hypoxia behaves in both a chronic fashion related to the limitation of oxygen diffusion from vessels (tumor cells located beyond the 100 to 150 μm diffusion limit of the nearest vessel become hypoxic)[75] and in an acute fashion in which oxygenation varies transiently in accordance with waxing and waning blood flow.[76,77] The irregular structure of the microvasculature is not the only factor contributing to impaired tumor blood flow and hypoxia. The high interstitial fluid pressure observed in non-peripheral regions of most tumors,[78] which is due to lack of adequate lymphatic drainage and

elevated leakiness of blood vessels,[79] contributes to transient perfusion and acute hypoxia by intermittently collapsing the small, capillary-like vessels. Overall, the characteristics of tumor microvasculature contribute to a hostile microenvironment that is generally nutrient-deprived, acidic, hypoxic, high-pressure, and experiences erratic, inadequate perfusion.[80] As in normal tissues, endothelial cells within tumors must perform highly specialized functions such as regulating smooth muscle tone and coagulation, facilitate fluid and solute exchange, as well as control haemostasis and inflammatory responses in order to support survival and replication of parenchymal cells.[81]

Until recently, endothelial cells were thought to have limited potential for acute radiation injury, but instead play an impactful role in the formation of late radiation effects. Endothelial cells have a slow turnover rate in normal tissues,[82,83] since they place energetic emphasis on cellular differentiation to perform specialized functions as opposed to directing energy towards replication. In response to fractionated radiation therapy, the vascular endothelium of cardiac, renal, pulmonary, brain, bone, skin, bowel, and urinary bladder tissues is known to develop degenerative and fibrotic changes such as hyaline, fibrinoid, or collagenous thickening of vessel walls that impede blood flow (sometimes provoking thrombosis) months to years after irradiation.[84] A notable characteristic of vessels that persist in tissues experiencing late radiation damage is the presence of "sausage segments" where endothelial cell depopulation followed by reactive hyperplasia occurs and generates focal constrictions.[85] The development of stereotactic radiosurgery to treat arteriovenous malformations and other brain tumors (both benign and malignant) generated deep concern over the potential for late effects to brain tissue, since the brain is a highly vascularized organ, and studies typically examined effects at ten or more

months after treatment.[86] Acute reactions of endothelial cells to large doses of radiation delivered in one fraction were not previously thought to be important in radiotherapy.

Studies that pre-date the emergence of stereotactic radiation therapy's application to malignant brain malignancies and extracranial tumors may have come across evidence of a dose threshold above which endothelial cells respond in a manner that would not have been observed in studies of late effects. Song and Levitt observed marked and lasting decreases in functional vascular volume (blood volume per mass of tissue) and increases up to thirty times baseline vessel permeability (as measured by extravasated plasma) after irradiation of rodent tumors with 30 to 60 Gy in one fraction.[87,88] This was in contrast with treatments in the same studies in which a low dose of 2.5 Gy or less produced slight decreases in functional vascular volume for six to twelve hours after irradiation but returned to pre-irradiation levels,[87,88] and also at odds with an earlier study that treated rodent tumors with numerous fractions of low doses, determining that the tumor parenchyma regresses prior to the vascular degeneration, leading to "super-vascularization" of the tumor and reoxygenation.[89] By stimulating endothelial cell proliferation in the eyes of dogs via lamellar keratectomy before treating each eye with single doses of up to 18 Gy, Gillette *et al.* calculated the doses that prevent acute neovascularization in 50% of cases (NVD_{50}) to be 9.5 Gy immediately after endothelial cells were triggered to proliferate and 10 Gy six hours after induction of endothelial cell proliferation.[90] A study in human tumor xenografts showed that tumor microvascular damage was quantifiable and significant to the point of loss of function as early as one week after high-dose irradiation (10, 15, or 20 Gy).[91] Closer examination of the immediate effects of high-dose irradiation (in this case, 17.5 to 25 Gy) showed that considerable normal endothelial cell death occurs within twenty four hours of irradiation, suggesting interphase cell death rather than mitotic cell death which

would not be prominent so early in cells with slow turnover rates.[92] Additional work on the acute death of endothelial cells confirmed that they undergo apoptosis very shortly after high-dose radiation exposure.[93,94] Although sparse evidence had been collected, it seemed as though high dose, single-fraction treatment above a threshold around 9 or 10 Gy triggered tumor endothelial cells to undergo apoptosis in the early stages following irradiation. These conclusions did not sum up to a generally interesting story until technological advances allowed SRT to become more prevalent in treating cancer; suddenly the acute effects of large doses delivered in one to a few fractions became extremely relevant.

In 1994, the mechanism by which ionizing radiation induces an acute apoptotic response in cultured endothelial cells was shown to be ceramide-mediated.[95] Ceramide is a second messenger molecule known to form enriched platforms in the cell membrane where receptor molecules may gather and transmit apoptotic stimuli in response to addition of cellular stressors, such as tumor necrosis factor α, heat shock treatment, or ultraviolet light.[96] When ionizing radiation causes cell damage, available endogenous acid sphingomyelinase enzymes (ASMase) translocate from intracellular lysosomes to the extracellular space and catalyze the conversion of sphingomyelin lipids into ceramide.[97] It happens that endothelial cells maintain massive amounts of active, endogenous ASMase enzymes, measured to be up to twenty times greater than ASMase levels in other cells such as macrophages.[98] Studies showing that ASMase-deficient lymphoblasts derived from individuals with Niemann-Pick disease and vascular endothelial cells in ASMase knock-out mice both fail to undergo apoptosis following a large dose of ionizing radiation (20 Gy) solidified the connection between high-dose irradiation and endothelial cell apoptosis. Apoptosis is not observed in endothelial cells as a response to irradiation with low doses delivered in one or multiple fractions.[99] A threshold dose of 8 to 10

Gy was suggested by Paris *et al.* in a study describing prevention of endothelial cell apoptosis in ASMase knock-out mouse intestinal villi.[100] In this study, whole body doses high enough to cause death from gastrointestinal syndrome (15 to 16 Gy in mice), a process originally thought to be mediated by clonogenic death of intestinal crypt stem cells, failed to produce endothelial cell death in the absence of ASMase, leading ASMase knock-out mice to die of hematopoetic syndrome since intestinal crypt stem cells were not affected by fatal loss of villus microvasculature.[100] A multitude of models describing radiation-induced cell death have been proposed, but none of them predicted that parenchymal cell death (in normal or neoplastic tissues) could be brought about *as a direct result of* endothelial cell death and the acute destruction of functional blood supply that must be subsequent to endothelial cell apoptosis. The interpretation of results in this study was highly debated.[101-103] Suit and Withers argued that stem cell death subsequent to vascular ablation would be ischemic in nature but their own *in vivo* experiments studying dose-dependent intestinal crypt stem cell survival produced survival curves that were not indicative of hypoxia (i.e. one would expect surviving fractions of hypoxic cells to decrease at less steep rates than well-oxygenated cells).[101] However, Suit and Withers' experiments were conducted using 6.6 Gy, below the threshold of endothelial cell apoptosis, so no hypoxic interactions would be expected.[103] The hypothesis of radiation-induced clonogenic cell death was determined from mathematical models of survival data measured in individual cell types rather than complex organ systems comprised of numerous, interacting cell types. The overall response to radiation may result from a more complex interplay of cellular responses, which may not be modeled accurately in simple, *in vitro* systems. Additional studies using ASMase knock-out mice and their wild-type littermates as hosts for fibrosarcoma and melanoma xenografts showed that high doses (20 Gy in one fraction) caused endothelial cell apoptosis and

microvascular damage when ASMase was present (i.e. in wild-type mice).[104] In contrast to ASMase knock-outs, in which endothelial cells were unable to signal for apoptosis via ceramide in response to irradiation, vasculature was structurally and functionally intact after 20 Gy single-dose exposure and tumors grew up to 400% larger in wild-type mice.[104] It has been suggested that an improved understanding of ceramide-mediated apoptosis and related vascular damage could lead to development of therapeutic modulators for the treatment of cancers with single fraction, high-dose irradiation.[105,106]

It has been proposed that endothelial cell apoptosis induced by high-dose single fraction irradiation causes subsequent death of associated parenchymal cells via hypoxic or ischemic mechanisms. This mechanism has yet to be conclusively proven, but several studies of high-dose single fraction irradiation lend credibility to the concept. High doses delivered in single fractions to animal tumor models have been shown to result in decreased tumor vascular density (both in terms of functional vascular volume and vessel length density), and increase extravasation of plasma proteins.[87,88,107-112] Single fraction, high-dose irradiation has also been shown to cause endothelial dysfunction by impacting the ability of vascular endothelium to respond to vasodilatory stimuli such as acetylcholine.[113-118] Impaired vascular function and/or decreased vascular coverage within tumors may be responsible for the observed perfusion decreases following irradiation with one large dose.[109,111,119-122] A perfusion deficit caused by radiation-induced vascular damage would likely increase the severity of hypoxic conditions within a tumor, and increased regions of focal hypoxia have been observed following single high-dose irradiation.[123] It remains unknown how and in what order of events the observations of such post-irradiation vascular dysfunction, decreased functional vascular volume, increased vascular permeability, decreased perfusion and increased hypoxia occur.

A two day delay in harvesting of rodent tumor cells treated with one fraction of 10 to 20 Gy for assessment of clonogenic survival *in vitro* resulted in decreased tumor cell survival relative to *in vivo-in vitro* excision immediately after irradiation.[124,125] The increase in tumor cell kill when tumor cells remained *in situ* for two days coincided with observations of severe vascular injury and decreases in functional vascularity of 50%.[124, 125] More recent studies using the *in vivo-in vitro* excision assay with human fibrosarcoma xenografts noted that tumor cells left *in situ* for three to five days had drastically decreased survival relative to tumor cells excised immediately after treatment with one fraction of 20 Gy.[126] It was proposed based on these experiments that the total tumor cell kill is the sum of direct damage to tumor cells, which die via mitotic cell death as classical radiation biology dictates, and tumor cell killing from the destruction of functional vasculature from high-dose treatment.[126-128] While the roles of tumor microenvironment are undoubtedly important in the survival and progression of tumor cells, it was previously believed that tumor stromal components, including tumor endothelial cells, were not involved in tumor cell killing.[129-131] However, since tumor microenvironmental parameters such as perfusion, hypoxia, and interstitial fluid pressure depend strongly on the morphology and function of vascular stroma, it seems reasonable to believe that endothelial cell apoptosis could lead to increased tumor cell death. This is particularly important when considering the increasing use of single fraction, high-dose irradiation used in SRT to treat a wide variety of tumors. The work described herein pursues an improved understanding of tumor cell radiosensitivity in the high-dose region of clonogenic survival curves and examines parameters related to vascular function in *in vivo* studies using SRT to treat canine soft tissue sarcomas. It is our hope that an improved understanding of the tumor biologic response to single high dose

irradiation will allow for improved design of radiation therapy protocols and enhanced efficacy of treatment for numerous types of cancer.

REFERENCES

1. Colvett K. The history of radiation oncology. *Southern Med J* 2006; 99: 1155-1156.
2. Thames HD. Early fractionation methods and the origins of the NSD concept. *Acta Oncologica* 1988; 27: 89-103.
3. Coutard H. Roentgnetherapy of epitheliomas of the tonsillar region, hypopharynx and larynx from 1920 to 1926. *Am J Roentgenol* 1932; 28: 313-331.
4. Coutard H. Principles of x-ray therapy of malignant diseases. *Lancet* 1934; 2: 1-8.
5. Hall EJ, Giaccia AJ. *Radiobiology for the Radiologist, 7th Ed.* Lippincott- Williams & Wilkins, Philadelphia, PA 2012.
6. Withers HR, McBride WH. Biologic basis of radiation therapy. In *Principles and Practice of Radiation Oncology, 3rd Ed.* Editors: Perez CA, Brady LW. Lippincott-Raven Publishers, Philadelphia 1997.
7. Timmerman RD, Kavanagh BD. Stereotactic body radiation therapy. *Curr Probl Cancer* 2005; 29: 120-157.
8. Leksell L. The stereotaxic method and radiosurgery of the brain. *Acta Chirurg Scand* 1951; 102: 316-319.
9. Blomgren H, Lax I, Naslund I, *et al.* Stereotactic high dose fraction radiation therapy of extracranial tumors using an accelerator- Clinical experience of the first 31 patients. *Act Oncol* 1995; 34: 861-870.
10. Hamilton AJ, Lulu BA, Fosmire H, *et al.* Preliminary clinical experience with linear accelerator-based spinal stereotactic radiosurgery. *Neurosurgery* 1995; 36: 311-319.

11. Uematsu M, Shioda A, Tahara, K, *et al.* Focal, high dose, and fractionated modified stereotactic radiation therapy for lung carcinoma patients: A preliminary experience. *Cancer* 1998; 82: 1062-1070.

12. Herfarth KK, Debus J, Lohr F, *et al.* Stereotactic single-dose radiation therapy of liver tumors: Results of a phase I/II trial. *J Clin Oncol* 2001; 19: 164-170.

13. Uematsu M, Shioda A, Suda A, *et al.* Computed tomography-guided frameless stereotactic radiotherapy for Stage I non-small-cell lung cancer: A 5-year experience. *Int J Radiat Oncol Biol Phys* 2001; 51: 666-670.

14. Wulf J, Hadinger U, Oppitz U, *et al.* Stereotactic radiotherapy of targets in the lung and liver. *Strahlenther Onkol* 2001; 177: 645-655.

15. Nagata Y, Negoro Y, Aoki T, *et al.* Clinical outcomes of 3D conformal hypofractionated single high-dose radiotherapy for one or two lung tumors using a stereotactic body frame. *Int J Radiat Oncol Biol Phys* 2002; 54: 1041-1046.

16. Hof H, Herfarth KK, Munter M, *et al.* Stereotactic single-dose radiotherapy of Stage I non-small-cell lung cancer (NSCLC). *Int J Radiat Oncol Biol Phys* 2003; 56: 335-341.

17. Timmerman RD, Papiez L, McGarry R, *et al.* Extracranial stereotactic radioablation: Results of a phase I study in medically inoperable stage I non-small cell lung cancer. *Chest* 2003; 124: 1946-1955.

18. Wulf J, Haedinger U, Oppitz U, *et al.* Stereotactic radiotherapy for primary lung cancer and pulmonary metastases: A noninvasive treatment approach in medically inoperable patients. *Int J Radiat Oncol Biol Phys* 2004; 60: 186-196.

19. Wersall PJ, Blomgren H, Lax I, *et al.* Extracranial stereotactic radiotherapy for primary and metastatic renal cell carcinoma. *Radiother Oncol* 2005; 77: 88-95.

20. Wulf J, Guckenberger M, Haedinger U, *et al.* Stereotactic radiotherapy of primary liver cancer and hepatic metastases. *Acta Oncol* 2006; 45: 838-847.
21. Yamada Y, Bilsky MH, Lovelock DM, *et al.* High-dose, single-fraction image-guided intensity-modulated radiotherapy for metastatic spinal lesions. *Int J Radiat Oncol Biol Phys* 2008; 71: 484-490.
22. Gunven P, Blomgren H, Lax I, *et al.* Curative stereotactic body radiotherapy for liver malignancy. *Med Oncol* 2009; 26: 327-334.
23. Inoue T, Shimizu S, Onimaru R, *et al.* Clinical outcomes of stereotactic body radiotherapy for small lung lesions clinically diagnosed as primary lung cancer on radiologic examination. *Int J Radiat Oncol Biol Phys* 2009; 75: 683-687.
24. Habermehl D, Herfarth KK, Bermejo JL, *et al.* Single-dose radiosurgical treatment for hepatic metastases- therapeutic outcome of 138 treated lesions from a single institution. *Rad Oncol* 2013; 8: 1-9.
25. King CR, Freeman D, Kaplan I, *et al.* Stereotactic body radiotherapy for localized prostate cancer: Pooled analysis from a multi-institutional consortium of prospective phase II trials. *Radiother Oncol* 2013; 109: 217-221.
26. Hanahan D, Weinberg RA. Hallmarks of cancer: The next generation. *Cell* 2011; 144: 646-674.
27. Withers HR. Biologic basis for altered fractionation schemes. *Cancer* 1985; 55: 2086-2095.
28. Withers HR. The four R's of radiotherapy. In *Advances in Radiation Biology, Vol. 5*, Academic Press, San Francisco, CA. 1975.

29. Fertil B, Malaise EP. Intrinsic radiosensitivity of human cell lines is correlated with radioresponsiveness of human tumors: Analysis of 101 published survival curves. *Int J Radiat Oncol Biol Phys* 1985; 11: 1699-1707.

30. Elkind MM, Whitmore GF. *The Radiobiology of Cultured Mammalian Cells*. Gordon and Breach, New York, NY 1967.

31. Curtis SB. Lethal and potentially lethal lesions induced by radiation- A unified repair model. *Radiat Res* 1986; 106: 252-270.

32. Kiefer J. Quantitative mathematical models in radiation biology. *Radiat Environ Biophys* 1988; 27: 219-232.

33. Park C, Papiez L, Zhang S, *et al.* Universal survival curve and single fraction equivalent dose: Useful tools in understanding potency of ablative radiotherapy. *Int J Radiat Oncol Biol Phys* 2008; 70: 847-852.

34. Kavanagh BD, Newman F. Toward a unified survival curve: In regard to Park *et al.* (*Int J Radiat Oncol Biol Phys* 2008;70:847-852) and Krueger *et al.* (*Int J Radiat Oncol Biol Phys* 2007;69:1262-1271). *Int J Radiat Oncol Biol Phys* 2008; 71: 958-959.

35. McKenna FW, Ahmad S. Fitting techniques of cell survival curves in high-dose region for use in stereotactic body radiation therapy. *Phys Med Biol* 2009; 54: 1593-1608.

36. Guerrero M, Li A. Extending the linear-quadratic model for large fraction doses pertinent to stereotactic radiotherapy. *Phys Med Biol* 2004; 49: 4825-4835.

37. Wang JZ, Huang Z, Lo SS, *et al.* A generalized linear-quadratic model for radiosurgery, stereotactic body radiation therapy, and high-dose rate brachytherapy. *Sci Transl Med* 2010; 2: 39ra48.

38. Andisheh B, Edgren M, Belkic Dz, *et al.* A comparative analysis of radiobiological models for cell surviving fractions at high doses. *Technol Cancer Res Treat* 2013; 12: 183-192.

39. Yaes RJ. Linear-quadratic model isoeffect relationships for proliferating tumor-cells for treatment with multiple fractions per day. *Int J Radiat Oncol Biol Phys* 1989; 17: 901-905.

40. Brenner DJ, Hlatky LR, Hahnfeldt PJ, *et al.* A convenient extension of the linear-quadratic model to include redistribution and reoxygenation. *Int J Radiat Oncol Biol Phys* 1995; 32: 379-390.

41. Fowler JF, Stern BE. Dose-rate factors in integral dose estimations [letter]. *Br J Radiol* 1958; 31: 316.

42. Fowler JF, Stern BE. Dose-rate effects: Some theoretical and practical considerations. *Br J Radiol* 1960; 33: 389-395.

43. Fowler JF. A review: The linear quadratic formula and progress in fractionated radiotherapy. *Br J Radiol* 1989; 62: 679-675.

44. Fowler JF. 21 Years of biologically effective dose. *Br J Radiol* 2010; 83: 554-568.

45. Jones B, Dale RG, Deehan C, *et al.* The role of biologically effective dose (BED) in clinical oncology. *Clin Oncol* 2001; 13: 71-81.

46. Dasu A, Toma-Dasu I. Prostate alpha/beta revisited- an analysis of clinical results from 14,168 patients. *Acta Oncol* 2012; 51: 963-974.

47. Williams MV, Denekamp J, Fowler JF. A review of α/β ratios for experimental tumors: Implications for clinical studies of altered fractionation. *Int J Radiat Oncol Biol Phys* 1985; 11: 87-96.

48. Hall EJ, Brenner DJ. The radiobiology of radiosurgery: Rationale for different treatment regimes for AVMs and malignancies. *Int J Radiat Oncol Biol Phys* 1993; 25: 381-385.

49. Marks LB. Extrapolating hypofractionated radiation schemes from radiosurgery data: Regarding *Hall et al. IJROBP 21: 819-825; 1991* and *Hall and Brenner, IJROBP 25; 381-385; 1993*. *Int J Radiat Oncol Biol Phys* 1995; 32: 274-275.

50. Kirkpatrick JP, Meyer JJ, Marks LB. The linear-quadratic model is inappropriate to model high dose per fraction effects in radiosurgery. *Semin Radiat Oncol* 2008; 18: 240-243.

51. Hall EJ, Brenner DJ. In response to Dr. Marks. *Int J Radiat Oncol Biol Phys* 1995; 32: 275-276.

52. Brenner DJ. The linear-quadratic model is an appropriate methodology for determining iso-effective doses at large dose per fraction. *Semin Radiat Oncol* 2008; 18: 234-239.

53. Zaider M. There is no mechanistic basis for the use of the linear-quadratic expression in cellular survival analysis. *Med Phys* 1998; 25: 791-792.

54. Garcia LM, Leblanc J, Wilkins D, *et al.* Fitting the linear-quadratic model to detailed data sets for different dose ranges. *Phys Med Biol* 2006; 51: 2813-2823.

55. Garcia LM, Wilkins DE, Raaphorst GP. α/β ratio: A dose range dependence study. *Int J Radiat Oncol Biol Phys* 2007; 67: 587-593.

56. Fowler JF, Tome WA, Fenwick JD, *et al.* A challenge to traditional radiation oncology. *Int J Radiat Oncol Biol Phys* 2004; 60: 1241-1256.

57. Miyakawa A, Shibamoto Y, Otsuka S, *et al.* Applicability of the linear-quadratic model to single and fractionated radiotherapy schedules: An experimental study. *Radiat Res* 2013; 87: 1-4.

58. Sheu T, Molkentine J, Transtrum MK, *et al.* Use of the LQ model with large fraction sizes results in underestimation of isoeffect doses. *Radiother Oncol* 2013; 109: 21-25.

59. Jones B, Dale RG. Radiobiology of high dose fractions. In *Stereotactic Body Radiotherapy: A Practical Guide* Editors Gaya A, Mahadevan A. Springer-Verlag, London, 2015.

60. Story M, Kodym R, Saha D. Exploring the possibility of unique molecular, biolotical, and tissue effects with hypofractionated radiotherapy. *Semin Radiat Oncol* 2008; 18: 244-248.

61. Song CW, Park H, Griffin RJ, *et al.* Radiobiology of stereotactic radiosurgery and stereotactic body radiotherapy. In *Technical Basis of Radiation Therapy* Editors Levitt SH, *et al.* Springer-Verlag, Berlin, Heidelberg, 2012.

62. Brown JM, Koong AC. High-dose single-fraction radiotherapy: Exploiting a new biology? *Int J Radiat Oncol Biol Phys* 2008; 71: 324-325.

63. Brown JM, Brenner DJ, Carlson DJ. Dose escalation, not "new biology," can account for the efficacy of stereotactic body radiation therapy with non-small cell lung cancer. *Int J Radiat Oncol Biol Phys* 2013; 85: 1159-1160.

64. Brown JM, Carlson DJ, Brenner DJ. The tumor radiobiology of SRS and SBRT: Are more than the 5 Rs involved? *Int J Radiat Oncol Biol Phys* 2014; 88: 254-262.

65. Brown JM, Diehn M, Loo BW. Stereotactic ablative radiotherapy should be combined with a hypoxic cell radiosensitizer. *Int J Radiat Oncol Biol Phys* 2010; 78: 323-327.

66. Kim SH, Lim DJ, Chung YG, *et al.* Expression of TNF-α and TGF-β1 in the rat brain after a single high-dose irradiation. *J Korean Med Sci* 2002; 17: 242-248.

67. Wersall PJ, Blomgren H, Pisa P, *et al.* Regression of non-irradiated metastases after extracranial stereotactic radiotherapy in metastatic renal cell carcinoma. *Acta Oncol* 2006; 45: 493-497.

68. Dewan MZ, Galloway AE, Kawashima N, *et al.* Fractionated but not single-dose radiotherapy induces an immune-mediated abscopal effect when combined with anti-CTLA-4 antibody. *Clin Cancer Res* 2009; 15: 5379-5388.

69. Lee Y, Auh SL, Wang Y, *et al.* Therapeutic effects of ablative radiation on local tumor require $CD8^+$ T cells: Changing strategies for cancer treatment. *Blood* 2009; 114: 589-595.

70. Lee WH, Sonntag WE, Mitschelen M, *et al.* Irradiation induces regionally specific alterations in pro-inflammatory environments in rat brain. *Int J Radiat Biol* 2010; 86: 132-144.

71. Finkelstein SE, Timmerman R, McBride WH, *et al.* The confluence of stereotactic ablative radiotherapy and tumor immunology. *Clin Developm Immunol* 2011; 2011: 1-7.

72. Tang C, Wang X, Soh H, *et al.* Combining radiation and immunotherapy: A new systemic therapy for solid tumors? *Cancer Immunol Res* 2014; 2: 831-838.

73. Folkman J. Angiogenesis. *Annu Rev Med* 2006; 57: 1-18.

74. Hashizume H, Baluk P, Morikawa S, *et al.* Openings between defective endothelial cells explain tumor vessel leakiness. *Am J Pathol* 2000; 156: 1363-1380.

75. Thomlinson RH, Gray LH. The histological structure of some human lung cancers and the possible implications for radiotherapy. *Br J Cancer* 1955; 9: 539-549.

76. Brown JM. Evidence for acutely hypoxic cells in mouse tumors and a possible mechanism for reoxygenation. *Br J Radiol* 1979; 52: 650-656.

77. Franko AJ, Sutherland RM. Radiation survival of cells from spheroids grown in different oxygen concentrations. *Radiat Res* 1979; 79: 454-467.

78. Heldin CH, Rubin K, Pietras K, *et al.* High interstitial fluid pressure- An obstacle in cancer therapy. *Nature Rev Cancer* 2004; 4: 806-813.

79. Boucher Y, Jain RK. Microvascular pressure is the principal driving force for interstitial hypertension in solid tumors- Implications for vascular collapse. *Cancer Res* 1992; 52: 5110-5114.

80. Vaupel P. Tumor microenvironmental physiology and its implications for radiation oncology. *Semin Radiat Oncol* 2004; 14: 198-206.

81. Pries AR, Kuebler WM. Normal Endothelium. In *The Vascular Endothelium I*. Editors Moncada S, Higgs A. Springer-Verlag, Berlin, Heidelberg, 2006.

82. Tannock IF, Hayashi S. The proliferation of capillary endothelial cells. *Cancer Res* 1972; 32: 77-82.

83. Hobson B, Denekamp J. Endothelial proliferation in tumours and normal tissues: Continuous labelling studies. *Br J Cancer* 1984; 49: 405-413.

84. Fajardo LF. Morphology of radiation effects on normal tissues. In *Principles and Practice of Radiation Oncology, 3rd Ed.* Editors: Perez CA, Brady LW. Lippincott-Raven Publishers, Philadelphia 1997.

85. Rubin P, Constine LS, Williams JP. Late effects of cancer treatment: Radiation and drug toxicity. In *Principles and Practice of Radiation Oncology, 3rd Ed.* Editors: Perez CA, Brady LW. Lippincott-Raven Publishers, Philadelphia 1997.

86. Schneider BF, Eberhard DA, Steiner LE. Histopathology of arteriovenous malformations after gamma knife radiosurgery. *J Neurosurg* 1997; 87: 352-357.

87. Song CW, Levitt SH. Quantitative study of vascularity in Walker carcinoma 256. *Cancer Res* 1971; 31: 587-589.

88. Song CW, Sung JH, Clement JJ, *et al.* Vascular changes in neuroblastoma of mice following x-irradiation. *Cancer Res* 1974; 34: 2344-2350.

89. Rubin P, Casarett G. Microcirculation of tumors part II: The supervascularized state of irradiated regressing tumors. *Clin Radiol* 1966; 17: 346-355.

90. Gillette EL, Maurer GD, Severin GA. Endothelial repair of radiation damage following beta irradiation. *Radiol* 1975; 116: 175-177.

91. Solesvik OV, Rofstad EK, Brustad T. Vascular changes in a human melanoma xenograft following single-dose irradiation. *Radiat Res* 1984; 98: 115-128.

92. Ljubimova NV, Levitman MK, Plotnikova ED, et al. Endothelial cell population dynamics in rat brain after local irradiation. *Br J Radiol* 1991; 64: 934-940.

93. Fuks Z, Persaud RS, Alferi A, *et al.* Basic fibroblast growth factor protects endothelial cells against radiation-induced programmed cell death *in vitro* and *in vivo.* *Cancer Res* 1994; 54: 2582-2590.

94. Langley RE, Bump EA, Quartuccio SG, *et al.* Radiation-induced apoptosis in microvascular endothelial cells. *Br J Cancer* 1997; 75: 666-672.

95. Haimovitz-Friedman A, Kan CC, Ehleiter D, *et al.* Ionizing radiation acts on cellular membranes to generate ceramide and initiate apoptosis. *J Exp Med* 1994; 180: 525-535.

96. Gulbins E. Regulation of death receptor signaling and apoptosis by ceramide. *Pharmacol Res* 2003; 47: 393-399.

97. Hannun YA, Obeid LM. Principles of bioactive lipid signaling: Lessons from sphingolipids. *Nature Rev Molec Cell Biol* 2008; 9: 139-150.

98. Marathe S, Schissel SL, Yellin MJ, *et al.* Human vascular endothelial cells are a rich and regulatable source of secretory sphingomyelinase: Implications for early atherogenesis and ceramide-mediated cell signaling. *J Biol Chem* 1998; 273: 4081-4088.

99. Cervelli T, Panetta D, Navarra T, *et al.* Effects of single and fractionated low-dose irradiation on vascular endothelial cells. *Atherosclerosis* 2014; 235: 510-518.

100. Paris F, Fuks Z, Kang A, *et al.* Endothelial apoptosis as the primary lesion initiating intestinal radiation damage in mice. *Science* 2001; 293: 293-297.

101. Suit HD, Withers HR. Endothelial cells and radiation gastrointestinal syndrome. *Science* 2001; 294: 1411.

102. Bendry JH, Booth C, Potten CS. In response to Paris *et al.* *Science* 2001; 294: 1411-1412.

103. Kolesnick R, Fuks Z, Venkatraman E. In response to Bendry *et al.* and Suit & Withers. *Science* 2001; 294: 1412-1413.

104. Garcia-Barros M, Paris F, Cordon-Cardo C, *et al.* Tumor response to radiotherapy regulated by endothelial cell apoptosis. *Science* 2003; 300: 1155-1159.

105. Kolesnick R, Fuks Z. Radiation and ceramide-induced apoptosis. *Oncogene* 2003; 22: 5897-5906.

106. Fuks Z, Kolesnick R. Engaging the vascular component of the tumor response. *Cancer Cell* 2005; 8: 89-91.

107. Song CW, Payne JT, Levitt SH. Vascularity and blood flow in X-irradiated Walker carcinoma 256 of rats. *Radiol* 1972; 104: 693-697.

108. Wong HH, Song CW, Levitt SH. Early changes in the functional vasculature of Walker carcinoma 256 following irradiation. *Radiol* 1973; 108: 429-434.

109. Acker JC, Marks LB, Spencer DP, *et al.* Serial *in vivo* observations of cerebral vasculature after treatment with a large single fraction radiation. *Radiat Res* 1998; 149: 350-359.

110. Tsai JH, Makonnen S, Feldman M, *et al.* Ionizing radiation inhibits tumor neovascularization by inducing ineffective angiogenesis. *Cancer Biol Ther* 2005; 4: 1395-1400.

111. Kim DWN, Huamani J, Niermann KJ, *et al.* Noninvasive assessment of tumor vasculature response to radiation-mediated, vasculature-targeted therapy using quantified power Doppler sonography: Implications for improvement of therapy schedules. *J Ultrasound Med* 2006; 25: 1507-1517.

112. Chen FH, Chiang CS, Wang CC, *et al.* Radiotherapy decreases vascular density and causes hypoxia with macrophage aggregation in TRAMP-C1 prostate tumors. *Clin Cancer Res* 2009; 15: 1721-1729.

113. Maynard KI, Stewart-Lee AL, Milner P, *et al.* X-irradiation attenuates relaxant responses in rabbit ear artery. *Br J Pharmacol* 1992; 105: 126-128.

114. Wiederman JG, Leavy JA, Amols H, *et al.* Effects of high-dose intracoronary irradiation on vasomotor function and smooth muscle histopathology. *Am Physiol Soc* 1994; 125-132.

115. Menendez JC, Casanova D, Amado JA, *et al.* Effects of radiation on endothelial function. *Int J Radiat Oncol Biol Phys* 1998; 41: 905-913.

116. Qi F, Sugihara T, Hattori Y, *et al.* Functional and morphological damage of endothelium in rabbit ear artery following irradiation with cobalt^{60}. *Br J Pharmacol* 1998; 123: 653-660.

117. Li J, De Leon H, Ebato B, *et al.* Endovascular irradiation impairs vascular function responses in noninjured pig coronary arteries. *Cardio Radiat Med* 2002; 3: 152-162.

118. Soloviev AI, Tishkin SM, Parshikov AV, *et al.* Mechanisms of endothelial dysfunction after ionized radiation: Selective impairment of the nitric oxide component of endothelium-dependent vasodilation. *Br J Pharmacol* 2003; 138: 837-844.

119. Emami B, Ten Haken RK, Nussbaum GH, *et al*. Effects of single-dose irradiation on tumor blood flow studied by ^{15}O decay after photon activation *in situ*. *Radiol* 1981; 141: 207-209.

120. Bussink J, Kaanders JHAM, Rijken PFJW, *et al.* Changes in blood perfusion and hypoxia after irradiation of a human squamous cell carcinoma xenograft tumor line. *Radiat Res* 2000; 153: 398-404.

121. Kioi M, Vogel H, Schultz G, *et al.* Inhibition of vasculogenesis, but not angiogenesis, prevents recurrence of glioblastoma after irradiation in mice. *J Clin Invest* 2010; 120: 694-704.

122. El Kaffas A, Al-Mahrouki A, Tran WT, *et al.* Sunitinib effects on radiation response of endothelial and breast tumor cells. *Microvasc Res* 2014; 92: 1-9.

123. Goda F, O'Hara JA, Rhodes ES, *et al.* Changes in oxygen tension in experimental tumors after a single dose of X-ray irradiation. *Cancer Res* 1995; 55: 2249-2252.

124. Clement JJ, Song CW, Levitt SH. Changes in functional vascularity and cell number following X-irradiation of a murine carcinoma. *Int J Radiat Oncol Biol Phys* 1976; 1: 671-687.

125. Clement JJ, Tanaka N, Song CW. Tumor reoxygenation and postirradiation vascular changes. *Radiol* 1987; 127: 799-803.

126. Song CW, Park I, Cho LC, *et al.* Is indirect cell death involved in response of tumor to stereotactic radiosurgery and stereotactic body radiation therapy? *Int J Radiat Oncol Biol Phys* 2014; 89: 924-925.

127. Song CW, Cho LC, Yuan J, *et al.* Radiobiology of stereotactic body radiation therapy/stereotactic radiosurgery and the linear-quadratic model. *Int J Radiat Oncol Biol Phys* 2013; 87: 18-19.

128. Song CW, Kim MS, Cho LC, *et al.* Radiobiological basis of SBRT and SRS. *Int J Clin Oncol* 2014; 19: 570-578.

129. Budach W, Taghian A, Freeman J, *et al.* Impact of stromal sensitivity on radiation response of tumors. *J Natl Cancer Inst* 1993; 85: 988-993.

130. Gerweck LE, Vijayappa S, Kurimasa A, *et al.* Tumor cell radiosensitivity is a major determinant of tumor response to radiation. *Cancer Res* 2006; 66: 8352-8355.

131. Ogawa K, Boucher Y, Kashiwagi S, *et al.* Influence of tumor cell and stroma sensitivity on tumor response to radiation. *Cancer Res* 2007; 67: 4016-4021.

CHAPTER 2

RADIOSENSITIVITY OF CANINE CANCER CELL LINES AND SURVIVAL AT HIGH DOSES

INTRODUCTION

The ability to predict radiation response in tumors and normal tissues on an individualized basis has been a long-time goal of radiation biologist and physicians.[1-2] Normal tissue tolerance limits, prognostic factors indicative of radiocurability, or tests to identify patients with impaired DNA damage repair mechanisms (e.g. individuals heterozygous for ataxia telangiectasia, Fanconi's anemia, etc.) could potentially be determined with pre-treatment modeling and would be extremely useful in the clinical application of radiation therapy.[1]

As previously discussed, animal models have been used in the hopes of developing such predictive assays and to increase understanding of radiation effects. While rodent models have the advantage of being able to host xenografted tumors of human genetic composition, but the conditions facilitating the xenograft, such as immunodeficiency or mixed murine stromal and human parenchymal components, makes it difficult to extrapolate results directly to human medicine. As opposed to models using xenografted tumors, spontaneously occurring tumors in dogs feature genetic similarities in the stages of initiation and progression of cancer that more closely reflect human cancer.[3-6] Companion animals share common environmental exposures to humans and represent a more naturally outbred population than rodents or other purpose-bred research animals.[3-6] Cancer is an age-related disease in both dogs and humans and age-adjusted cancer occurrence rates in dogs reflect those in humans.[3-5] In contrast to rodent models, immune system response, tumor size, and tumor cell kinetics of canine cancers are similar to humans.[3-6]

Cancer cell lines derived from spontaneously occurring canine tumors were chosen for the experiments described herein.

The most fundamental of models used to understand interactions of radiation with cells is the cell survival curve. Survival curves communicate information related to two populations of cells: those that are rendered unable to proliferate from radiation exposure, and those that have "survived" irradiation by maintaining clonogenic capabilities. The proportion of each population (essentially, dead or alive) is dose-dependent and varies tremendously across different cell types and different conditions manipulated during irradiation. Oxygenation levels, the presence or absence of feeder layers, asynchronogenicity or alternative manipulations of cell cycling, and other factors can influence cell survival, as well as whether cells were grown in primary culture as opposed to being immortalized cell lines. Even use of different assays to determine surviving fractions of cells, such as the clonogenic assay, the soft agar colony formation assay, or population growth assays, can affect the results of a cell survival curve.[7] While cell survival curves should not be expected to directly reflect *in vivo* radiation response, there is sufficient variability of surviving fraction values among cells from different individuals (more so than within multiple samplings of the same tissue in a single individual) to believe that *in vitro* assays of radiation response may have some predictive value worthy of study,[7] as long as it is remembered that such assays reflect no properties aside from reproductive integrity.[8]

The first dose-dependent survival curve was developed using the HeLa cervical carcinoma cell line in by Puck and Marcus in 1956.[8-10] The curve contained surviving fraction data in the range of 1 to 6 Gy, although a great amount of attention was drawn to survival at 2 Gy due to the common use of 2 Gy per fraction in radiation therapy protocols. In general, tumors considered to be traditionally radioresponsive corresponded with greater *in vitro* radiosensitivity

of cells derived from the same tumor tissues.[8,10,11] Most survival curves report surviving fractions below 6 to 8 Gy, a range in which data is more easily obtained. In order to explain how irradiated cells lose unlimited clonogenic capacity, numerous models were developed to fit cell survival curve data. One of the early models, the single-hit multitarget model described by Equation 1, was based on Target Theory in which the discrete and random interactions of ionizing radiation within cells produce molecular lesions that inactivate a number of unspecified "targets," presumably but not implicitly genetic in composition, in a process both necessary and sufficient for cell death.[10]

$$S = 1 - (1 - e^{-D/D_0})^n \qquad [1]$$

Survival (S) is described by dose (D), target number (n), and the mean lethal dose (D_0, or the dose required to deliver one inactivating event per cell). While this model implies mechanistic biologic events, it is simply based upon a binomial distribution of probabilities of "hits" and "misses."[10] It is important to note that it lacks definitive connection to biological events, but it was developed from simple exponential models of cell survival in an effort to better describe the shoulder observed in the low dose region of cell survival curves. The target number describes the width of the shoulder and it has been proposed that cellular damage repair occurs at doses within the shoulder region. The single-hit multitarget model predicts that surviving fraction data extrapolates in an exponential fashion at high doses, which is visualized as a straight line on conventional semi-log survival curve plots.

The linear quadratic model, which has been discussed previously in detail, became favored over other models for its simplicity. In this case, survival (S) is described in terms of αD (the linear term) and βD^2 (the continuously bending quadratic term) components according to the theory of dual action of radiation.

$$S = e^{-(\alpha D + \beta D^2)} \quad [2]$$

The fact that the linear quadratic model predicts continuous bending of the curve in the high dose region was not troublesome in terms of traditional, fractionated radiation therapy in which doses above 2 Gy were uncommonly used. Following development of hypofractionated radiation protocols and SRT, the high-dose region garnered greater focus. In an effort to better describe the high-dose region while maintaining the characteristics of simplicity and good low-dose region fit that made the linear quadratic model popular, an effort was made to fuse the linear quadratic model to the single-hit multitarget model into a "universal survival curve."[12] A subsequent alteration of the universal survival curve to smooth out the "elbow" where low-dose, linear quadratic fitting joined high-dose multitarget fitting, produced the Kavanagh-Newman universal survival curve:[13]

$$S = e^{-K_0(1 - e^{-KgD})D} \quad [3]$$

While each model is used to explain biologic observations in terms of biophysical events, no model has a truly established biologic basis. Numerous mathematical expressions could be used to fit the survival curve shape, and the more variables and constants added the better the fit can be made, but goodness of fit of experimental data is not an acceptable replacement for direct proof of mechanistic principles. In an effort to further explore fitting of survival curve data, a modified linear quadratic function with an added component called γD^3 was used to increase bending in the high-dose region of survival curves, which made for useful comparisons with equations that predicted exponential trends in that region.

$$S = e^{-(\alpha D + \beta D^2 + \gamma D^3)} \quad [4]$$

Using multiple, established canine cancer cell lines, equations 1 through 4 were applied to dose-dependent survival data with the goal of improving understanding of modeling in the high-dose region of the curves. We hypothesized that existing models provide poor fitting of high-dose data, as they were originally designed to fit data in the low-dose region as pertaining to traditional, fractionated radiation therapy. It has been suggested that alternative biological responses occur above an 8 to 10 Gy threshold,[14] and since no model accounts for differential mechanistic behaviors at low versus high dose, it may be necessary to develop new models to describe high-dose effects.

MATERIALS AND METHODS

Canine Cell Lines

Eight canine cancer cell lines were obtained from Colorado State University's Flint Animal Cancer Center (courtesy of Dr. D. Thamm). Two osteosarcoma lines named Abrams and D17, Dennys hemangiosarcoma, STSA-1 soft tissue sarcoma, CTAC thyroid carcinoma, CMT-12 mammary carcinoma, K9TCC transitional cell carcinoma, and C2 mast cell tumor cell lines were used in this study. In addition, one normal canine endothelial cell line, CnAOEC, was studied as purchased from Cell Applications, Inc. (San Diego, California). Cancer cells were grown, maintained, and irradiated in either RPMI (HyClone Laboratories, Inc., South Logan, Utah, USA) or, in an effort to improve plating efficiencies by increasing the glucose content of the cellular environment, DMEM (Mediatech, Inc., Manassas, Virginia, USA) media. 10% fetal bovine serum (Peak Serum, Inc., Fort Collins, Colorado, USA) and 1% penicillin/streptomycin/amphotericin B antibiotic and antimycotic solution (Mediatech, Inc., Manassas, Virginia, USA) were added to culture media. Canine endothelial cells were grown, maintained, and irradiated in Canine Endothelial Cell Basal Medium (Cell Applications, Inc.,

San Diego, California, USA) which contains serum and specialized components necessary for endothelial cells culture (e.g. growth factors). Cells were incubated at 37°C, 5% CO_2, and 80% humidity. All cells were maintained in monolayers and subcultured to sustain continuous, asynchronous, logarithmic growth.

Irradiation

Canine cancer cells were irradiated prior to their thirtieth subculture, and in many cases prior to their tenth to minimize chance of genetic drift and prevent complications of cell senescence related to reaching the Hayflick limit. Canine endothelial cells were irradiated before reaching their eighth subculture, as "normal" cell line viability decreases rapidly with increasing subcultures and is in that respect very different from cell lines derived from neoplasms. Cells were washed with HBSS and trypsinized (both solutions were used as received from Mediatech, Inc., Manassas, Virginia, USA) before being counted using a hemocytometer (Hausser Scientific, Horsham, Pennsylvania, USA) and diluted to quantitatively so that known numbers of cells were plated directly into vent-capped, 75 cm^2 cell culture flasks (Corning Inc., Corning, New York, USA) which, with the exception of zero dose control flasks, were irradiated without delay and at room temperature using a single posterior-anterior beam of 6 MV photons generated from a Varian Trilogy® linear accelerator (Varian Medical Systems, Inc., Palo Alto, California, USA).

Each experiment was carried out in triplicate; surviving fractions reported here represent mean values calculated from colony counts from three separate flasks of cells per dose level. Zero dose control flasks, typically containing 100 to 200 cells, were carried from the laboratory to the accelerator suite along with flasks intended for irradiation to account for effects of movement on cell reattachment and to insure applicability of calculated plating efficiencies to their corresponding experiments.

To generate electronic equilibrium and produce an even distribution of dose across the cell monolayer, flasks were placed snugly on top of 1 cm of tissue equivalent bolus ("Superflab" bolus, Mick Radio-Nuclear Instruments, Inc., Mt. Vernon, New York, USA) with additional bolus alongside the flask edges. Dose was delivered at a rate of approximately 600 cGy/min to values of 0, 2, 4, 6, 8, 10, 12, 13, 14, or 15 Gy, as determined by point calculations.

Clonogenic Assay

Irradiated cells were evaluated for retention of unlimited replicative capacity using the standard clonogenic assay method.[15] Cells were not removed from their flasks following irradiation and were allowed to incubate undisturbed for 1.5 to nearly 3 weeks, until colonies reached a size that was visible to the naked eye. It was noted that flasks treated with high doses (which, by design and necessity, usually contained up to a million cells per flask) required longer incubation periods before visible colonies could be distinguished from a background of cells that would eventually die off. Cell culture media was changed as needed throughout the incubation period. The large numbers of cells contained in aforementioned flasks intended for high-dose irradiations maintained metabolic activity after radiation treatment and consumed media nutrients at high rates until the 2.5 to 3 week post-irradiation point, at which point evidence of cell death could be visualized under a microscope. After incubation, colonies were fixed in a solution of 15 mL glacial acetic acid mixed with 40 mL of 95% ethanol and 150 mL of deionized water. Fixed colonies were stained using a solution of 18% crystal violet and colonies estimated to contain more than 50 cells were counted using a Counter Pen (Control Co., Friendswood, Texas, USA).

Plating efficiencies (PE) for each set of experiments in every cell line were determined using the unirradiated (0 Gy) controls according to the following equation:

$$PE = \frac{Number\ of\ Colonies}{Number\ of\ cells\ seeded} x\ 100 \quad [5]$$

Plating efficiencies were typically much lower than 100% due to trauma associated with trypsinization during cell suspension for counting and dilution and differential success among cell types regarding reattachment capabilities. Some cell lines, particularly the canine endothelial cells, had consistently low plating efficiencies regardless of changes in media or conditions. Data with plating efficiencies above 40% were obtained from six of the cell lines. Plating efficiencies from zero dose control flasks associated with every set of experiments were taken into account when calculating surviving fraction (SF) at each dose level as follows:

$$SF = \frac{Number\ of\ Colonies}{Cells\ seeded\ x\ (\frac{PE}{100})} \quad [6]$$

Survival Curve Modeling

All survival curves were fit using non-linear regression techniques on Origin 6.1 software according to four, previously described models: the linear quadratic model, the single-hit multitarget model, the Kavanagh-Newman universal survival curve, and a modified linear quadratic expression containing a "γD^3" parameter.

RESULTS

Surviving fraction as a function of dose was determined in eight canine cancer cell lines and one normal canine endothelial cell line (Figure 2.1). Among the canine cancer cell lines, Abrams and D17 osteosarcoma cells, Dennys hemangiosarcoma cells, CMT-12 mammary carcinoma cells, and K9TCC transitional cell carcinoma cells generally fell into a category of greater radioresistance, with divergence from the more radiosensitive STSA-1 soft tissue sarcoma cells, CTAC thyroid carcinoma cells, and C2 mast cell tumor cells above 2 Gy. Separation of the two groups in terms of differences in survival at a given dose increased as dose

increased up to 12 to 13 Gy, at which point the two groups of survival curves seemingly began to converge, with the exception of the Dennys hemangiosarcoma line which produced the highest surviving fractions of all cell lines in the 12 to 15 Gy dose range. A mean surviving fraction value at 13 Gy in the K9TCC line appeared to be very low relative to expectations based on K9TCC cell surviving fraction values at lower doses; it is possible that this point is an outlier, in spite of the fact that plating efficiency for the set of experiments producing this point was relatively high (68.2%) compared to other experiments with K9TCC (in which plating efficiency was between 18.3 and 24.3%).

The normal canine endothelial cell line, CnAOEC, had survival characteristics similar to the more radiosensitive canine cancer cell lines (STSA-1, CTAC, and C2), although due to low plating efficiency (13.6%) and difficulty in obtaining high-dose data, surviving fraction in CnAOEC cells was not determined above 12 Gy. Data above 15 Gy was not achieved in any cell line in spite of numerous experimental attempts and attempts using larger (150 cm^2) flasks to hold more cells. All attempts at collecting data at 18 or 20 Gy failed to produce surviving colonies. In a classic radiobiology textbook, Elkind and Whitmore claimed that the surviving fraction limit of the clonogenic assay for determining dose-dependent survival was 10^{-4}.[10] However, the data shown in Figure 2.1 reached surviving fractions in the range of 10^{-5} due to careful handling of cells and persistent attempts at determining optimum numbers of cells to seed into flasks in a trial-and-error process. Of note, the data in the high-dose range with surviving fractions around 10^{-5} had increased variability relative to data at lower doses, as visualized by the increased range of the error bars denoting one standard deviation of the mean on high dose data points.

Non-linear regression analysis allowed for data from each cell line to be fitted using the linear quadratic, single-hit multitarget, and Kavanagh-Newman expressions and also using a modified, curvier version of linear quadratic model that includes a "γD^3" component. Parameters of interest in the linear quadratic equation, including calculated α/β ratios for each cell line, were summarized in Table 2.1. A wide range of α/β ratios were calculated, from the lowest for K9TCC at 0.6 Gy, to the highest for STSA-1 at 227 Gy. Parameters used in the single-hit multitarget model such as mean lethal dose, D_0, and target number, n, were summarized in Table 2.2. D_0 values fell within a reasonable range of about 1.8 to 3.1 Gy and n values were found to be between 0.8 and 3.5. Table 2.3 displays values in each cell line for the components of the Kavanagh-Newman universal survival curves and Table 2.4 contains α, β, and γ values from the hypothetical, modified linear quadratic survival curves. Addition of the "γD^3" component had the effect of decreasing α values in eight of the nine cell lines in a comparison of modified linear quadratic versus linear quadratic modeling. In four of the cell lines, the β component took on a negative value when "γD^3" was added to the linear quadratic formula. What this could mean in the context of the proposed dual radiation action-based mechanism of linear quadratic formalism is unclear; radiation exposure would certainly not induce the annealing of intertrack DNA breaks. Figures 2.2 through 2.10 display the results of fitting for the four survival curve models in each of the eight canine cancer cell lines and one normal canine endothelial cell line. Goodness of fit can be compared visually and on the basis of the chi-squared divided by degrees of freedom (χ^2/DoF) values, which are summarized in Tables 2.1 through 2.4. Larger chi-squared values represent greater discrepancy between observed data and modeled fit, and dividing chi-squared by the degrees of freedom produces a relative measure of

goodness of fit where values much larger than one indicate that the model does not appropriately fit the data. How well each model fit data varied widely among the nine different cell lines.

Hypoxia Subsequent to Irradiation

In addition to experiments evaluating clonogenic survival under normoxic conditions, the impact of hypoxia subsequent to irradiation was studied in terms of dose-dependent cell survival. Abrams osteosarcoma cells were cultured under normal, well-oxygenated conditions and irradiated before being placed in a C-Chamber hypoxia chamber (BioSpherix, Salem, North Carolina, USA) fed by oxygen and carbon dioxide levels controlled by ProOx 110 and ProCO2 electronic gas regulators (BioSpherix, Salem, North Carolina, USA). Different irradiate cultures were treated with different severities of hypoxia for durations of two to twenty four hours before being returned to normoxic incubation conditions. To test the most severe conditions of anoxia, the hypoxia chamber was set to its lowest limit of 0.1% O_2 and a GasPak^{TM} EZ anaerobe container sachet, which included an indicator strip that changed color in the presence of oxygen (BD Biosciences, San Jose, California, USA). Any remaining oxygen in the hypoxia chamber was absorbed by the inorganic carbonate, activated carbon, ascorbic acid and other components of the GasPak^{TM} throughout the duration of time in which the hypoxia chamber was sealed. The seal the hypoxia chamber door was reinforced by stretching Parafilm (Bemis Company Inc., Oshkosh, Wisconsin, USA) over the hypoxia chamber door.

DISCUSSION

In this study, two canine osteosarcoma cell lines were used: Abrams and D17. Osteosarcoma is the most commonly occurring primary bone cancer in dogs.[6,16] In terms of radiocurability, canine osteosarcoma is viewed as a radioresistant type of tumor and attempts

treating primary osteosarcoma using fractionated radiation therapy are typically conducted to palliate disease. In accordance with known clinical radioresistance, both the Abrams and D17 canine osteosarcoma cell lines produced survival curves among the group that had higher surviving fractions of cells in this study (data shown in black and red in Figure 2.1). In a previous study by Fitzpatrick *et al.*, the D17 osteosarcoma line was irradiated with doses up to 9 Gy to determine a surviving fraction at 2 Gy (SF_2) of 0.63 ± 0.3 with an α value of 0.08 and a β value of 0.08, producing an α/β ratio of 1.0.[17] Fitzpatrick *et al.* conducted additional experiments in three other canine osteosarcoma cell lines named POS, HMPOS, and COS31, which behaved differently from D17 by having SF_2 values between 0.60 and 0.64, α values at 0.16 Gy^{-1} for each line, β values between 0.03 and 0.05 Gy^{-2}, and α/β ratios between 3.5 and 5.6 Gy.[17] In our study, the SF_2 for Abrams osteosarcoma cells was measured directly as 0.666 ± 0.068 and SF_2 for D17 cells was measured as 0.807 ± 0.093 (see Table 2.5). Linear quadratic modeling of Abrams and D17 survival data in the range from 2 to 15 Gy produced α values of 0.135 ± 0.026 Gy^{-1} and 0.034 ± 0.019 Gy^{-1} and β values of 0.016 ± 0.004 Gy^{-2} and 0.023 ± 0.003 Gy^{-2}, respectively. The calculated α/β ratio for Abrams osteosarcoma cells was 8.4 Gy, which suggests along with other parameters measured or calculated in Abrams cells that the Abrams line behaves more similarly to the aforementioned POS, HMPOS, and COS31 osteosarcoma cell lines than to D17 cells. Our values obtained for D17 cells, such as the α/β ratio of 1.5 Gy, were similar to published results. A more recent report by Maeda *et al.* irradiated the same canine cell lines as used in our study (i.e. obtained from the same source) with 1 to 5 Gy and determined that SF_2 values for Abrams and D17 osteosarcoma cells were 0.65 and 0.70, respectively.[18] The differences between reported values and values obtained in this study were small and possibly due to variation in cellular behavior modifications following different numbers of subculture events.

A greater difference was seen when comparing our results in Abrams and D17 cell lines to SF_2 and α/β parameters of canine osteosarcoma cells from primary culture. Harris derived primary cultures from nine different canine osteosarcoma cases and found a moderate degree of variability in SF_2 (which ranged from 0.425 to 0.839) and α/β ratios (1.9 to 14.6 Gy).[19] SF_2 values are known to depend on whether cells are from an established cell line or from primary culture and on the chosen assay method used to determine survival (colony formation, soft agar assay, population growth assay, etc.).[20] Inherent individual variability may also explain the variability seen from primary canine osteosarcoma cultures in contrast with the relatively consistent values from D17 and Abrams cell lines reported here and in the literature. The concept that individuals differ in their response to radiation is the underlying principle driving the study of *in vitro* radiosensitivity.[1,2,20] The inherent radiosensitivities of human osteosarcoma cell lines have been studied and analyzed using the linear quadratic equation and the single-high multitarget model that predated it.[21,22] When applying the single-high multitarget model to our results using canine osteosarcoma cell lines (Table 2.2) D_0 values of 3.14 ± 0.37 and 2.90 ± 0.33 Gy and n values of 1.66 ± 0.31 and 2.96 ± 0.65 were generated for Abrams and D17 cells, respectively. A human osteosarcoma cell line called TX-4 was irradiated at doses up to 9 Gy to result in a D_0 value of 1.4 Gy and n of 1.9 in experiments with very low plating efficiencies (between 3 and 12%).[21] Human osteosarcoma cell lines called SaOS-2 and U2OS-2 were treated with doses up to 6 Gy to establish D_0 values of 1.46 and 1.42, respectively.[22] Overall, it seems that the parameters of canine osteosarcoma cell lines established in this study are more similar to parameters found from primary canine osteosarcoma cell culture than to human osteosarcoma cell lines, although no study from the literature managed to obtain data in osteosarcoma cells (neither human nor canine, established line nor primary) in the high-dose region above 10 Gy.

Our data show a steep decrease in survival of Abrams and D17 osteosarcoma cells that starts around 12 Gy and is consistently lower with respect to surviving fraction values than predicted by linear quadratic, single-hit multitarget, and Kavanagh-Newman models. Several reports in the literature claim that linear quadratic modeling overestimates cell killing in the high dose region,[21,22] which conflicts with our results shown in Figures 2.2 and 2.3. However, it has been noted from a clinical perspective that treatment outcomes using single fraction or hypofractionated, high dose SRT seem to outperform expectations based on linear quadratic formalism,[23] and increased cell killing relative to the predictions of the model is highly congruent with our results in canine osteosarcoma and other canine cell lines (visualized in Figures 2.2, 2.3, 2.5, 2.6, 2.9, and 2.10). The linear quadratic model provided a superior fit of Abrams and D17 cell data relative to the single-hit multitarget model or the Kavanagh-Newman model (which incorporates components of both linear quadratic and single-hit multitarget expressions). However, fitting of these models at doses between 12 and 15 Gy was poor (Figures 2.2 and 2.3). Data in the low dose range of these survival curves seemed to be preferentially weighted in the fitting process; adjusting the range of data fitted by non-linear regression using the linear quadratic formula to a exclude doses lower than 4 to 6 Gy similarly displayed heavy preference for fitting data at the initial region of the curve at the expense of fitting data at the far right of the curve. The only model that was able to fit data in the high dose region of the survival curve was the hypothetical, modified linear quadratic model. The additional bending capabilities achieved by using a "γD^3" parameter allowed this model to reach data at very low surviving fractions (on the order of 10^{-3} to 10^{-5}), resulting in a slight overestimation of cell kill in Abrams and a very close fit to data in D17 osteosarcoma cells (refer to the pink lines in Figures 2.2 and 2.3). While the applicability of linear quadratic formalism to

traditional, fractionated radiation therapy is undisputed, our data suggest that the linear quadratic model does not always apply to cell survival at high doses, and that modifications of the model can help to improve fitting. The biologic interpretation of added components to the linear quadratic expression has not been explored. It is rational to assume that the more variables an expression contains, the better it will be able to fit data. It is possible that by virtue of being a three-variable model, our hypothetical "γD^3" model outperformed the two-variable models used in this study. It is also possible that the linear quadratic model and its derivations lack an additional biologic component that does not come into play in low dose irradiation.

Song *et al.* has suggested that the missing biologic components leading to increased cell killing at high doses are "indirect" cell killing following endothelial cell apoptosis and tumor vascular damage.[24] Given the importance placed on the behavior of irradiated endothelial cells in the rationale for conducting this study, the dose-dependent survival response of the canine hemangiosarcoma cell line, called Dennys, was of particular interest. It is important to note, however, that this study used the standard clonogenic assay to quantify retention of clonogenic capacity following radiation exposure and did not address the mechanism of cell death in cells that failed to form colonies. Hemangiosarcoma is a malignancy of endothelial cells and usually affects the spleen, but can also be present in the right atrium of the heart, the skin and subcutaneous tissues, the liver, lungs, kidneys, oral cavity, muscle, bone, urinary bladder, and peritoneum in dogs.[16] Canine hemangiosarcoma is highly metastatic and a vast majority of clinical cases possess diffuse or systemic metastatic disease at the time of presentation, meaning that if surgery or radiation therapy are used the intent is primarily palliation.[16,25] In limited reports of such palliative efforts, fractionated radiation therapy has achieved good short-term results.[25] The Dennys canine hemangiosarcoma cell line was among the Abrams and D17

osteosarcoma cell lines with respect to relative radioresistance (data represented in green in Figure 2.1). However, while Abrams and D17 surviving fractions decreased sharply above 12 Gy, the shape of the survival curve for Dennys cells was shallower in the high dose region and allowed for accurate fitting using the linear quadratic model. In this region of the Dennys survival curve, single-hit multitarget modeling and Kavanagh-Newman equation fitting slightly underestimated cell killing and fitting with the modified "γD^3" linear quadratic equation slightly overestimated cell killing (Figure 2.4). The SF_2 of Dennys hemangiosarcoma cells was measured as 0.659 ± 0.071 and linear quadratic fitting produced an α/β ratio of 11.9 Gy from an α value of 0.167 ± 0.011 Gy^{-1} and a β value of 0.014 ± 0.002 Gy^{-2} (Table 2.1). Parameters derived from single-hit multitarget, Kavanagh-Newman, and modified linear quadratic modeling are summarized in Tables 2.2, 2.3, and 2.4. Classically, tumor tissues are thought to have high α/β ratios around 10 Gy, similarly to acutely responding normal tissues. Dennys hemangiosarcoma complies with this principle and should be expected to respond well to fractionated radiation therapy. However, little data is available to correlate *in vitro* parameters with clinical outcomes due to the metastatic nature of canine hemangiosarcoma and the fact that a vast majority of cases opt for systemic chemotherapy rather than radiation therapy.[25]

In contrast with hemangiosarcomas, radiation therapy is an option for curative intent treatment of canine soft tissue sarcomas.[26] A diverse collection of mesenchymal tumors that share similar biologic behaviors fall under the category of soft tissue sarcoma, including fibrosarcomas, neurofibrosarcomas, malignant fibrous hisiocytomas, hemangiopericytomas, myxosarcomas, and liposarcomas.[26] While soft tissue sarcomas are considered resistant to traditional fractionated radiation therapy (i.e. 2 Gy per day) with relatively low cumulative doses (40-48 Gy), modest dose escalation to 3 Gy per fraction delivered every other day to a total of 63

Gy was shown to improve tumor response.[27] The STSA-1 canine soft tissue sarcoma cell line used in our study produced a survival curve that fell into place among the relatively radiosensitive cell lines (note the data shown in royal blue in Figure 2.1). Survival data at 15 Gy was the most difficult of all dose levels to obtain and was not successfully collected in several cell lines, but among the surviving fractions measured at 15 Gy, STSA-1 produced the lowest values. The SF_2 of STSA-1 (0.319 ± 0.042) was also the lowest in terms of survival relative to any other cell line (Table 2.5). The quality of these data may be called into question, as plating efficiencies for STSA-1 cells were consistently low, falling between 12.0 and 34.2% in all experiments. As with both canine osteosarcoma cell lines, the three established survival curve models (linear quadratic, single-hit multitarget, and Kavanagh-Newman) failed to bend sufficiently to reach surviving fraction data in the high dose region. Fitting the modified "γD^3" linear quadratic equation to STSA-1 data had a similar effect as in Abrams osteosarcoma cells: the "γD^3" equation fit with a greater degree of bending but overestimated cell killing at 12, 13, and 14 Gy. The survival curve parameters following the single-hit multitarget model using seven different human soft tissue sarcoma cell lines have been reported, with D_0 values between 0.91 and 1.52 Gy (mean D_0 was 1.20 Gy) and n values between 1.33 and 4.95 (mean n was 3.57).[28] Irradiation of the human soft tissue sarcoma cell lines resulted in SF_2 values between 0.24 and 0.53 with a mean of 0.39 with similarly low plating efficiencies (1.2 to 24.8%)[28] as measured in the STSA-1 cell line. Overall, with a calculated D_0 value of 1.977 ± 0.045 Gy and n of 0.849 ± 0.029 (Table 2.2) the STSA-1 canine soft tissue sarcoma cell line produced survival data that seemed to be within the limits of normal variability across tumors when compared to parameters reported in the literature for human soft tissue sarcoma cell lines. Given the fact that

soft tissue sarcomas encompass multiple histologically distinct tumor types in both human and dogs, the similarities seen in cell line characteristics are remarkable.

In addition to the cell lines derived from canine sarcomas discussed above, three varieties of canine carcinoma cell lines were studied. CMT-12 canine mammary carcinoma, CTAC thyroid carcinoma, and K9TCC transitional cell carcinoma lines were irradiated in an effort to understand cellular survival response in the high dose region. In veterinary medicine, mammary carcinomas in dogs are almost universally treated with surgery,[16] but are informally recognized as generally radioresponsive tumor types. Our data showed that CMT-12 mammary carcinoma cells were among the more radioresistant types of cancer cells (data in turquoise in Figure 2.1), with the largest SF_2 (0.874 ± 0.040, see Table 2.5) of all nine cell lines studied herein. Linear quadratic fitting of CMT-12 cells failed to describe data in the high dose region, underestimating cell kill at 14 and 15 Gy (Figure 2.6). All other models behaved similarly to the linear quadratic model in this respect, with the single-hit multitarget model providing the poorest fit and the most drastic underestimation of cell killing. While the CMT-12 cell line responded similarly to the Abrams and D17 osteosarcoma cell lines in most respects, they differed in that the "γD_3" linear quadratic equation failed to bend sufficiently to describe high dose data from the CMT-12 cell line (Figure 2.6). In comparison to human breast cancer cell lines fitted using the single-hit multitarget model, our CMT-12 cells were considerably more radioresistant. In a study evaluating eight human breast cancer cell lines, the mean SF_2 was 0.30 (ranging from 0.23 to 0.54), mean D_0 was 1.15 Gy (range of 0.83 to 1.69 Gy), and mean n 5.02 (range of 1.6 to 14.2).[28] The CMT-12 canine "breast cancer" cell line resulted in a D_0 value of 2.94 ± 022 Gy, which is higher in terms of mean lethal dose than any of the eight previously studied human breast cancer cell lines. As mentioned previously, single-hit multitarget modeling failed to describe high dose

data from CMT-12 cells, so comparisons of D_0 values may not be appropriate; however, the fact that CMT-12 cells had a much higher SF_2 value than human breast cancer cell lines is not affected by modeling and suggests on its own merit that this canine mammary carcinoma cell line is more radioresistant than typical human mammary carcinoma cells.

As with mammary carcinoma, canine thyroid carcinoma is usually treated surgically. However, limited reports have described effective local control of canine thyroid carcinoma achieved using external beam radiation therapy to total doses of 48 Gy delivered in coarse fractions of 4 Gy on an alternate-day schedule.[29,30] Our *in vitro* studies using the CTAC canine thyroid carcinoma cell line are in accordance with the concept of general radiosensitivity of malignant thyroid cells (Figure 2.1). The SF_2 measured in CTAC cells was 0.657 ± 0.029 (Table 2.5), and the SF_4, which is more relevant to reports of clinical outcomes using 4 Gy per fraction,[29] was 0.262 ± 0.048. In comparison to four different human thyroid carcinoma cell lines, which had SF_2 values ranging from 0.23 to 0.51 and α/β ratios of 15.4, 15.6, 16.6 Gy, and one line at 4.8 Gy,[31] the canine CTAC cells were more radioresistant at lower doses and resulted in an α/β ratio of 2.4 Gy (Table 2.1). Experiments in the four human cell lines were conducted up to 8 Gy, so no comparison between human and canine thyroid carcinoma cell lines may be achieved for the high dose region. Also, experiments in human cell lines reported using a "high" dose rate cobalt-60 source to irradiate thyroid carcinoma cells, but what they considered high at 45.9 cGy per hour was much lower than dose rates produced by the Varian Trilogy® linear accelerator used in this study (approximately 600 cGy per minute). Dose rate effects may play a role in the observed differences in cellular responses between cell lines. In the CTAC cell line, the linear quadratic model was superior to other models in fitting data from the CTAC cell line; single-hit multitarget and Kavanagh-Newman modeling underestimated cell kill and the

modified linear quadratic model with an added "γD^3" parameter overestimated cell kill in CTAC cells (Figure 2.7).

Transitional cell carcinoma of the urinary bladder is typically treated in dogs using a multimodal approach that can include fractionated, external beam radiotherapy, but the risk of late effects to pelvic organs such as the colon, rectum, ureters, and other sensitive structures limit both fraction size and volume of tissue that can be safely treated.[32] A previous study of the intrinsic radiosensitivity of canine transitional cell carcinoma cells determined that observed cellular radioresistance was in line with relatively poor clinical response.[33] Three canine bladder cancer cell lines, named K9-TCC-PU-Sh, K9-TCC-PU-Mx, and K9-TCC-PU-Nk, were determined to have SF_2 values of 0.63, 0.63, and 0.56, respectively.[33] The K9TCC cell line used in our experiments had a SF_2 value of 0.819 ± 0.074, which was more radioresistant than previously studied cell lines. Previously studied canine transitional cell carcinoma cell lines had α/β ratios of 3.14, 4.0, and 2.67 Gy, which were all much higher than the α/β ratio determined in this study of 0.6 Gy. A single data point in the high dose region of our K9TCC survival curve may be responsible for differences in linear quadratic modeling of our data versus published data. Obtaining survival data from K9TCC cells was extremely difficult; cells in logarithmic growth tended to form aggregates and had very low plating efficiencies (usually 18.3 to 24.3%). A single data point measured at 13 Gy appeared to be an outlier relative to surviving fraction data generated for 12 Gy and lower (Figure 2.8), but the plating efficiency of the experiment in which the 13 Gy data was collected was abnormally good (68.2%). Despite numerous attempts, no additional data at 14 or 15 Gy was able to be collected, so the status of the unusual 13 Gy data point remains questionable. Excluding this point, the remainder of these data were described well by both linear quadratic and Kavanagh-Newman survival curves. Single-hit multitarget

modeling underestimated cell killing around 12 Gy very slightly and modified "γD^3" linear quadratic survival overestimated cell killing at 12 Gy, although it showed the most promise with respect to modeling the 13 Gy data.

The final canine cancer cell line used in this study was the C2 mast cell tumor line. Canine mast cell tumors are the most common cutaneous tumors in dogs and are known to be highly responsive to radiation therapy.[30, 34-36] Our data indicate that C2 mast cell tumor cells are indeed highly sensitive to radiation; the surviving fractions at 6, 8, and 10 Gy were the lowest of any cell line studied here. The SF_2 of C2 cells (0.421 ± 0.078, shown in Table 2.5) was only surpassed by STSA-1 canine soft tissue sarcoma cells in radiosensitivity. In the low dose range, C2 cells were somewhat well described by all models, with divergence from predicted surviving fractions beginning above 6 Gy (Figure 2.9). In the high dose region, linear quadratic, single-hit multitarget, and Kavanagh-Newman models underestimated cell killing. The modified "γD^3" linear quadratic model failed to fit a majority of these data in dramatic fashion. The α/β ratio for C2 cells was calculated to be 35.3 Gy (Table 2.1). It has been shown that C2 canine mast cell tumor cells undergo dose-dependent apoptotic cell death upon irradiation,[37] thus behaving similarly to lymphocytes and possibly to endothelial cells. While apoptotic cell death is not an outcome directly evaluated in clonogenic survival assays, it is well established that some cells preferentially apoptose as opposed to undergoing mitotic cell death, and that inherent radiosensitivity is affected by such predispositions.

Due to the suggested role of endothelial cell apoptosis in tumor control achieved in SRT, a canine endothelial cell line called CnAOEC was also evaluated for dose-dependent survival using the standard clonogenic assay. CnAOEC, a cell line developed from canine endothelial cells of aortic origin, was the only non-neoplastic cell line used in this study, and the cell line

displayed limited tolerance for subculture and low plating efficiency (13.6%) as to be expected from a "normal" cell line. CnAOEC cells were among the more radiosensitive cells studied (SF_2 was 0.467 ± 0.089, see Table 2.5 and Figure 2.1), and while data above 12 Gy was not obtained in this cell line, fitting of all models began to underestimate cell killing at 8, 10 and 12 Gy (Figure 2.10). The four survival models used in this study produced very similar survival curves with no obviously superior model for fitting canine endothelial cells (note the similarity in red, blue, green, and pink lines in Figure 2.10). The linear quadratic model produced an α of 0.376 ± 0.042 Gy^{-1} and a β of 0.007 ± 0.010 Gy^{-2}, resulting in an extremely large α/β ratio of 52.6 Gy (Table 2.1). Single-hit multitarget model fitting of CnAOEC cells produced a D_0 value of 2.22 ± 0.24 Gy and n of 1.19 ± 0.20 (Table 2.2).

Previous studies have attempted to quantify inherent radiosensitivity of endothelial cells in several species in efforts to understand the role of endothelium in late normal tissue damage. A study in conduced 1984 used cultured rabbit aortic endothelial cells to measure a D_0 of 120 rad (1.20 Gy) and n of 7 from survival data collected between 0 and 8 Gy.[38] Plating efficiencies of this study were reported as being between 40 and 60%,[38] which seems suspiciously high relative to CnAOEC. Another early study used pig endothelial cells derived from the aorta and vessels in white matter of the brain to determine D_0 of 1.57 ± 0.05 Gy and n of 1.21 ± 0.09 and D_0 of 1.47 ± 0.12 Gy and n of 1.74 ± 0.35, respectively.[39] Bovine aortic endothelial cells were used in a 1986 study to determine a D_0 of 101 rad (1.01 Gy) and n of 1.9, with more reasonable reported plating efficiencies of 11%.[40] Additional studies using bovine aortic endothelial cells calculated D_0 values of 1.07 ± 0.07 and 1.12 ± 0.01, noting that the culture conditions such as feeder layers or mimetics of extracellular matrix components can impact the outcome of survival curve parameters.[41,42] Human umbilical vein endothelial cells were evaluated for dose-dependent

survival with plating efficiencies between 15 and 20%, producing a D_0 value of 1.65 Gy and n of 2.2.[43] It was later determined that the tissue from which endothelial cells were derived can have an effect on resulting radiation sensitivity measurements.44 For example, endothelial cells extracted from human skin were significantly more radiosensitive than endothelial cells derived from human hepatic sinusoidal tissue, with endothelial cells harvested from brain, ovarian, pulmonary, and umbilical vein tissues having survival characteristics in between.44 While our CnAOEC cells produced a D_0 value slightly higher than values reported in the literature for rabbit, bovine, and human endothelium, it is important to note that multiple factors contribute to survival curve parameters, including cell type, culture conditions, dose rate, and species and tissue origin of cells, which may explain variability of results.

Having obtained SF_2 and SF_8 values experimentally in eight canine cancer cell lines and one normal canine cell line, the rank order of cell lines from most radiosensitive to most radioresistant was visualized in Figure 2.11. Rank was conserved with a few minor changes when comparing SF_2 to SF_8 (e.g. radiosensitive STSA-1 cells were ranked first in terms of SF_2 and second in SF_8, similarly radiosensitive C2 cells were second in SF_2 and first in SF_8, and radioresistant CMT-12 cells were ranked last in both dose groups). In SRT, doses larger than 8 Gy are typically used and effects following a single fraction of 24 Gy were of interest in this study. To calculate surviving fraction at 24 Gy (SF_{24}), two methods were used. First, given that three fractions of 8 Gy would total 24 Gy, the SF_8 values for each cell line were cubed to calculate SF_{24}. Alternatively, the high-dose data from each cell line was used to extrapolate data up to 24 Gy in a linear fashion, which was decided to be the most conservative estimation method (an example is shown in Figure 2.12). Resulting values are presented in Table 2.5. The two methods of calculating SF_{24} produced wildly different results (Table 2.5). The more

conservative method of estimation (extrapolated SF_{24}) resulted in the smallest surviving fraction values, often several orders of magnitude smaller than corresponding $(SF_8)^3$ values. When rank order of each cell line for SF_2 and SF_8 were compared to extrapolated SF_{24} rank order, it was found that the most radiosensitive cell lines at low doses were the most radioresistant at high doses and the most radioresistant cell lines at low doses had the smallest surviving fractions at 24 Gy (Figure 2.11). At some point the cellular response to radiation must change with increasing doses; clearly the cell survival curves do not change with increasing dose in proportion to each other. We propose that some alternative biologic response mechanism is triggered at very high doses of radiation. Furthermore, since predicted SF_{24} values based on high-dose data were much smaller in terms of survival than would be expected based on predictions from low dose data (i.e. SF_8) the use of very high doses may improve the efficacy of cell killing to a greater extent than previously expected.

In accordance with observations of post-irradiation transient perfusion deficits in animal models,[45] and with preliminary data measuring a decrease in partial pressure of oxygen two hours after treatment of a canine soft tissue sarcoma with a single fraction of 20 Gy (discussed further in Chapter 3), we hypothesized that decreases in tumor oxygenation following single fraction high dose radiation therapy may contribute to increased tumor cell killing. Using a hypoxia chamber, irradiated Abrams osteosarcoma cells were exposed to 1% oxygen for two hours and 0.1% oxygen for durations of thirty minutes, two hours, twenty four hours, and seventy two hours to mimic severe perfusion and oxygenation deficits. It is important to note that cells were not hypoxic during exposure to radiation, but only subsequent to irradiation, since the survival of cells in hypoxia during radiation treatment is well established in the literature.[46-48] Although studies began with the most severe of hypoxic conditions, cell survival results failed to

differentiate from control irradiated Abrams cells that were not exposed to subsequent hypoxia (Figure 2.13). Additional experiments testing a post-irradiation treatment under anoxic conditions for twenty four hours also failed to produce measureable differences from control cells in terms of cell survival (Figure 2.13). It was determined that the contribution of hypoxia subsequent to irradiation, which may occur *in vivo* following vascular damage induced by single fraction high dose radiation treatment, to tumor cell kill could not be evaluated effectively in the system described herein due to the fact that the hypoxia chamber used did not generate a hypoxic environment in a timely fashion. The hypoxia chamber system took thirty to forty five minutes to generate hypoxic levels of 0.1 to 0.2% after having opened the door to place cell flasks inside. This latency period of thirty to forty five minutes post-irradiation in which cells had access to oxygen was a tremendous technical difficulty considering DNA damage repair processes are initiated immediately after radiation damage is detected and generally complete the "fast phase" or majority of the DNA repair process, either by non-homologous end joining or by homologous recombination repair, in approximately one hour following radiation exposure.[49,50] If a hypoxia-induction system could be built to generate immediate hypoxic conditions for irradiated cells, the lack of oxygen available to cells during their attempts to repair radiation-induced DNA damage may promote failure of repair and increased cell killing. A large collection of literature has shown that hypoxia causes downregulation in numerous genes that code for proteins involved in non-homologous repair and homologous recombination repair,[51-57] supporting our hypothesis that hypoxia subsequent to irradiation could contribute to tumor cell killing via impaired DNA double strand break repair processes. Future studies utilizing a superior hypoxia chamber system will be better equipped to test our hypothesis.

CONCLUSIONS

While cell survival curves are prominent in the literature, rarely are data collected in the high dose region above 6 to 10 Gy. Low and high dose survival data were obtained in eight canine cancer cell lines and one normal canine endothelial cell line to test the applicability of the linear quadratic model, the single-hit multitarget model, the Kavanagh-Newman universal survival curve, and a modified "γD^3" linear quadratic equation to high dose data. Cell lines divided into two distinct populations in terms of dose-dependent survival (Figure 2.1). Abrams and D17 osteosarcoma, Dennys hemangiosarcoma, CMT-12 mammary carcinoma and K9TCC transitional cell carcinoma cell lines comprised the more radioresistant group and STSA-1 soft tissue sarcoma, CTAC thyroid carcinoma, C2 mast cell tumor, and CnAOEC endothelial cell lines grouped together to show more radiosensitive trends. In the cases of canine osteosarcoma cell lines (both Abrams and D17), only the modified "γD^3" linear quadratic equation was able to approach fitting high dose data. Similarly, linear quadratic, single-hit multitarget, and Kavanagh-Newman equations underestimated cell killing in the STSA-1 soft tissue sarcoma, CMT-12 mammary carcinoma, C2 mast cell tumor, and CnAOEC normal endothelial cell lines at doses above approximately 12 Gy. On the other hand, linear quadratic modeling seemed to be adequate for Dennys hemangiosarcoma, K9TCC transitional cell carcinoma, and CTAC thyroid carcinoma cell lines. Different models provided the best fits to data from different cell lines, with no single model producing uniformly accurate estimation of cell killing.

Surviving fractions in each cell line measured at 2 Gy and at 8 Gy were compared with respect to rank of cell lines from most radiosensitive to most radioresistant. In order to predict cell survival at 24 Gy, a dose of relevance to SRT, two methods were used. First, measured SF_8 values were cubed to calculate equivalent surviving fractions for SF_{24}. Next, the high-dose

region of the survival curve in each cell line was used to extrapolate in the most conservative estimation (i.e. simple exponential extrapolation on a semi-log plot) of cell survival at doses above those that can be determined experimentally. SF_{24} values calculated from $(SF_8)^3$ were markedly higher than SF_{24} values derived from extrapolation of high dose data, indicating that some additional mechanism is contributing to increased cell killing after exposure to very high doses of radiation. This mechanism is occurring within isolated cells, as opposed to in diverse tissue systems containing different types of cells. Since the conservative estimate of SF_{24} from extrapolation of high-dose data was more strongly based on measured values (three to four data points, as opposed to one data point in SF_8) the rank order of all nine cell lines was evaluated using SF_2, SF_8, and extrapolated SF_{24}. Order was maintained with only small changes in rank when comparing measured SF_2 with SF_8, but the rank changed radically between SF_8 and SF_{24}, in which case many cell lines ranked as having the highest surviving fractions at low doses had the lowest surviving fractions at 24 Gy and vice versa. The change in rank order at high doses suggests that radioresistant cells, and possibly their corresponding tumors *in vivo*, may become radiosensitive when treated with very large doses of radiation, bolstering an argument in favor of using SRT in radiation therapy. However, studies *in vitro* must be carefully interpreted as they do not directly translate to biologic behavior *in vivo.* Additional studies are necessary to understand the response of tissues to single fraction, high-dose irradiation.

We hypothesized that single high dose irradiation induces vascular damage *in vivo* and attempted to use canine cancer cell lines *in vitro* to evaluate the effects of hypoxia subsequent to irradiation in an effort to mimic the decreased perfusion and oxygen levels observed in some animal models following exposure to large doses of ionizing radiation. It was concluded that our equipment was inadequate for inducing hypoxia in a manner that reflected perfusion and oxygen

changes *in vivo*. Further studies using methods capable of inducing immediate hypoxia, rather than the thirty to forty five minute delay in generating hypoxic conditions described herein, may be better able to test our hypothesis.

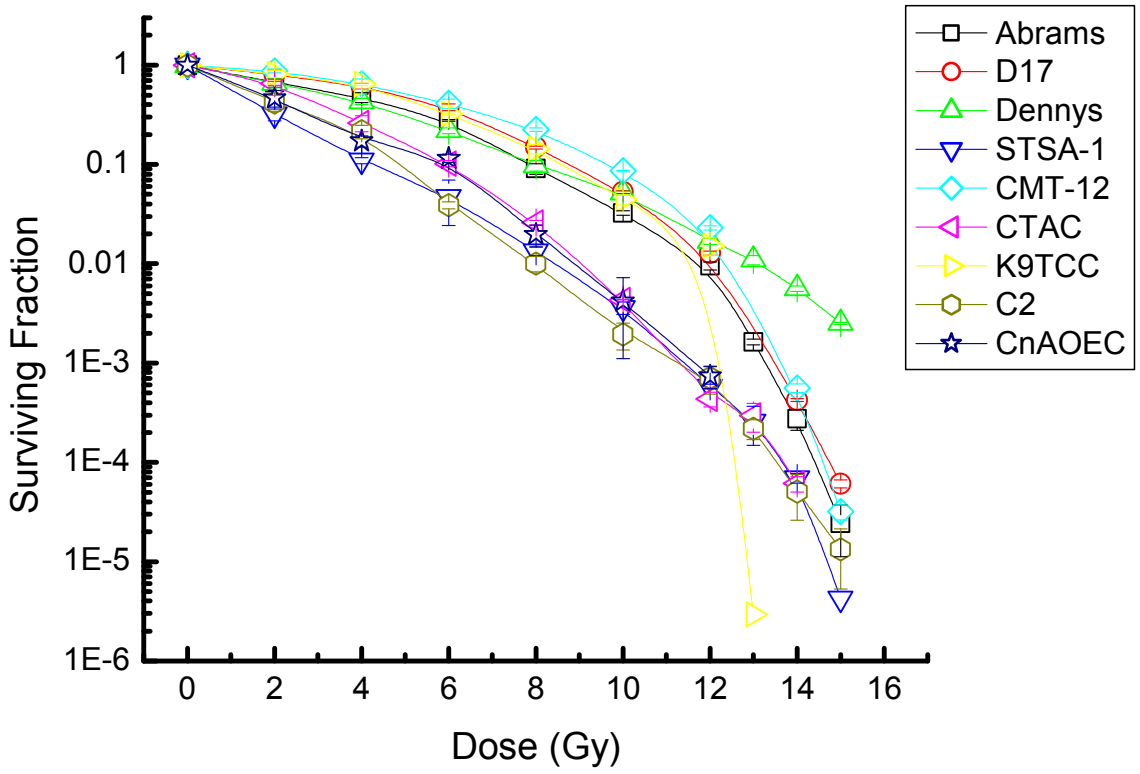

Figure 2.1: Survival of eight canine cancer cell lines and one normal canine endothelial cell line (CnAOEC). Abrams and D17 cells were derived from canine osteosarcomas, Dennys from hemangiosarcoma, STSA-1 from soft tissue sarcoma, CMT-12 from mammary carcinoma, CTAC from thyroid carcinoma, K9TCC from transitional cell carcinoma, and C2 from a mast cell tumor. Each data point represents the mean surviving fraction calculated from colony counting in three separate experiments for each dose. Error bars represent associated standard deviation of the mean. Lines represent general trends and are not fitted models of any kind.

Table 2.1: Parameters of Linear Quadratic modeling in eight canine cancer cell lines and one normal canine endothelial cell line (CnAOEC).

Cell Line	Plating Efficiency (%)	α (Gy^{-1})	β (Gy^{-2})	α/β (Gy)	χ^2/DoF
Abrams	53.0-87.2	0.135±0.026	0.016±0.004	8.4	0.00072
D17	47.1	0.034±0.019	0.023±0.003	1.5	0.00058
Denny	87.0	0.167±0.011	0.014±0.002	11.9	0.00013
STSA-1	12.0-34.2	0.554±0.018	0.002±0.006	277	0.00004
CTAC	47.3-63.8	0.120±0.020	0.049±0.006	2.4	0.00016
CMT-12	46.0-56.4	0.021±0.007	0.021±0.001	1.0	0.00009
K9TCC	18.3-24.3*	0.017±0.024	0.027±0.004	0.6	0.00079
C2	45.1-61.8	0.389±0.040	0.011±0.011	35.3	0.00039
CnAOEC	13.6	0.376±0.041	0.007±0.010	52.6	0.00054

*Plating efficiency of experiments producing one possibly outlying surviving fraction value at 13 Gy was 68.2%

Table 2.2: Parameters of Single-Hit Multitarget modeling in eight canine cancer cell lines and one normal canine endothelial cell line (CnAOEC).

Cell Line	Plating Efficiency (%)	D_0 (Gy)	n	χ^2/DoF
Abrams	53.0-87.2	3.138±0.372	1.663±0.309	0.00143
D17	47.1	2.900±0.336	2.958±0.651	0.00178
Denny	87.0	3.088±0.203	1.599±0.157	0.0004
STSA-1	12.0-34.2	1.977±0.045	0.849±0.029	0.00001
CTAC	47.3-63.8	1.807±0.034	2.661±0.091	0.00002
CMT-12	46.0-56.4	2.935±0.222	3.469±0.531	0.00081
K9TCC	18.3-24.3*	2.641±0.320	3.502±0.858	0.0019
C2	45.1-61.8	2.171±0.253	1.115±0.195	0.0004
CnAOEC	13.6	2.222±0.244	1.190±0.197	0.00041

*Plating efficiency of experiments producing one possibly outlying surviving fraction value at 13 Gy was 68.2%

Table 2.3: Parameters of Kavanagh-Newman Universal Survival Curve (USC) modeling in eight canine cancer cell lines and one normal canine endothelial cell line (CnAOEC).

Cell Line	**Plating Efficiency (%)**	**K_0**	**K_g**	**χ^2/DoF**
Abrams	53.0-87.2	0.279±0.038	0.376±0.142	0.00199
D17	47.1	0.651±0.539	0.054±0.053	0.00098
Denny	87.0	0.275±0.019	0.525±0.126	0.00075
STSA-1	12.0-34.2	0.586±0.027	1.306±0.350	0.0001
CTAC	47.3-63.8	0.485±0.020	0.286±0.020	0.00003
CMT-12	46.0-56.4	0.765±0.387	0.037±0.021	0.0002
K9TCC	18.3-24.3*	1.837±0.077	0.018±0.052	0.00087
C2	45.1-61.8	0.483±0.025	0.767±0.000	0.00199
CnAOEC	13.6	0.420±0.023	1.206±0.417	0.00038

*Plating efficiency of experiments producing one possibly outlying surviving fraction value at 13 Gy was 68.2%

Table 2.4: Parameters determined for a model similar to the Linear Quadratic with an added component, "γD^3," in eight canine cancer cell lines and one normal canine endothelial cell line.

Cell Line	**Plating Efficiency (%)**	**α (Gy^{-1})**	**β (Gy^{-2})**	**γ (Gy^{-3})**	**χ^2/DoF**
Abrams	53.0-87.2	0.261±0.017	-0.040±0.007	0.005±0.001	0.00006
D17	47.1	0.114±0.014	-0.010±0.005	0.003±0.001	0.00007
Denny	87.0	0.188±0.021	0.004±0.008	0.001±0.001	0.00012
STSA-1	12.0-34.2	0.552±0.079	0.001±0.049	0.001±0.007	0.00009
CTAC	47.3-63.8	0.165±0.085	0.019±0.052	0.005±0.007	0.00043
CMT-12	46.0-56.4	0.040±0.010	0.014±0.003	0.001±0.000	0.00005
K9TCC	18.3-24.3*	0.080±0.039	-0.001±0.016	0.003±0.002	0.00052
C2	45.1-61.8	0.687±0.026	-0.178±0.017	0.026±0.002	0.00002
CnAOEC	13.6	0.371±0.090	0.010±0.043	-0.0002±0.004	0.00072

*Plating efficiency of experiments producing one possibly outlying surviving fraction value at 13 Gy was 68.2%

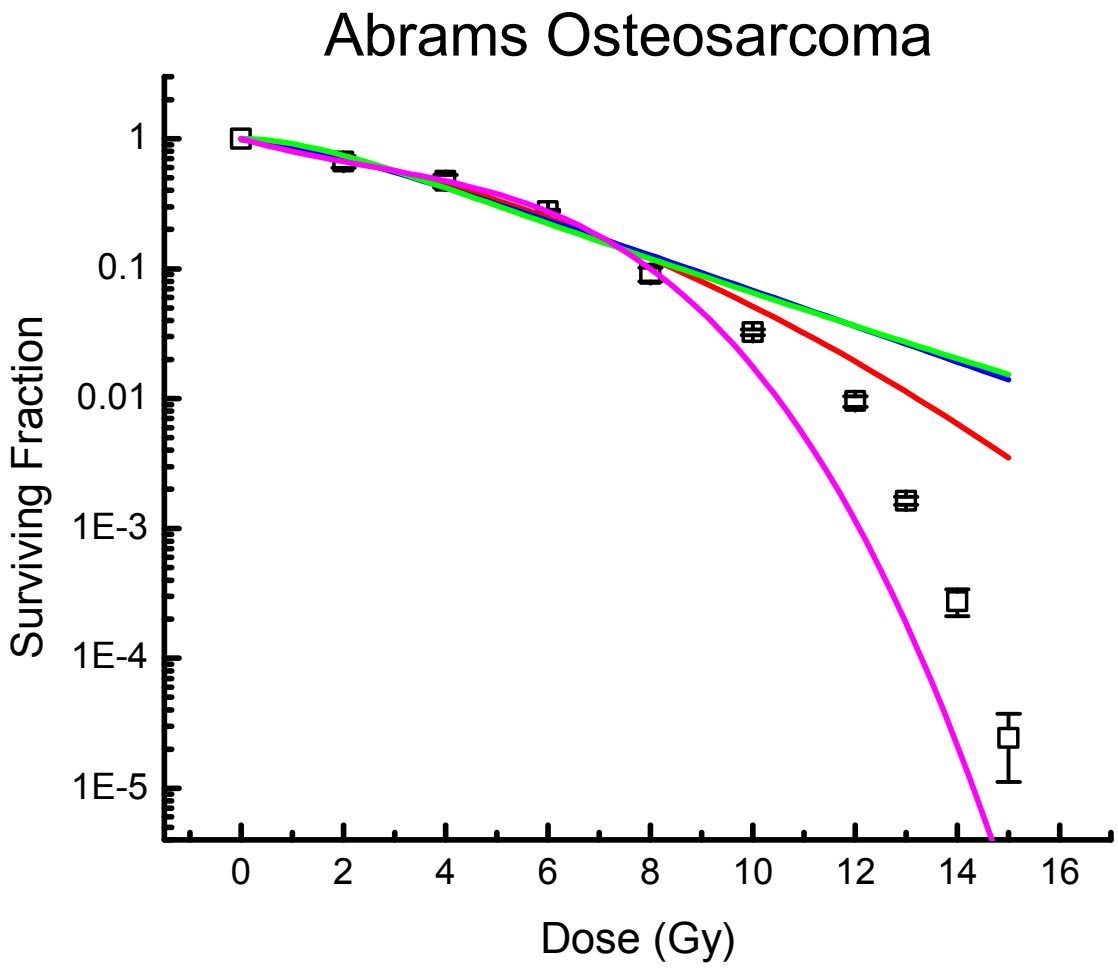

Figure 2: Modeling of dose-dependent survival data from Abrams canine osteosarcoma cells. Data points represent mean values of surviving fractions calculated from colony counts in three separate experiments. Error bars represent one standard deviation of the mean. The red line was generated via non-linear regression analysis using the linear quadratic model. The blue line was generated using the single-hit multitarget model. The green line was produced using the Kavanagh-Newman universal survival curve and the pink line was the result of fitting a modified linear quadratic equation in which survival (S) = $e^{-(\alpha D + \beta D^2 + \gamma D^3)}$.

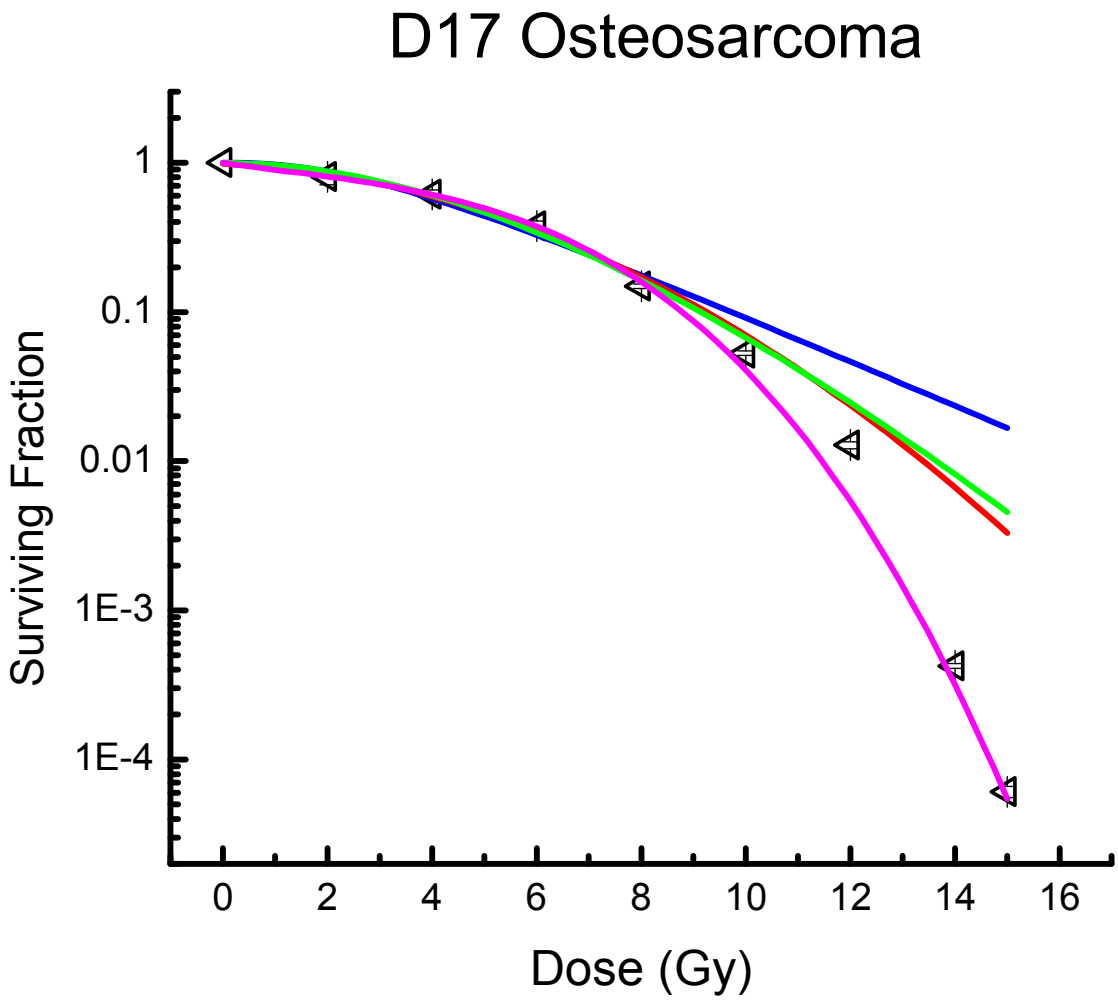

Figure 2.3: Modeling of dose-dependent survival data from D17 canine osteosarcoma cells. Data points represent mean values of surviving fractions calculated from colony counts in three separate experiments. Error bars represent one standard deviation of the mean. The red line was generated via non-linear regression analysis using the linear quadratic model. The blue line was generated using the single-hit multitarget model. The green line was produced using the Kavanagh-Newman universal survival curve and the pink line was the result of fitting a modified linear quadratic equation in which survival (S) = $e^{-(\alpha D + \beta D^2 + \gamma D^3)}$.

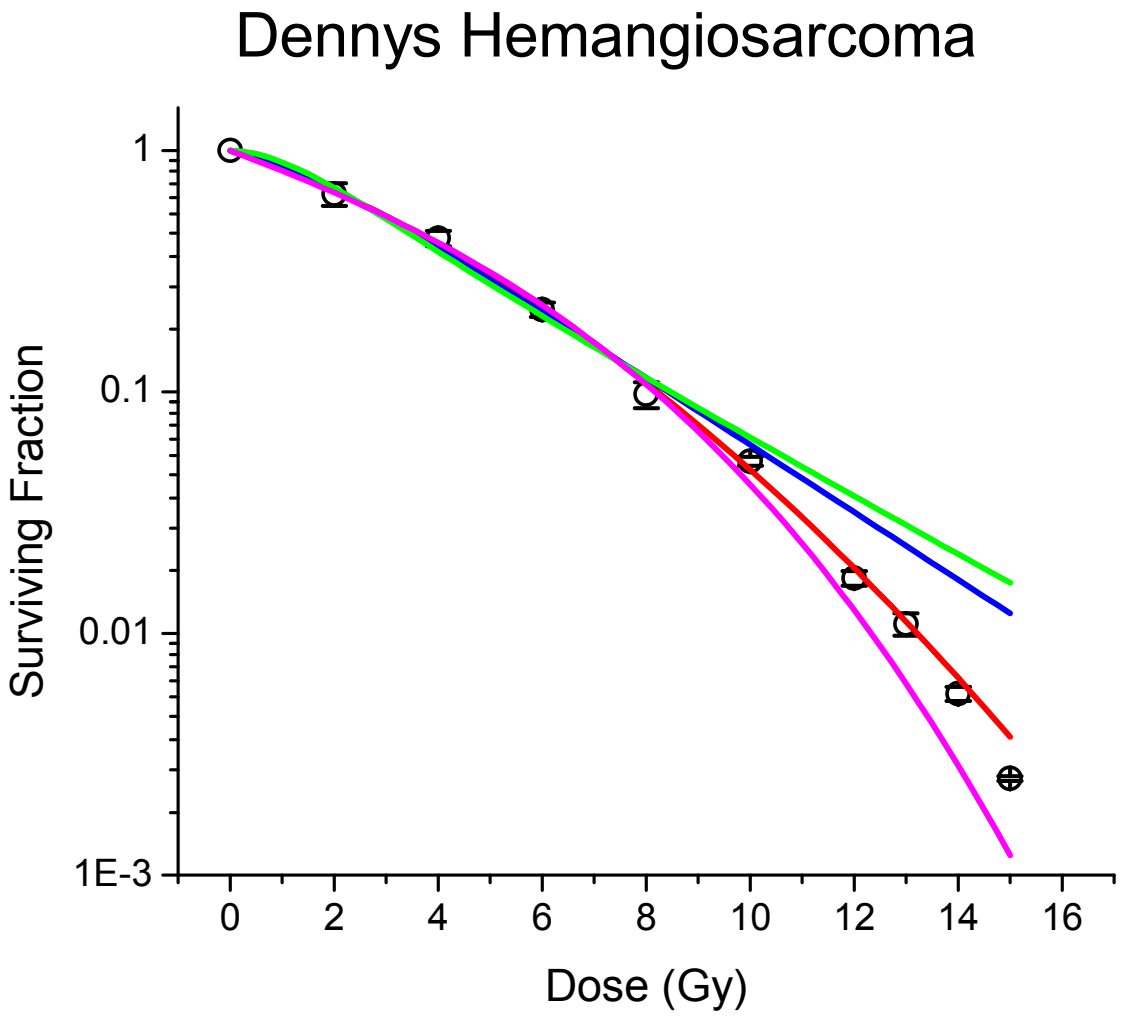

Figure 2.4: Modeling of dose-dependent survival data from Dennys canine hemangiosarcoma cells. Data points represent mean values of surviving fractions calculated from colony counts in three separate experiments. Error bars represent one standard deviation of the mean. The red line was generated via non-linear regression analysis using the linear quadratic model. The blue line was generated using the single-hit multitarget model. The green line was produced using the Kavanagh-Newman universal survival curve and the pink line was the result of fitting a modified linear quadratic equation in which survival (S) = $e^{-(\alpha D + \beta D^2 + \gamma D^3)}$.

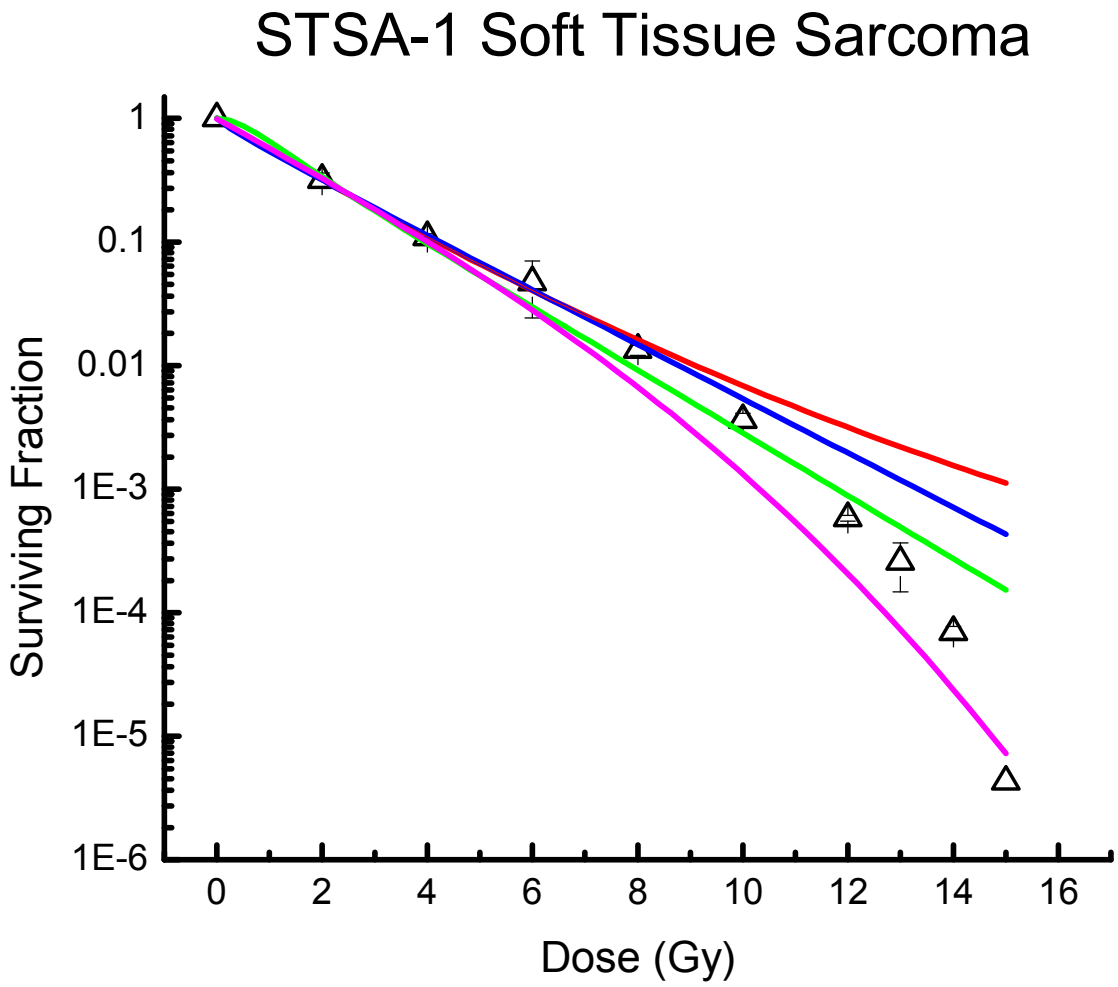

Figure 2.5: Modeling of dose-dependent survival data from STSA-1 canine soft tissue sarcoma cells. Data points represent mean values of surviving fractions calculated from colony counts in three separate experiments. Error bars represent one standard deviation of the mean. The red line was generated via non-linear regression analysis using the linear quadratic model. The blue line was generated using the single-hit multitarget model. The green line was produced using the Kavanagh-Newman universal survival curve and the pink line was the result of fitting a modified linear quadratic equation in which survival (S) = $e^{-(\alpha D + \beta D^2 + \gamma D^3)}$.

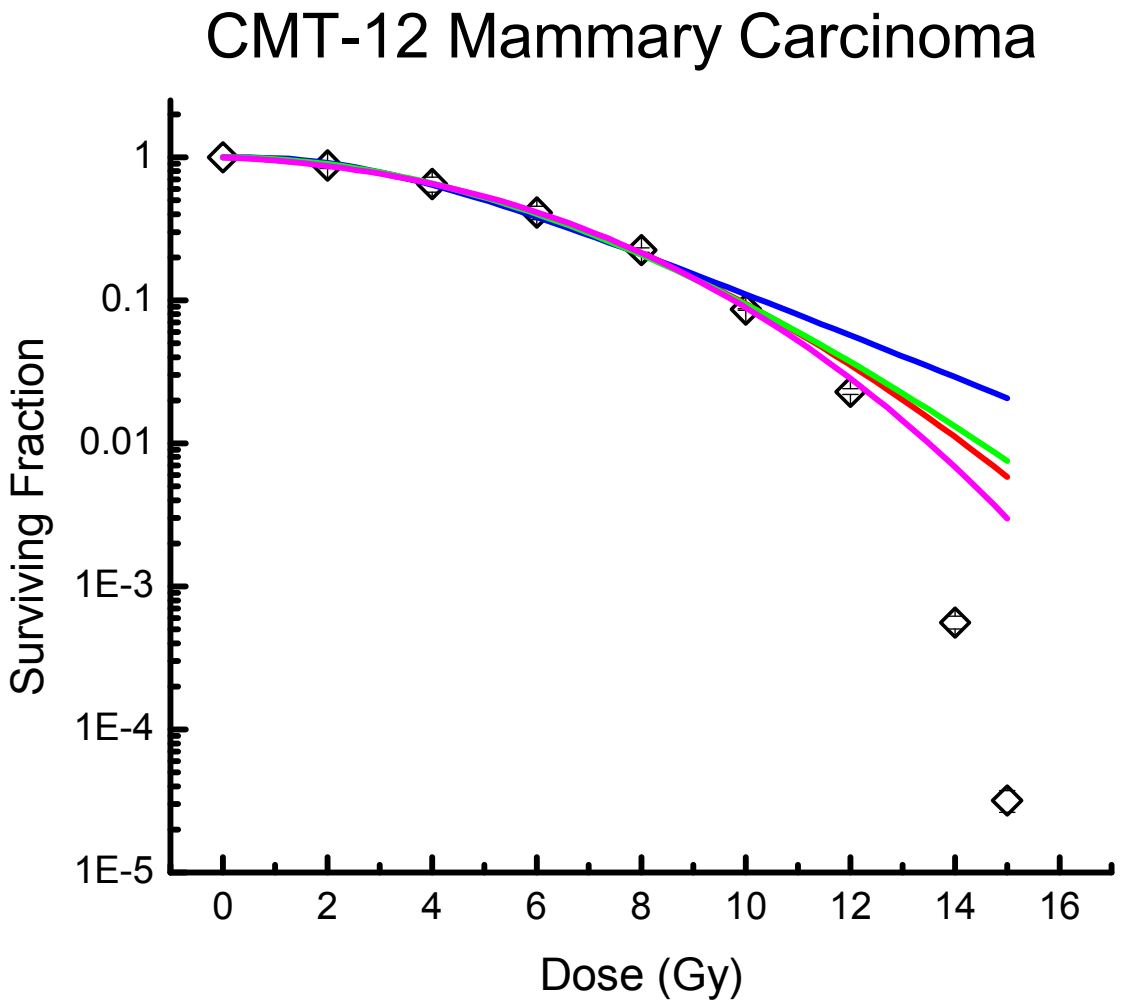

Figure 2.6: Modeling of dose-dependent survival data from CMT-12 canine mammary carcinoma cells. Data points represent mean values of surviving fractions calculated from colony counts in three separate experiments. Error bars represent one standard deviation of the mean. The red line was generated via non-linear regression analysis using the linear quadratic model. The blue line was generated using the single-hit multitarget model. The green line was produced using the Kavanagh-Newman universal survival curve and the pink line was the result of fitting a modified linear quadratic equation in which survival (S) = $e^{-(\alpha D + \beta D^2 + \gamma D^3)}$.

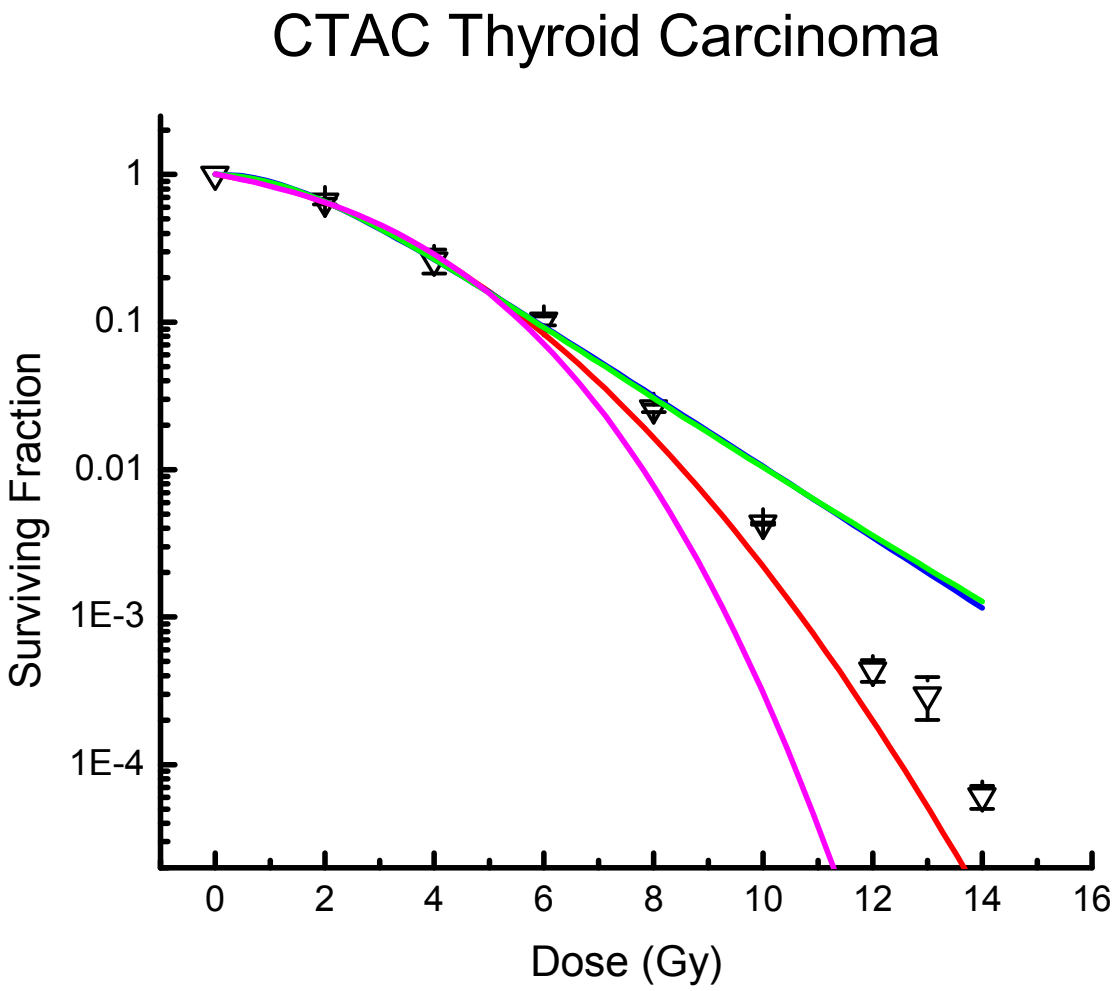

Figure 2.7: Modeling of dose-dependent survival data from CTAC canine thyroid carcinoma cells. Data points represent mean values of surviving fractions calculated from colony counts in three separate experiments. Error bars represent one standard deviation of the mean. The red line was generated via non-linear regression analysis using the linear quadratic model. The blue line was generated using the single-hit multitarget model. The green line was produced using the Kavanagh-Newman universal survival curve and the pink line was the result of fitting a modified linear quadratic equation in which survival (S) = $e^{-(\alpha D + \beta D^2 + \gamma D^3)}$.

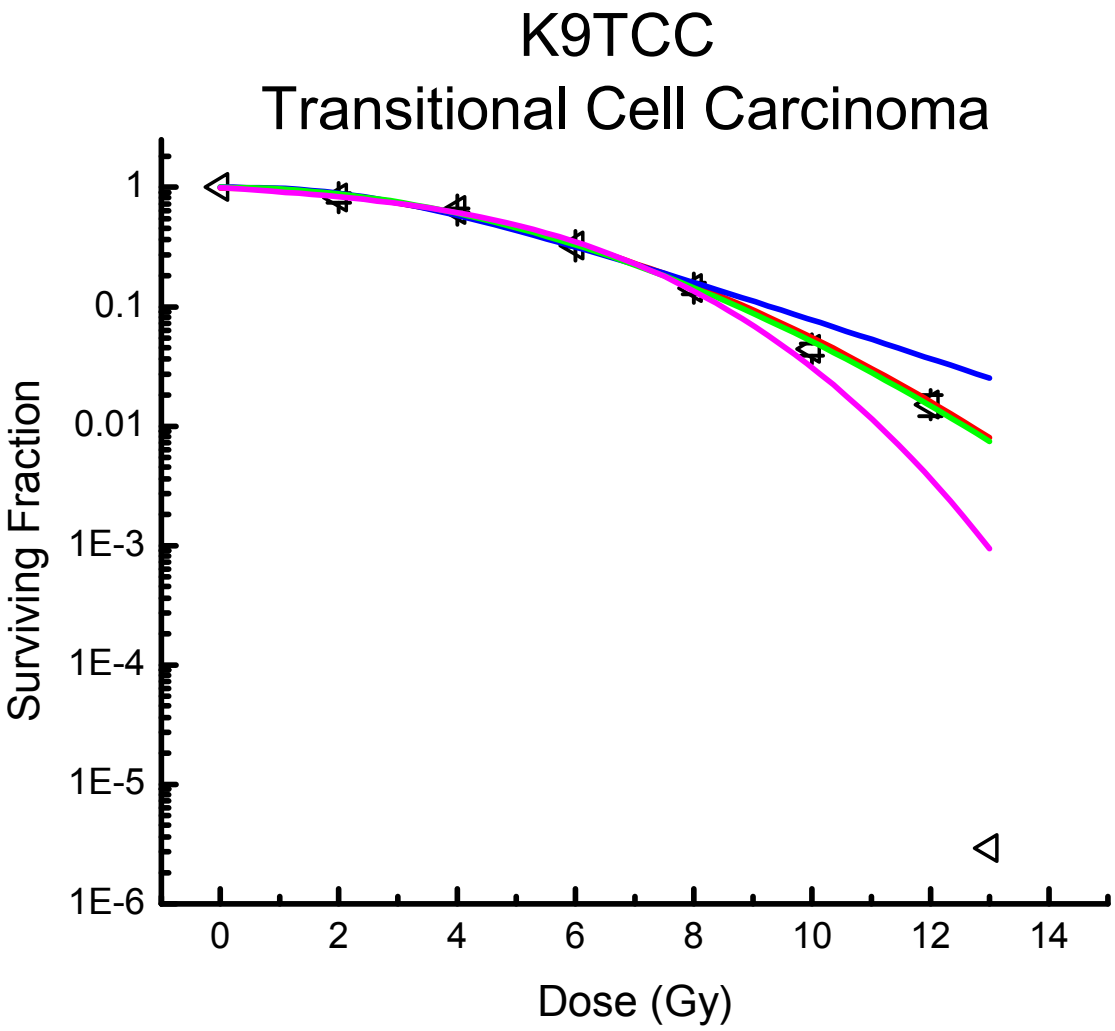

Figure 2.8: Modeling of dose-dependent survival data from K9TCC canine transitional cell carcinoma cells. Data points represent mean values of surviving fractions calculated from colony counts in three separate experiments. Error bars represent one standard deviation of the mean. The red line was generated via non-linear regression analysis using the linear quadratic model. The blue line was generated using the single-hit multitarget model. The green line was produced using the Kavanagh-Newman universal survival curve and the pink line was the result of fitting a modified linear quadratic equation in which survival (S) = $e^{-(\alpha D + \beta D^2 + \gamma D^3)}$.

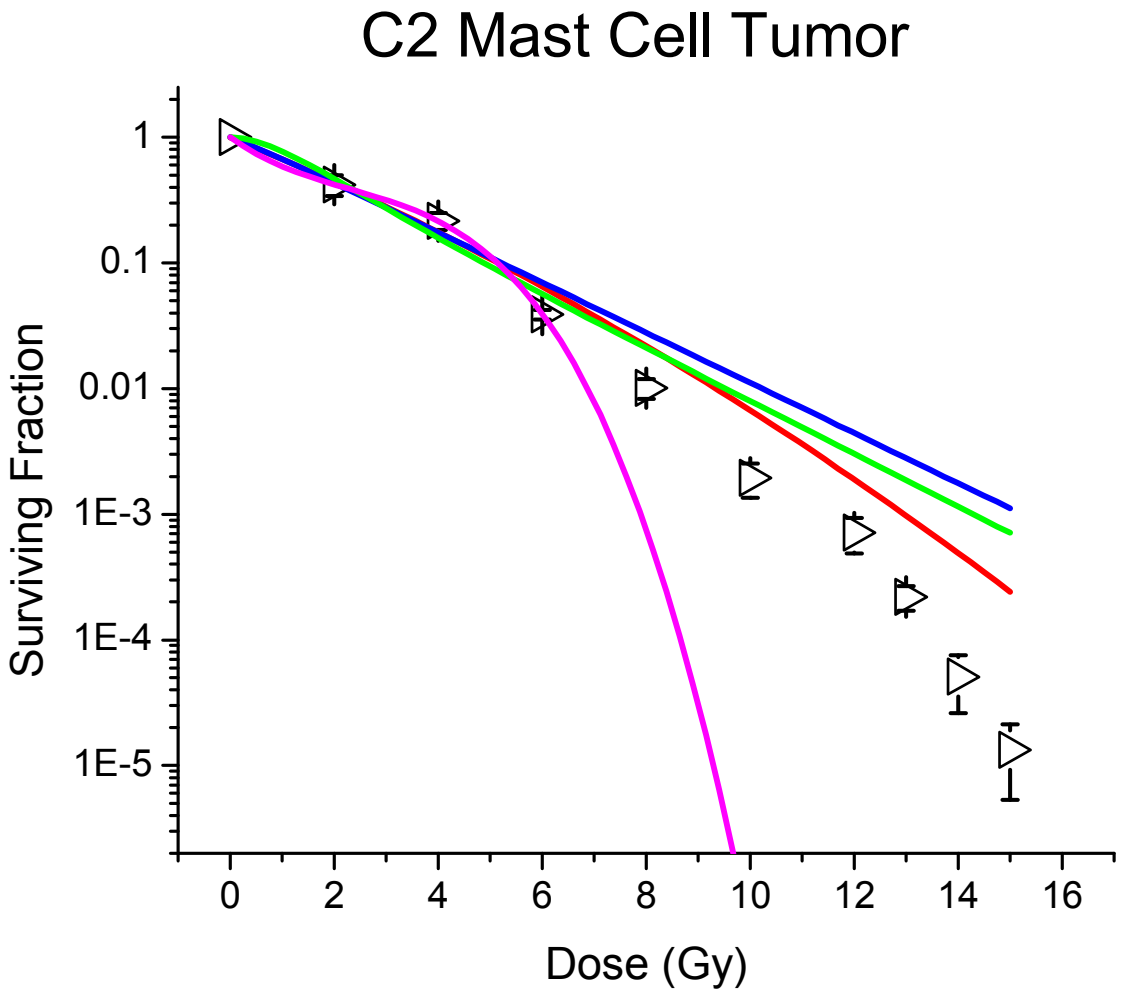

Figure 2.9: Modeling of dose-dependent survival data from C2 canine mast cell tumor cells. Data points represent mean values of surviving fractions calculated from colony counts in three separate experiments. Error bars represent one standard deviation of the mean. The red line was generated via non-linear regression analysis using the linear quadratic model. The blue line was generated using the single-hit multitarget model. The green line was produced using the Kavanagh-Newman universal survival curve and the pink line was the result of fitting a modified linear quadratic equation in which survival (S) = $e^{-(\alpha D + \beta D^2 + \gamma D^3)}$.

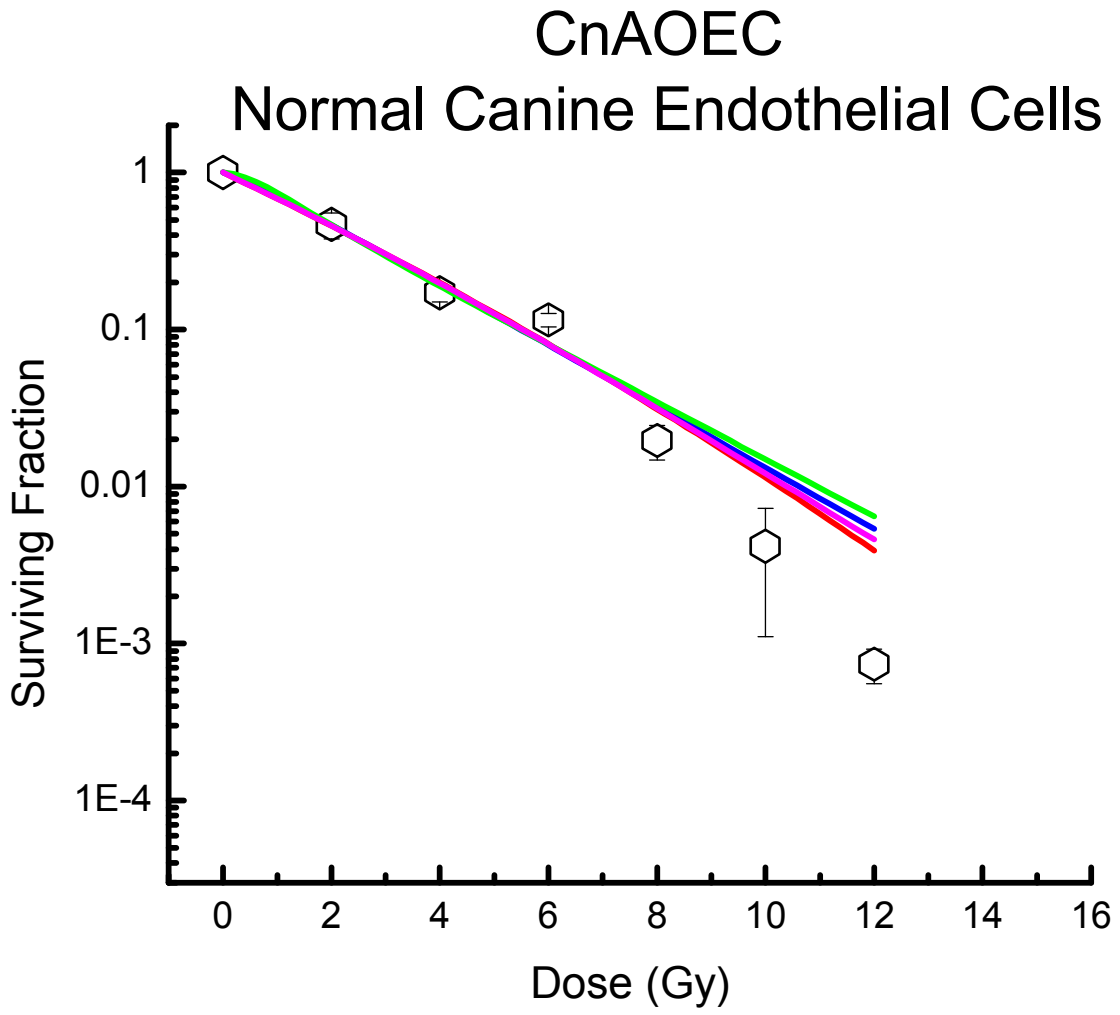

Figure 2.10: Modeling of dose-dependent survival data from CnAOEC canine endothelial cells. Data points represent mean values of surviving fractions calculated from colony counts in three separate experiments. Error bars represent one standard deviation of the mean. The red line was generated via non-linear regression analysis using the linear quadratic model. The blue line was generated using the single-hit multitarget model. The green line was produced using the Kavanagh-Newman universal survival curve and the pink line was the result of fitting a modified linear quadratic equation in which survival (S) = $e^{-(\alpha D + \beta D^2 + \gamma D^3)}$.

Table 2.5: Surviving fractions measured at 2 Gy (SF_2) and 8 Gy (SF_8), and calculated for 24 Gy via the cubed values of SF_8 or extrapolation to 24 Gy using the high dose region of survival curve data in eight canine cancer cell lines and one canine endothelial cell line.

Cell Line	**SF_2**	**SF_8**	**$(SF_8)^3$**	**SF_{24}**
STSA	0.319 ± 0.042	0.013 ± 0.001	2.41×10^{-6}	5.42×10^{-17}
C2	0.421 ± 0.078	0.010 ± 0.002	1.03×10^{-6}	7.69×10^{-11}
CnAOEC	0.467 ± 0.089	0.020 ± 0.005	7.65×10^{-6}	2.23×10^{-8}
CTAC	0.657 ± 0.029	0.026 ± 0.001	1.78×10^{-5}	8.73×10^{-12}
Dennys HAS	0.659 ± 0.071	0.098 ± 0.012	9.30×10^{-4}	1.78×10^{-6}
Abrams OSA	0.666 ± 0.068	0.091 ± 0.011	7.46×10^{-4}	7.93×10^{-15}
D17 OSA	0.807 ± 0.093	0.149 ± 0.005	3.30×10^{-3}	1.61×10^{-12}
K9TCC	0.819 ± 0.074	0.143 ± 0.016	2.94×10^{-3}	4.13×10^{-47}
CMT12	0.874 ± 0.040	0.225 ± 0.008	1.13×10^{-2}	2.01×10^{-16}

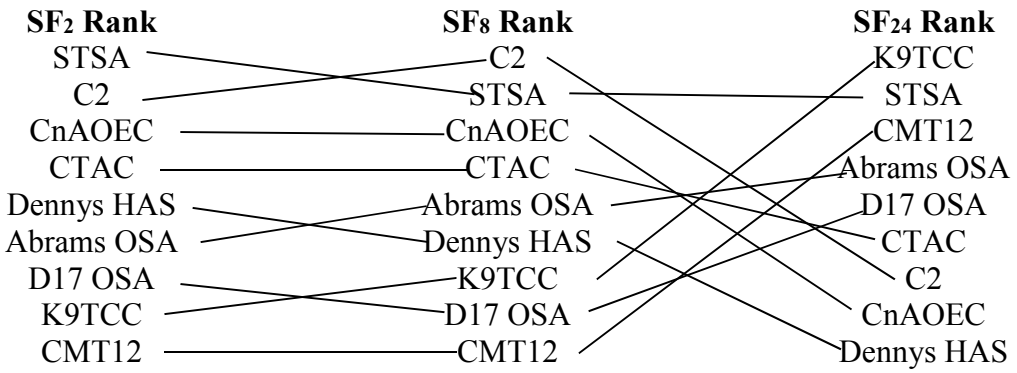

Figure 2.11: The relationships between surviving fraction rank of each canine cell line (eight cancer lines and one normal endothelial cell line) at 2, 8, and 24 Gy. Cell lines are listed in order from lowest values (radiosensitive) at the top to highest values (radioresistant) at the bottom of each list. SF_2 and SF_8 values were determined experimentally and SF_{24} was extrapolated from measured surviving fraction values in the high-dose region of the survival curve.

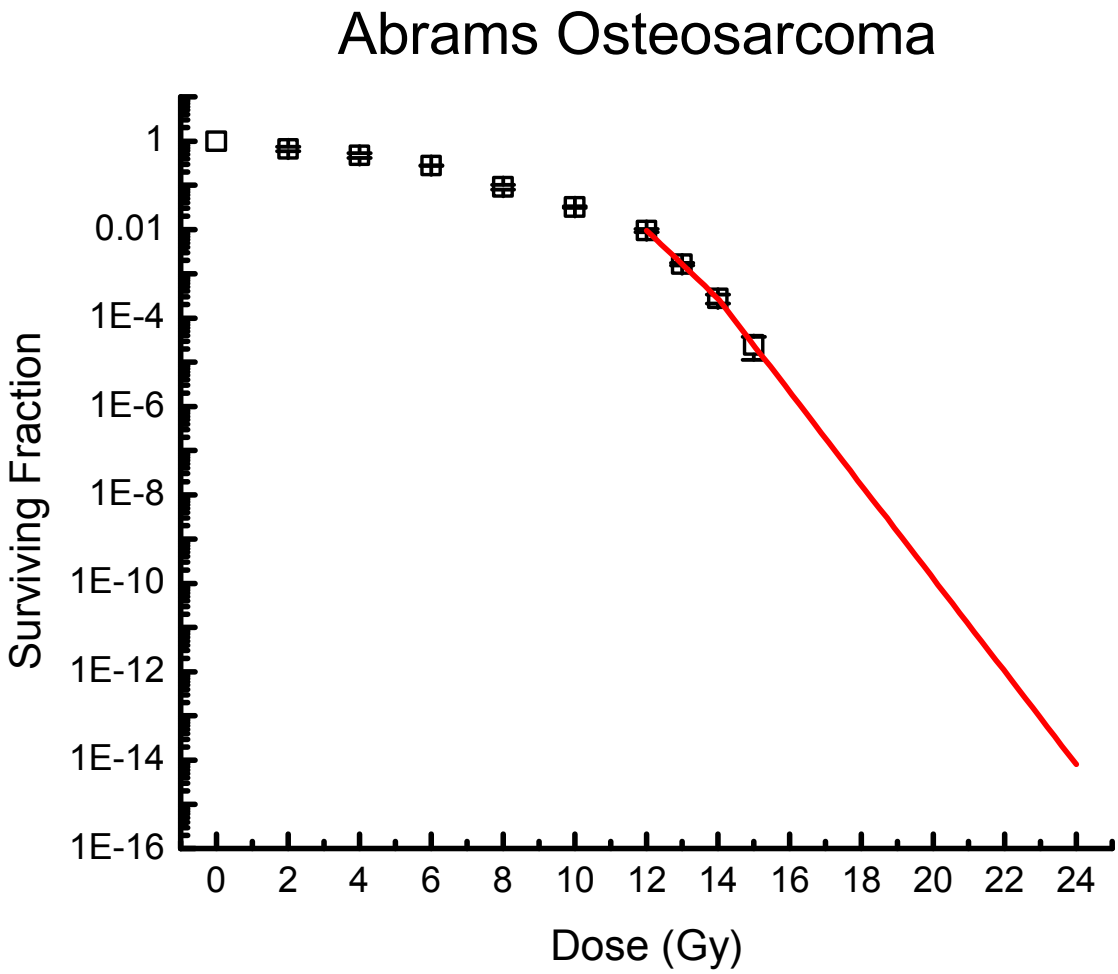

Figure 2.12: Extrapolation of high-dose data to estimate surviving fraction at 24 Gy (shown here in Abrams canine osteosarcoma cells).

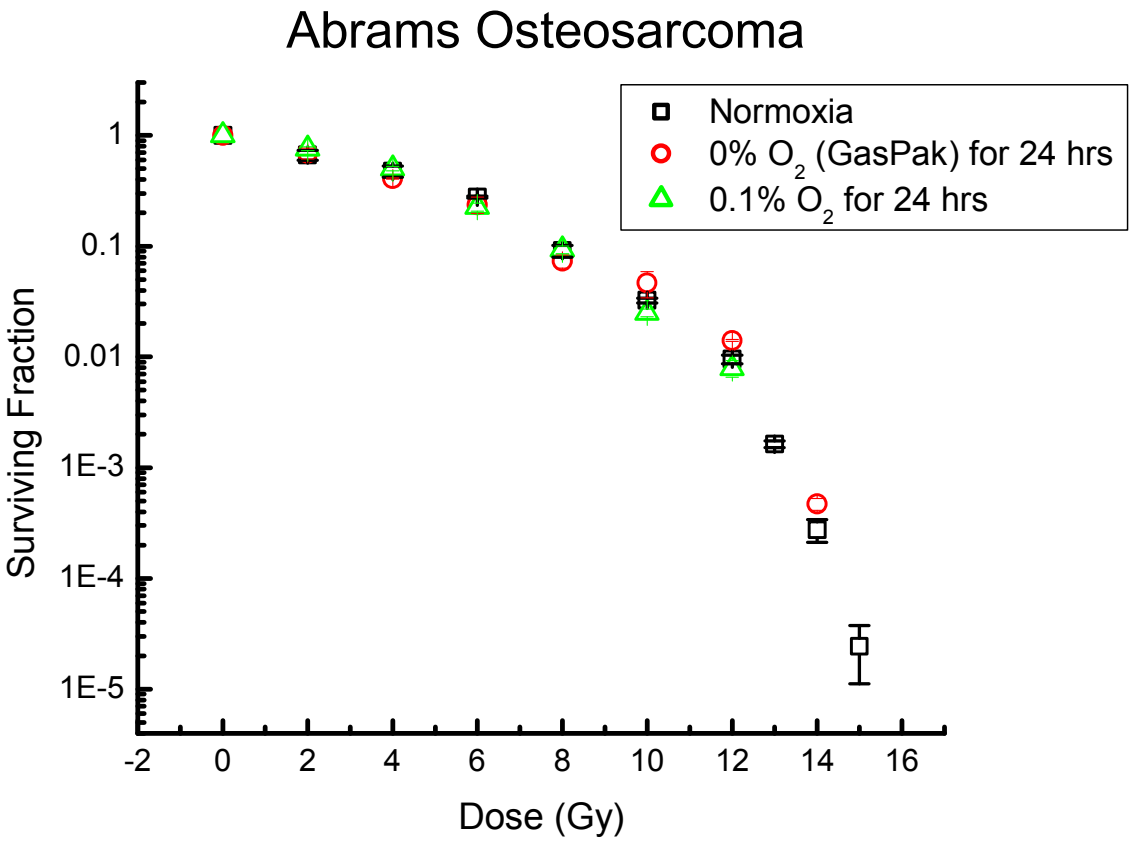

Figure 2.13: Cell survival versus dose in Abrams canine osteosarcoma cells treated with varying degrees of hypoxia immediately after irradiation. Cells shown here were treated with 0.1% oxygen for 24 hours and at 0% oxygen achieved using a GasPak™. Each data point represents the mean surviving fraction of experiments run in triplicate. Error bars represent one standard deviation of the mean. No difference was observed among treatment groups.

REFERENCES

1. Peters LJ. Inherent radiosensitivity of tumor and normal tissue cells as a predictor of human tumor response. *Radiother Oncol* 1990; 17: 177-190.
2. West CML. Intrinsic radiosensitivity as a predictor of patient response to radiotherapy. *Br J Radiol* 1995; 68: 827-837.
3. Vail DM, MacEwen EG. Spontaneously occurring tumors of companion animals as models for human cancer. *Cancer Investig* 2000; 18: 781-792.
4. Paoloni M, Khanna C. Translation of new cancer treatments from pet dogs to humans. *Nature Rev Cancer* 2008; 8: 147-156.
5. Gordon I, Paoloni M, Mazcko C, *et al.* The comparative oncology trials consortium: Using spontaneously occurring cancers in dogs to inform the cancer drug development pathway. *PLoS Med* 2009; 6: 1-5.
6. Withrow SJ, Wilkins RM. Corss talk from pets to people: Translational osteosarcoma treatments. *Inst Lab Anim Res J* 2010; 51: 208-213.
7. Suit HD, Baumann M, Skates S, *et al.* Clinical interest in determinations of cellular radiation sensitivity. *Int J Radiat Biol* 1989; 56: 725-737.
8. Hall EJ, Giaccia AJ. *Radiobiology for the Radiologist, 7th Ed.* Lippincott- Williams & Wilkins, Philadelphia, PA 2012.
9. Puck TT, Marcus PI. Actions of X-rays on mammalian cells. *J Exp Med* 1956; 103: 653-666.
10. Elkind MM, Whitmore GF. *The Radiobiology of Cultured Mammalian Cells*. Gordon and Breach, New York, NY 1967.
11. Deacon J, Peckham MJ, Steel GG. The radioresponsiveness of human tumours and the initial slope of the cell survival curve. *Radiother Oncol* 1984; 2: 317-323.

12. Park C, Papiez L, Zhang S, *et al.* Universal survival curve and single fraction equivalent dose: Useful tools in understanding potency of ablative radiotherapy. *Int J Radiat Oncol Biol Phys* 2008; 70: 847-852.

13. Kavanagh BD, Newman F. Toward a unified survival curve: In regard to Park *et al.* (*Int J Radiat Oncol Biol Phys* 2008;70:847-852) and Krueger *et al.* (*Int J Radiat Oncol Biol Phys* 2007;69:1262-1271). *Int J Radiat Oncol Biol Phys* 2008; 71: 958-959.

14. Garcia-Barros M, Paris F, Cordon-Cardo C, *et al.* Tumor response to radiotherapy regulated by endothelial cell apoptosis. *Science* 2003; 300: 1155-1159.

15. Franken NAP, Rodermond HM, Stap J, *et al.* Clonogenic assay of cells *in vitro*. *Nature Protocols* 2006; 1: 2315-2319.

16. Withrow SJ, MacEwen EG, Page R. *Withrow and MacEwen's Small Animal Clinical Oncology, 3rd Ed.* Elsevier Health Sciences, St. Louis, Missouri, 2013.

17. Fitzpartick CL, Farese JP, Milner RJ, *et al.* Intrinsic radiosensitivity and repair of sublethal radiation-induced damage in canine osteosarcoma cell lines. *Am J Vet Radiol* 2008; 69: 1197-1202.

18. Maeda J, Yurkon CR, Fujisawa H, *et al.* Genomic instability and telomere fusion of canine osteosarcoma cells. *PLOS One* 2012; 7: 1-12.

19. Harris GA. *Intrinsic radiosensitivity of canine normal and tumor cells to both high and low dose rate*. Doctoral Dissertation. Colorado State University, Fort Collins, CO, 1997.

20. Suit HD, Baumann M, Skates S, *et al* Clinical interest in determination of cellular radiation sensitivity. *Int J Radiat Biol* 1989; 56: 725-737.

21. Garcia LM, Leblanc J, Wilkins D, *et al.* Fitting the linear-quadratic model to detailed data sets for different dose ranges. *Phys Med Biol* 2006; 51: 2813-2823.

22. Sheu T, Molkentine J, Transtrum MK, *et al.* Use of the LQ model with large fraction sizes results in underestimation of isoeffect doses. *Radiother Oncol* 2013; 109: 21-25.
23. Nahum AE. The radiobiology of hypofractionation. *Clin Oncol* 2015; 27: 260-269.
24. Song CW, Park I, Cho LC, *et al.* Is indirect cell death involved in response of tumor to stereotactic radiosurgery and stereotactic body radiation therapy? *Int J Radiat Oncol Biol Phys* 2014; 89: 924-925.
25. Smith AN. Hemangiosarcoma in dogs and cats. *Vet Clin Small Anim* 2003; 33: 533-552.
26. Maudin GN. Soft tissue sarcomas. *Vet Clin Nor Am Small Anim Pract* 1997; 27: 139-147.
27. McKnight JA, Mauldin GN, McEntee MC, *et al.* Radiation treatment for incompletely resected soft tissue sarcomas in dogs. *J Am Vet Med Assoc* 2000; 217: 205-210.
28. Ruka W, Taghian A, Gioioso D, *et al.* Comparison between the *in vitro* intrinsic radiation sensitivity of human soft tissue sarcoma and breast cancer cell lines. *J Surg Oncol* 1996; 61: 290-294.
29. Theon AP, Marks SL, Feldman ES, *et al.* Prognostic factors and patterns of treatment failure in dogs with unresectable differentiated thyroid carcinomas treated with megavoltage irradiation. *J Am Vet Med Assoc* 2000; 216: 1775-1779.
30. Moore AS. Radiation therapy for the treatment of tumours in small companion animals. *Vet J* 2002; 164: 176-187.
31. Challeton C, Branea F, Schlumberger M, *et al.* Characterization and radiosensitivity at high or low dose rate of four cell lines derived from human thyroid tumors. *Int J Radiat Oncol Biol Phys* 1997; 37: 163-169.

32. Nolan MW, Kogan L, Griffin LR, *et al.* Intensity-modulated and image-guided radiation therapy for treatment of genitourinary carcinomas in dogs. *J Vet Intern Med* 2012; 26: 987-995.

33. Parfitt SL, Milner RJ, Salute ME, *et al.* Radiosensitivity and capacity for radiation-induced sublethal damage repair of canine transitional cell carcinoma (TCC) cell lines. *Vet Comp Oncol* 2011; 9: 232-240.

34. LaDue T, Price, GS, Dodge R, *et al.* Radiation therapy for incompletely resected canine mast cell tumors. *Vet Radiol Ultrasound* 1998; 39: 57-62.

35. Chaffin K, Thrall DE. Results of radiation therapy in 19 dogs with cutaneous mast cell tumor and regional lymph node metastasis. *Vet Radiol Ultrasound* 2002; 43: 392-95.

36. Mayer MN. Radiation therapy for canine mast cell tumors. *Can Vet J* 2006; 47: 263-265.

37. Sekis I, Gerner W, Willmann M, *et al.* Effect of radiation on vascular endothelial growth factor expression in the C2 canine mastocytoma cell line. *Am J Vet Radiol* 2009; 70: 1141-1150.

38. Martin DF, Fischer JJ. Radiation sensitivity of cultured rabbit aortic endothelial cells. *Int J Radiat Oncol Biol Phys* 1984; 10: 1903-1906.

39. Penhaligon M, Laverick M. Radiation response of endothelial cells *in vitro*. *Br J Radiol* 1985; 58: 913-914.

40. Rhee JG, Lee I, Song CW. The clonogenic response of bovine aortic endothelial cells in culture to radiation. *Radiat Res* 1986; 106: 182-189.

41. Haimovitz-Friedman A, Vlodavsky I, Chaudhuri A, *et al.* Autocrine effects of fibroblast growth factor in repair of radiation damage in endothelial cells. *Cancer Res* 1991; 51: 2552-2558.

42. Fuks Z, Vlodavsky I, Andreef M, *et al.* Effects of extracellular matrix on the response of endothelial cells to radiation *in vitro. Eur J Cancer* 1992; 28A; 725-731.

43. Hei TK, Marchese MJ, Hall EJ. Radiosensitivity and sublethal damage repair in human umbilical cord vein endothelial cells. *Int J Radiat Oncol Biol Phys* 1987; 13: 879-884.

44. Park MT, Oh ET, Song MJ, *et al.* Radio-sensitivities and angiogenic signaling pathways of irradiated normal endothelial cells derived from diverse human organs. *J Radiat Res* 2012; 53: 570-580.

45. Xu J, Yan X, Gao R, *et al.* Effect of irradiation on microvascular endothelial cells of parotid glands in the miniature pig. *Int J Radiat Oncol Biol Phys* 2010; 78: 897-903.

46. Powers WE, Tolmach LJ. A multicomponent X-ray survival curve for mouse lymphosarcoma cells irradiated *in vivo*. *Nature* 1963; 197: 710-711.

47. Hall EJ, Bedford JS, Oliver R. Extreme hypoxia- Its effect on survival of mammalian cells irradiated at high and low dose-rates. *Br J Radiol* 1966; 39: 302-307.

48. Hall EJ, Bedford JS. Threshold hypoxia- Its effect on survival of mammalian cells irradiated at high and low dose-rates. *Br J Radiol* 1966; 39: 896-900.

49. Metzger L, Iliakis G. Kinetics of DNA double-strand break repair throughout the cell cycle as assayed by pulsed field gel electrophoresis in CHO cells. *Int J Radiat Biol* 1991; 59: 1325-1339.

50. Jackson SP. Sensing and repairing DNA double-strand breaks. *Carcinogenesis* 2002; 23: 687-696.

51. Meng AX, Jalali F, Cuddihy A, *et al.* Hypoxia down-regulates DNA double strand break repair gene expression in prostate cancer cells. *Radiother Oncol* 2005; 76: 168-176.

52. Bindra RS, Gibson SL, Meng A, *et al.* Hypoxia-induced down-regulation of BRCA1 expression by E2Fs. *Cancer Res* 2005; 65: 11597-11604.

53. Bindra RS, Schaffer PJ, Meng A, *et al.* Alterations in DNA repair gene expression under hypoxia- Elucidating the mechanisms of hypoxia-induced genetic instability. *Ann NY Acad Sci* 2005; 1059: 184-195.

54. Bindra RS, Crosby ME, Glazer PM. Regulation of DNA repair in hypoxic cancer cells. *Cancer Metastasis Rev* 2007; 26: 249-260.

55. Bindra RS, Glazer PM. Repression of RAD51 gene expression by E2F4/p130 complexes in hypoxia. *Oncogene* 2007; 26: 2048-2057.

56. Chan N, Koritzinsky M, Zhao H, *et al.* Chronic hypoxia decreases synthesis of homologous recombination proteins to offset chemoresistance and radioresistance. *Cancer Res* 2008; 68: 605-614.

57. Klein TJ, Glazer PM. The tumor microenvironment and DNA repair. *Semin Radiat Oncol* 2010; 20: 282-287.

CHAPTER 3

VASCULAR FUNCTION FOLLOWING STEREOTACTIC RADIATION THERAPY USING 2, 8, OR 24 GY TO SPONTANEOUSLY OCCURRING CANINE SOFT TISSUE SARCOMAS

INTRODUCTION

Much of what we know about tumor and normal tissue responses to high-dose single fraction irradiation have come from studies in purpose-bred and pet dogs. As previously described, cancers in dogs are considered to be excellent models for human disease due to characteristics such as outbred genetics, intact immune systems, similar environmental exposures, age-related incidence of disease, overall tumor size, and tumor cell kinetics.[1-3] In many tumor types histological features of tumors of canine and human origin are identical,[2-3] and the overall heterogeneity of human tumor microenvironment and treatment response is more closely reflected in spontaneously occurring tumors of dogs than by other animals models.[2-3] Studying canine tumors has the advantage of observing results in a timely manner, as canine cancers progress at a more rapid rate than human cancers (although this is in proportion to life span and is therefore reflective of human disease).[1,2] In addition, the standard of care for many canine cancers is unestablished, which facilitates ease of testing new therapeutic modalities within the limits of ethical treatment policies.[1-3]

Studies using spontaneously occurring canine tumors to examine clinical response to single high-dose irradiation delivered in the form of intraoperative radiation therapy (IORT) greatly increased understanding of radiation late effects to normal tissues.[4] In IORT, a tumor is surgically exposed for cytoreduction and normal tissues are moved aside or shielded with thin sheets of lead to protect them from exposure to a high dose of radiation delivered in one

treatment, or "boost," (with notably larger margins than those used in SRT) before surgical closure.[4] In general, tumor control results from IORT were disappointing and the high dose per fraction treatment produced severe late tissue toxicities.[4-7] Even when prodigious efforts were made to physically exclude normal tissues from receiving high doses, experimental treatments utilizing IORT were limited by normal tissue tolerance to doses that were unlikely to result in tumor control (leading clinicians to combine IORT with post-surgical, fractionated radiation therapy to improve clinical outcome).

To treat using stereotactic radiation therapy, clinicians go to great lengths to protect normal tissues from high-dose irradiation, although this is done using careful immobilization, image guidance, and beam intensity modulation rather than physical exclusion of dose-limiting tissues in the surgical procedures of IORT. In parallel to studies showing increased efficacy of SRT to treat radiation resistant tumor types in humans, SRT has been used increasingly in veterinary medicine,[8] particularly in the case of canine appendicular osteosarcoma.

Canine osteosarcoma is a well-established model for human osteosarcoma since it is similar relative to basic biologic characteristics and occurs in dogs at a higher frequency than in humans, thus facilitating experimentation for the purposes of translational medicine.[9,10] Traditional fractionated radiation therapy is known to be unsuccessful as a single therapeutic agent in curative intent treatment of canine osteosarcoma,[11,12] although it has been used successfully in multimodal approaches to achieve limb-sparing treatment for this disease.[13] Palliative, hypofractionated radiation therapy utilizing protocols that deliver 6, 8, or 10 Gy in one treatment per week for three to four weeks, is commonly used to achieve palliation of pain frequently associated with osteosarcoma.[14-17] Preliminary studies exploring application of 20 to 30 Gy in a single fraction to canine appendicular osteosarcoma determined that SRT may be a

viable, limb-sparing treatment modality, possibly enhanced in combination with chemotherapy.[18,19] A study conducted at the Flint Animal Cancer Center enrolled over eighty canine patients with spontaneously occurring appendicular osteosarcoma to evaluate the efficacy of a 12 Gy per three fraction SRT protocol (one fraction per day for three days to achieve a total of 36 Gy) with adjuvant bisphosphonate and carboplatin chemotherapy.[20,21] In stark contrast to the poor outcomes from traditional fractionated radiation therapy, the SRT protocol achieved greater than 90% tumor control with a mean survival time of 310 days, which was comparable to standard of care results from amputation but was non-invasive, free from severe complications and generally well tolerated.[20,21] The results of these studies prompted interest in determining *why* SRT achieved tumor control in a tumor type that did not respond to traditional fractionated radiation therapy. What mechanisms were leading to local tumor control in these bone tumors following treatment with high doses that were not occurring after low dose treatment?

Endothelial cell apoptosis occurring above a dose threshold of 8 to 10 Gy has been shown in murine models,[22,23] and it was proposed that such endothelial cell damage may be a component in a biologic response leading to tumor control from SRT. Biopsies from spontaneously occurring canine tumors treated with either 3 or 18 Gy in a single fraction were evaluated using TUNEL staining for apoptotic cells and immunofluorescence staining of CD31 proteins on the surface of endothelial cells.[24] Twenty four hours after irradiation with 18 Gy, vascular endothelial cell apoptosis was observed in greater numbers than those measured in pre-irradiation samples, while irradiation with 3 Gy did not increase endothelial cell apoptosis from pre-irradiation values.[24] It was also noted that the partial pressure of oxygen measured in these tumors decreased twenty four hours after treatment with 18 Gy in three out of four tumors, a finding that differed from results using 3 Gy in which partial pressure of oxygen showed signs of

reoxygenation at twenty four hours if the tumors had been hypoxic (having a median partial pressure of oxygen below 10 mmHg) prior to treatment.[25] Among the hypoxic tumors that showed increased oxygen values after treatment with 3 Gy (i.e. reoxygenation) and in several, better-oxygenated tumors, the interstitial fluid pressure measured using "wick-in-needle" techniques was shown to decrease.[25] In order to evaluate the time frame in which vascular effects may be occurring relative to radiation therapy treatment, one dog (named "Maggie") with a spontaneously occurring soft tissue sarcoma located on the caudal thigh (Figure 3.1) was treated with a single dose of 20 Gy using SRT (treatment planning summarized in Figure 3.2) while oxygen measurements and biopsies were taken at multiple time points before and after dose delivery. It was determined that the acute vascular response within three to five hours of irradiation was of greatest interest, since percent endothelial cell apoptosis determined from immunofluorescently stained biopsies (Figure 3.4) was increased relative to pre-irradiation (Figure 3.5) and oxygen was observed to transiently decrease (Figure 3.6) during that time frame.

The relationship between tumor microenvironment and tumor vascular function is highly interdependent, but no previous work has established that tumor microvasculature and microenvironment respond in a unique manner at high doses in ways that impact clinical tumor control. We hypothesize that unlike the low doses administered in finely fractionated radiation therapy, high doses delivered in a single fraction induce acute tumor vascular dysfunction, consequently altering tumor microenvironment within hours of radiation treatment. Acute changes in tumor blood supply and vascular function may contribute to the increased tumor cell kill observed in SRT. From a more specific standpoint, we hypothesize that changes in the tumor microenvironment occur in more than one phase and responses such as worsening of

hypoxia or perfusion deficits may be the result of different types of time-dependent vascular changes (i.e. vascular change producing very acute responses on the scale of one to three hours, versus vascular damage causing measureable effects after twenty four or forty eight hours). The overreaching goal of our work is to elucidate the novel biological mechanism underlying the clinical tumor response to SRT. Understanding the mechanism by which SRT achieves tumor control will inform radiation therapy protocol design, leading to improved treatment efficacy and potentially allowing for identification of targets (e.g. ASMase upregulation) which may be modified to achieve therapeutic gain.

We evaluated parameters related to tumor vascular function and microenvironment in an acute time frame in spontaneously occurring soft tissue sarcomas following low (2 Gy), medium or possibly threshold (8 Gy), and high (24 Gy) doses delivered stereotactically and in a single fraction. Canine soft tissue sarcomas are considered to be radioresistant and of low metastatic risk while being locally aggressive with a propensity toward developing hypoxic regions within tumor parenchyma.[26,27] Soft tissue sarcomas were selected for study due to their relatively high incidence in dogs and with the understanding that surgery was a secondary and highly viable treatment option to fall back upon in the event of adverse effects. Microenvironmental parameters related to vascular function that were investigated in this study were oxygenation, interstitial fluid pressure, and tumor perfusion. Each parameter was measured in a single location within the tumor during the pre-irradiation and acutely post-irradiation time frame to monitor for immediate changes in vascular function, and again in nearby locations at twenty four and forty eight hours after irradiation.

In order to address hypothesized mechanistic events following single fraction high dose irradiation in canine soft tissue sarcomas, it was proposed that several assays that evaluated

vascular response on a highly acute time scale within hours of irradiation rather than days or weeks should be used. Figure 3.7 displays potential responses of tumor vasculature and parenchyma, two interdependent subcategories of a tumor, in different time frames following high dose irradiation. Due to observations of peak endothelial cell apoptosis around six hours post-irradiation in stained biopsies from our preliminary studies (experiments that shall be replicated in this study) and in accordance the literature,[28] it would be expected that microenvironmental changes subsequent to endothelial cell apoptotic events would begin to occur during or after that time frame. Massive endothelial cell death and vascular catastrophe could explain decreases in oxygenation and perfusion over the course of the next twenty four to forty eight hours, but such events could not explain changes in the one to three hour timeframe. Multiple changes to endothelial cell behavior may be induced by large doses of radiation prior to the cells' orderly progression into apoptosis. The cells must first secrete ASMase to begin a ceramide-mediated cascade towards apoptosis.[29,30] Irradiated endothelial cells may respond to DNA damage with a loss of several specialized functions, including the ability to generate nitric oxide and the related ability to trigger a vasodilatory response. Decreased bioavailability of nitric oxide and failure to vasodilate when stimulated by vasoactive molecules such as acetylcholine are defining characteristics of vascular dysfunction,[31,32] which may occur rapidly enough to explain microenvironment changes within a few hours of irradiation. Oxidative stress, a cellular state of being that is to be expected following exposure to ionizing radiation due to the generation of free radicals and reactive oxygen species, can contribute to reduced bioavailability of nitric oxide.[33] As with hypoxia, oxidative stress may show a biphasic response including an immediate wave of radical species during radiation exposure and any subsequent oxidative stress from cellular response mechanisms. Overall, it is our objective to evaluate tumor vascular

response to single fraction high dose irradiation using methods and assays that focus on biologic events at different points in the timeline between radiation exposure and cell death.

The study of parameters related to tumor hypoxia and perfusion *in vivo* required regulation of inspired oxygen to replicate the arterial blood partial pressure of oxygen (pAO_2) of an awake patient. Maintaining the dogs on 100% oxygen, as is typical for veterinary anesthesia, was not desirable in this study because increasing inspired oxygen produces an increase in tissue oxygen tension in tumors.[34] In contrast to veterinary medicine, radiation therapy in adult humans is not conducted under general anesthesia and oxygenation of tissues from breathing room air is typical. Anesthesia was maintained using compressed air/oxygen blending techniques to achieve normal pAO_2 levels, which were between 80 and 85 mmHg at the elevation of Colorado State University.

MATERIALS AND METHODS

Nine dogs presenting with large, superficially located, histologically-confirmed soft tissue sarcomas were enrolled in our clinical trial at Colorado State University's Flint Animal Cancer Center. All clinical trial procedures consented to by each dog owner and approved by the Colorado State University Internal Animal Care & Use Committee (IACUC). Dogs were randomized into one of three treatment groups: irradiation with a single fraction of 2, 8, or 24 Gy. All dogs were positioned for CT scanning in a Gemini TruFlight Big Bore PET/CT scanner (Philips Healthcare, Best, The Netherlands) using immobilization devices such as vacuum pillows, bite blocks, face masks, etc. that were necessary and appropriate for SRT. Each dog's immobilization setup was kept for use in positioning for treatment. CT scans were conducted with additional contrast enhancement in eight of the nine dogs, allowing for contrast uptake

within the tumor to be evaluated in terms of Hounsfield Units (HU). CT scans were used to generate radiation therapy plans with Eclipse™ treatment planning software (Varian Medical Systems, Inc., Palo Alto, California, USA), utilizing inverse treatment planning algorithms. Dose was delivered to the gross tumor volume (GTV), which was determined jointly by a faculty radiation oncologist and a radiologist, using the Varian Trilogy® linear accelerator (Varian Medical Systems, Inc., Palo Alto, California, USA) at a sharp gradient in which prescribed doses conform tightly to the treatment volume and dose drop-off outside that target is steep, sparing adjacent normal tissues. The steep dose gradient was achieved using inverse treatment planning, multileaf collimator-based beam modulation, and positioning verification, which was conducted for each patient using on-board cone beam CT. Planning target volume (PTV) margins were set based on tumor location, ranging from 3 to 5 mm. Plan data for dose to the 99% of the GTV and 95% of the CTV in each dog prior to assignment of dogs into treatment groups is displayed in Table 3.1. All radiation therapy treatment plans were generated to deliver 24 Gy to each dog's tumor; once a dog was randomized into the 2, 8, or 24 Gy treatment group, the plan was adjusted to deliver dose in two fractions (2 and 22 Gy or 8 and 16 Gy) or left as a single dose of 24 Gy. Examples of dose volume histograms displaying dose to the GTV and PTV in cases where dogs were randomized into the 2 or 8 Gy treatment groups are shown in Figures 3.8 and 3.9.

Prior to radiation treatment, all dogs were anesthetized using individualized anesthetic protocols that typically incorporated atropine and hydromorphone as premedications. In general, induction of anesthesia was conducted using diazepam and propofol prior to intubation and dogs were maintained on isoflurane and a mixture of oxygen with room air. Mixtures of compressed air and oxygen were regulated using a Bird® Low Flow Air/O_2 Blender (CareFusion Corporation, San Diego, California, USA). An arterial line was placed and blood was collected for analysis

with a Radiometer ABL800 Flex blood gas analyzer (Radiometer America, Brea, California, USA). Air and oxygen were mixed in appropriate proportions to achieve an arterial blood gas partial pressure of oxygen around 80 mmHg (actual measurements ranged from 73.9 to 108 mmHg and fine tuning of admixture was often conducted to adjust measured values toward 80 mmHg prior to probe placement). Fentanyl and propofol were used in addition to the inhalant anesthetic to maintain anesthesia as needed.

Hair overlying the tumors and over adjacent skin was shaved and cleaned with Hibiclens® antiseptic surgical scrub and alcohol and a location for insertion of probes was selected based on planning CT scans with the intent of avoiding fatty or necrotic regions within the tumor. Small incisions were made through the skin and cathethers of appropriate sizes (16 to 20 gauge) to accommodate probes for oxygen, interstitial fluid, and perfusion measurements were inserted into the tumor tissues. After the catheter stylets were withdrawn, probes could be inserted into the tissues through the catheter sleeve. All probes were wiped with alcohol before being placed in tumor tissues and remained in place throughout irradiation and for three hours subsequent to the end time of dose delivery. Continuous measurements of partial pressure of oxygen, interstitial fluid pressure, and blood flow were taken before, during, and for three hours after irradiation with minimal repositioning of probes. Following measurements at three hours post-treatment, probes were withdrawn and the dogs were recovered from anesthesia and housed in the Colorado State University James L. Voss Veterinary Teaching Hospital overnight. Twenty four and forty eight hours after radiation therapy, each dog was anesthetized a second and third time and maintained on an oxygen and room air admixture in both cases, for oxygen, interstitial fluid pressure, and perfusion measurements. At the conclusion of sampling forty eight hours after the initial delivery of dose, dogs that were randomized into the 2 Gy or 8 Gy

treatment groups were treated with an additional dose of 22 Gy or 16 Gy, respectively, delivered in one fraction to achieve a total dose of 24 Gy, thus allowing every dog enrolled in this study to receive equal total dose. All dogs participating in this clinical trial were scheduled for three and six month follow up appointments to assess toxicities and tumor response (ideally tumor shrinkage) for future comparisons of clinical outcomes among dogs treated with 2 and 22 Gy versus 8 and 16 Gy and versus 24 Gy in one fraction. The veterinary radiation oncologist tasked with placing probes into tumor tissue was blinded to the assignment of dogs into treatment groups until after all measurements had been collected. In addition to continuous measurements of oxygen, interstitial fluid pressure, and perfusion, tumor biopsies and systemic blood samples were taken from each dog before radiation therapy, immediately after dose delivery, and at one, two, three, twenty four, and forty eight hours after dose delivery. It was anticipated that biopsies and blood samples would be used for additional analyses of the impact of 2, 8, or 24 Gy on tumor vascular function. Biopsies were taken using a 14 gauge needle in a TruCut biopsy gun and immediately placed in a cassette and submerged in a chilled 4% paraformaldehyde solution. Blood samples were collected using 5 mL lavender top vacutainers containing EDTA (BD Diagnostics, Franklin Lakes, New Jersey, USA) to separate plasma from whole blood and using 5 mL red top vacutainers (BD Diagnostics, Franklin Lakes, New Jersey, USA) that allowed whole blood to clot for the separation of serum.

Probes for Measurement of Oxygen, Interstitial Fluid Pressure, and Perfusion

Partial pressure of oxygen at a single location in each tumor was measured using Oxylite^{TM} NX-LAS-9/O/E "large area sensor" probes (Oxford Optronics Ltd., Abingdon, Oxford, UK), which averaged absolute measurements of partial pressure of oxygen in mmHg among an 8 mm^2 sampling area into a single reading that was collected in real-time by an

Oxylite™ one channel oxygen monitoring system (Oxford Optronics Ltd., Abingdon, Oxford, UK). Oxylite™ probes achieved oxygen measurements using a luminescence-based optical sensory system in which a platinum-based fluorophore in the tip of each probe is excited via light conducted fiber-optically to the probe tip. Fluorescent light is then emitted from the probe tip and quenched by dissolved oxygen molecules in the tissues, allowing a fraction of the incident light to return via the fiber-optic cable. The concentration of dissolved oxygen in the tissues is inversely proportional to the lifetime of the fluorophore emission, thus allowing for quantification of partial pressure of oxygen in a sampled tissue volume. Proper function of probes was verified before each use by submerging each probe in a 211 mM aqueous solution of sodium sulfate heated to 37°C, which quenched dissolved oxygen and produced probe readings of approximately zero mmHg. The Oxylite™ system is the current gold-standard for *in vivo* and *in vitro* oxygen monitoring, as it does not consume dissolved oxygen in the measurement process as do comparable oxygen measurement technologies. Oxylite™ measurements were collected using a PowerLab 4/35 multichannel analog-to-digital converter and signal modifier/signal amplifier (AD Instruments Inc., Colorado Springs, Colorado, USA). Data was displayed and collected in real-time using LabChart 8 data acquisition and analysis software (AD Instruments Inc., Colorado Springs, Colorado, USA).

Interstitial fluid pressure measurements were made using a Mikro-Tip® catheter pressure transducer (Millar Inc., Houston, Texas, USA) and relayed via a FE221 single-channel bridge amplifier (AD Instruments, Colorado Springs, Colorado, USA) to the PowerLab 4/35 multichannel signal modifier/signal amplifier (AD Instruments Inc., Colorado Springs, Colorado, USA). Interstitial fluid pressure data were collected in real-time and displayed simultaneously alongside oxygen and flow data using LabChart 8 software (AD Instruments Inc., Colorado

Springs, Colorado, USA). The pressure transducer probe allows for continuous measurement of interstitial fluid pressure in a single location, whereas older methods of measuring interstitial fluid pressure such as the "wick-in-needle" technique can only take one measurement per location. Pressure transducer probes were submerged in 37^{o}C water and allowed to equilibrate for thirty minutes before undergoing a two-point calibration in the range of 2 to 15 mmHg using a Delta-Cal^{TM} pressure transducer tester (Utah Medical Products, Inc., Midvale, Utah, USA). Following any situation in which pressure readings appeared to be inaccurate, a second calibration was performed after data was acquired.

Perfusion measurements were made using laser Doppler flow probes, in this case Type M two-fiber cables with attached semi-disposable, implantable, monofiber probe ends (Transonic Systems, Inc., Ithica, New York, USA). Probe fiber-optic systems emit a low intensity beam of monochromatic light to illuminate a small volume of tissue (in this case sampling volume is assumed to be 1 mm^3, but actual volumes depend on optical properties of the tissue). Reflective components within the tissue scatter light in all directions and light reflected back to the probe by moving components, such as red blood cells, experiences a frequency change relative to incident light. Red blood cell flow in terms of mL x min^{-1} x 100 g^{-1} (or "percent tissue perfusion units") of tissue may be calculated using Doppler theory based on the shift in scattered light frequency. Blood flow data was collected using a Transonic® BLF21 Series laser Doppler monitor (Transonic Systems, Inc., Ithica, New York, USA), which communicated directly with the PowerLab 4/35 multichannel signal modifier/signal amplifier (AD Instruments Inc., Colorado Springs, Colorado, USA). Blood flow data was measured in real-time and displayed with oxygen and interstitial fluid pressure data on LabChart 8 software (AD Instruments Inc., Colorado Springs, Colorado, USA). Flow probe sampling was set to a time constant of 0.1

seconds to allow for recording of instantaneous data with pulsatility (as opposed to averaged data), which displayed waveforms in accordance with the dog's pulse. The flow probes were particularly sensitive to motion artifacts, which were clearly distinguishable among a background of consistent waveforms (Figures 3.10 and 3.11).

Statistical Analysis

Oxygen, interstitial fluid pressure, and blood flow data were collected continuously and simultaneously over time in each dog for approximately one hour leading up to radiation therapy treatment, during the delivery of dose (which could take up to one hour), and for the subsequent three hours as well as for seven to ten minute segments at approximately twenty four and forty eight hours after the time at which dose delivery concluded. For each time point of interest (pre-irradiation, immediately post-irradiation as well as 1 hour, 2 hours, 3 hours, 24 hours, and 48 hours later), thirty second-long segments of data at one minute intervals were averaged to a single mean value for a total of nine to fifteen minutes, depending on how much high quality data was obtained at each time point. In the event that motion artifacts obscured data in a selected segment, the data around the artifact was collected with the exclusion of the artifact and in some cases where the artifact engulfed the entire thirty second segment, that segment was excluded entirely. Linear regression analysis on ranked data (a non-parametric test) was performed using SAS v9.4 statistical software (SAS Institute Inc., Cary, North Carolina, USA) to determine if any significant changes in oxygenation, interstitial fluid pressure, or blood flow relative to pre-irradiation levels could be detected among treatment groups. A summary of statistical findings is compiled in Appendix A.

Tumor Biopsies

Biopsies stored in refrigerated 4% paraformaldehyde were later embedded in paraffin wax, cut via microtome, and transferred onto slides for immunohistochemical staining. Staining of apoptotic cells was achieved using terminal nick end labeling (TUNEL), which enzymatically inserts bromodeoxyuridine onto the broken 3'-OH termini generated by endonucleases during apoptosis,[35] and of vascular endothelium using labeled anti-CD31 antibodies which attach to the CD-31 (a *PECAM* gene product) cell surface proteins expressed by endothelial cells and a few other cell types (including platelets and megakaryocytes).[36] Percent endothelial cell apoptosis could then be quantified for each biopsy collection time point in each dog.

Blood Samples

Blood samples taken at pre-irradiation, post-irradiation, 1, 2, 3, 24, and 48 hour time points were kept on ice in vacutainers until the earliest opportunity to be centrifuged. After centrifugation, plasma from the lavender top tubes and serum from the red top tubes were extracted and transferred to cryovials for storage at -80^{o}C. Plasma samples could then be thawed and diluted in deionized water for analysis using ion chromatography to determine nitrite and nitrate concentrations as long-lived biomarkers of endothelial-derived nitric oxide. Rat plasma samples spiked with known concentrations of sodium nitrite (Sigma-Aldrich, St. Louis, Missouri, USA) or sodium nitrate (Sigma-Aldrich, St. Louis, Missouri, USA) were used to construct the standard curves shown in Figures 3.12 and 3.13. Serum samples were intended for commercially available assays of ASMase activity (using the Acid Sphingomyelinase Activity Colorimetric Assay Kit by BioVision Inc., Milpitas, California, USA) and oxidative stress (using the TBARS Assay Kit by Cayman Chemical Co., Ann Arbor, Michigan, USA). Absorbance data from one of several attempts at the ASMase activity colorimetric assay is shown in Figure 3.14.

RESULTS

Clinical Trial Participants

Nine dogs between the ages of 9 and 13 years old (median 12 years) were enrolled in the clinical trial. Two of the enrolled dogs were Golden Retrievers, one was a Boston Terrier, one was a Standard Poodle, and six were of mixed breed. Three dogs were castrated males and six were spayed females, and all presented with superficially located soft tissue sarcomas (two Grade I, five Grade II, and two Grade III STS). Tumor volumes were highly variable, ranging from 36.44 cm^3 to 2,196.63 cm^3 (median 353.63 cm^3), as determined in contouring of gross tumor volume using Eclipse™ software. Characteristics of each dog are summarized in Table 3.2. Contrast uptake from the planning CT scans of each dog's tumor at the point where probes were placed (verified using positioning cone-beam CT scans) in the pre-contrast injection scan, arterial contrast influx phase, venous contrast efflux phase, and contrast at three minutes after injection are shown in Table 3.3.

Oxygenation

Pre-irradiation oxygen measurements in all three treatment groups varied tremendously among individuals. Linear regression analysis of pre-contrast CT values taken at the position of probe placement had a somewhat strong, negative correlation with pre-irradiation oxygen measurements once dogs with incorrectly placed probes were removed (Figure 3.15). Probe positioning highly influenced oxygen readings and care was taken to avoid regions of the tumor that were likely not tumor tissue, either having readings indicative of normoxic tissues (e.g. subcutaneous fat) or zero oxygen readings which occur in hemorrhagic or necrotic regions of tumor tissue. However, in one dog the probe was not long enough to reach tumor tissues below the subcutaneous fat layer, and oxygen measurements were accordingly high. In dogs treated

with a single fraction of 2 Gy, two categories of responses were observed. The first was a clinically significant decrease in oxygenation in a large tumor that was very well oxygenated prior to irradiation (belonging to "Sidney," see Figure 3.16). At no point did radiation exposure cause this tumor to become hypoxic. The other response observed in dogs treated with 2 Gy was a mild reoxygenation response, where oxygen levels either increased immediately or decreased slightly and recovered to a level of oxygenation that was higher than pre-irradiation by 48 hours. In the preliminary statistics conducted, none of the changes in oxygenation in the 2 Gy treatment group were considered significantly different from pre-irradiation values. The lack of statistical significance in spite of clearly observable changes from pre-irradiation values (see Figures 3.16 through 3.21) emphasizes the existence of tremendous variability in oxygenation levels within an individual tumor and among tumors belonging to different individuals. Such variability is known to be generated by mechanisms of acute and chronic hypoxia, and suggests that a much larger sample size should be studied in any effort to evaluate statistically significant changes in oxygenation.

Oxygen levels measured in tumors treated with a single fraction of 8 Gy showed a different response in each of the three dogs in that treatment group. First, a seemingly well-oxygenated tumor from "Simon" showed little change in partial pressure of oxygen following radiation therapy. Upon closer inspection of the cone-beam CT image taken to verify this dog's position for therapy, it was determined that the oxygen probe was not properly placed in tumor tissue due to inadequate length of the probe and instead lodged within a thick layer of subcutaneous fat (having negative Hounsfield units on CT, see Table 3.3) encapsulating the tumor parenchyma. Another tumor, verified as being placed in actual tumor tissue but having relatively high pre-irradiation oxygen levels, showed classic reoxygenation by twenty four hours

and even further reoxygenation at forty eight hours (see data for "Grunt" in Figure 3.18). The third tumor in this group showed very slight increases in oxygen levels within the first three hours relative to baseline (which were not statistically significant) but did not reoxygenate at longer time points (note data for "Piper" in Figures 3.18 and 3.19). Statistical results indicated that the one hour oxygen measurements taken in each dog in the 8 Gy treatment group were significantly decreased relative to baseline, but this outcome does not take into account the case of the misplaced probe.

Oxygen levels in tumors treated with a single fraction of 24 Gy all showed some degree of (statistically significant) increased oxygen at one or two hours post-treatment and decreased from there, showing no reoxygenation response and in some cases decreased oxygen levels at twenty four hours relative to pre-irradiation (Figures 3.20 and 3.21). In all three tumors oxygen levels increased slightly between twenty four and forty eight hours. The observed trend toward increased tumor oxygenation within one to two hours of irradiation followed by a decrease by three hours appeared to be consistent among all three dogs in this group and could not have been caused by endothelial cell apoptosis, which peaks at a later time point. Observations in this time frame, particularly the drop in oxygen levels between two and three hours, are of considerable interest and may be better explained by related studies of nitrite and nitrate quantification as a marker for nitric oxide bioavailability or assays of oxidative stress and ASMase activity.

Interstitial Fluid Pressure

Millar pressure transducer readings of interstitial fluid pressure allowed for observation of two different types of responses in tumor treated with a single fraction of 2 Gy. Two tumors in this group showed very little change in interstitial fluid pressure following irradiation (see data for "Tuli" and "Sassy" in Figures 3.22 and 3.23). One tumor, which was previously discussed as

being well oxygenated and large in size (approximately two liters in volume, as shown in Table 3.2), showed steady increases in pressure up to three hours post-irradiation before decreasing back to pre-irradiation levels by forty eight hours (see data for "Sidney" in Figures 3.22 and 3.23). In this case, a considerable amount of bleeding occurred upon puncture of the skin in an effort to collect biopsy samples, making it is possible that the observed increase in tumor interstitial fluid pressure was related to bleeding and clotting processes.

Tumors irradiated with a single fraction of 8 Gy either showed minimal change over the course of forty eight hours (see data for "Piper" and "Grunt" in Figures 3.24 and 3.25) or, in one case, increased steadily throughout the forty eight hour time period. As in the 2 Gy group, the tumor with continuously increasing interstitial fluid pressure also had normoxic oxygen readings and was in fact the dog in which the Oxylite^{TM} probe was immersed in fat. Whether or not the Millar pressure probe was also placed in fat is uncertain.

Interstitial fluid pressures of tumors treated with a single fraction of 24 Gy all showed decreased pressure at twenty four hours relative to pre-irradiation values, and possibly slight increases in pressure between twenty four and forty eight hours (Figure 3.26). Changes in interstitial fluid pressure within the three hour post-irradiation time frame seemed to be minimal (Figure 3.27).

Perfusion

Laser Doppler flow probe measurements are expressed in terms of percent tissue perfusion units and are under the assumption that the volume of tissue sampled has the appropriate optical properties such that light emission illuminates a tissue volume of 1 mm^3. This assumption has not been proven in canine soft tissue sarcomas, so all perfusion data is shown as percentages relative to pre-irradiation values (Figures 3.28 through 3.30). Blood flow

measurements were highly sensitive to motion artifacts caused by manipulation of the tumor or events of light anesthesia in which dogs may breathe out of sync with the respirator. All measurements showed waveforms characteristic of pulsing blood, indicating that observed flow was that of red blood cells through the tumor microvascular network. Few obvious trends in perfusion were detected within groups and a high degree in variability of responses was observed.

DISCUSSION

Classic reoxygenation in two of three tumors treated with 2 Gy was observed while the third tumor of the 2 Gy treatment group was well oxygenated to prior to radiation therapy and remained well oxygenated throughout the study. In a previous study monitoring oxygenation at 24 hours after 3 Gy, it was noted that well oxygenated tumors remained oxygenated.[25] In contrast, the oxygenation status of six out of seven tumors that were originally hypoxic (having partial pressure of oxygen measurements less than 10 mmHg) improved 24 hours after treatment with a dose of 3 Gy.[25] The measured tumor reoxygenation following 2 Gy is consistent with other reports of increased tumor oxygen levels during traditional, fractionated radiation therapy.[29-31]

Mixed responses in oxygenation of tumors in the 8 Gy treatment group (excluding data collected from "Simon," in which the oxygen probe was placed within subcutaneous fat) may be showing the summative effects of intermediate levels of endothelial cell dysfunction (possibly within a few hours of radiation exposure) and endothelial cell apoptosis (the more likely cause of observed changes at twenty four and forty eight hours). Other studies have measured counter-intuitive and mixed vascular responses to such "intermediate" doses; one study found increased

oxygen but decreased number of perfused vessels and unchanged radiobiologically hypoxic cell fraction in tumors twenty four hours after a single fraction treatment of 10 Gy.[32] While a dose threshold for endothelial cell apoptosis has been suggested as 8 to 10 Gy, apoptotic events have been shown increase with increasing dose (specifically from 12 to 14 to 15 Gy).[33,34] In order to cause appreciable effects in the microenvironment, it is possible that more endothelial cells must be induced to undergo apoptosis than the minimum threshold would cause. Since the studies determining the dose threshold for endothelial cell apoptosis made use of inbred mouse models,[33,34] it is also possible that variations in response are normal and to be expected based on genetic variability of individual members of more outbred populations (such as our canine subjects).

No reoxygenation effect was observed at twenty four hours in the 24 Gy treatment group. There was some variation in oxygen measurements between irradiation and two hours post-irradiation and oxygen was shown to decrease by twenty four hours with a slight and gradual recovery by forty eight hours. Decreased partial pressure of oxygen is linked to ischemic disease and free radical-mediated reperfusion injury, which could be a contributing factor to increased tumor cell kill following tumor microvascular dysfunction or endothelial cell death from high-dose irradiation. The observations of decreased partial pressure of oxygen at twenty four hours after 24 Gy is distinctly different from transient and inconsistent micro-fluctuations seen in partial pressure of oxygen during fractionated radiation therapy.[35]

Interstitial fluid pressures measurements in all tumors, before or after irradiation, resulted in high values characteristic of tumors as opposed to normal tissues, which have interstitial fluid pressures between -3 and 3 mmHg.[36] Interstitial fluid pressure measurements in two dogs, “Sidney” (possessing a well-oxygenated tumor treated with 2 Gy) and “Simon” (in which the

probes were likely placed within fatty tissues) were highly suspicious and may be excluded from future analyses. Otherwise, no obvious trends in interstitial fluid pressure were seen in the 2 and 8 Gy treatment groups. However, interstitial fluid pressure in all dogs belonging to the 24 Gy treatment group was decreased relative to pre-irradiation pressures after twenty four hours. While apoptotic events in endothelium and tumor parenchyma may occur as early as three to six hours after irradiation,[37] it may be possible that such acute vascular changes do not produce observable changes in total tumor microenvironment (specifically interstitial fluid pressure) for several more hours. Interstitial fluid pressure has been found to have a positive correlation with vessel segment length as well as vessel tortuosity,[38] and changes in vessel length and shape may not occur as quickly as endothelial cell dysfunction or apoptosis.

Analysis of tumor perfusion data produced no obvious trends. Each tumor seemed to tell a unique story. Such variation in pre-irradiation perfusion parameters and responses to irradiation may be indicative of rapid and intermittent changes in blood flow. Laser Doppler flowmetry has been used to measure high degrees of change in microregional blood flow; changes in magnitude by a factor of at least 1.5 were observed in 54% of the regions monitored over a 60 min period.[39] Constant, unpredictable fluctuations in blood flow may occur frequently within tumors and laser Doppler flowmetry at a single point in a tumor may not be the most appropriate method of evaluating large-scale changes in tumor perfusion. Magnetic resonance imaging (MRI) and electron paramagnetic resonance (EPR)-based methodologies may be more appropriate for the quantification of tumor perfusion and oxygenation.[40] Ultrasound methodologies utilizing Doppler principles could provide a superior alternative as well. Such methods were used in a study of normal pig parotid glands treated with 25 Gy in a single fraction, leading to the observation of rapidly decreased perfusion at four hours after irradiation

relative to unirradiated controls.[41] In the complex, post-irradiation tumor microenvironment multiple factors such as extravasation, changes in blood viscosity, or vascular collapse may influence perfusion in a small volume of the tumor, meaning larger volumes of irradiated tumor tissues should be evaluated.

CONCLUSIONS

The absence of a reoxygenation effect and presence of increased severity of hypoxia in tumors treated with a single fraction of 24 Gy indicates a difference in response to high doses as compared to the well-established reoxygenation response seen following the low doses used in traditional fractionated radiation therapy. Oxygen measurements in the 24 Gy group showed what could be a biphasic response, having sharp increases in partial pressure of oxygen at one to two hours after irradiation followed by a sharp decrease at three hours; responses that are unlikely to be caused by endothelial cell apoptosis, which should peak several hours later. Additional studies of the immediate response of vascular endothelium to single fraction high dose irradiation may determine whether endothelial cell dysfunction precedes apoptotic events and if so, the impact of radiation-induced endothelial cell dysfunction on tumor cell kill.

Interstitial fluid pressure measurements in tumors treated with 24 Gy showed similar decreases at twenty four hours after radiation therapy, which was also different from observations in tumors treated with 2 Gy. Canine soft tissue sarcomas treated with a single fraction of 8 Gy resulted in mixed responses, possibly due to an incomplete or variable damage response from being on the dose threshold of induction of endothelial cell apoptosis. Evaluation of perfusion using laser Doppler flowmetry was inconclusive and demonstrated overall that tumor perfusion is highly variable with respect to location and time.

Figure 3.1: "Maggie" the dog positioned for treatment of a large soft tissue sarcoma located on the caudal, left thigh treated with a single fraction of 20 Gy. The tumor has been shaved and marked for locations from which biopsies and oxygen measurements were taken before SRT, as well as 1, 2, 3, 4, 5, 12, 18, and 24 hours after SRT.

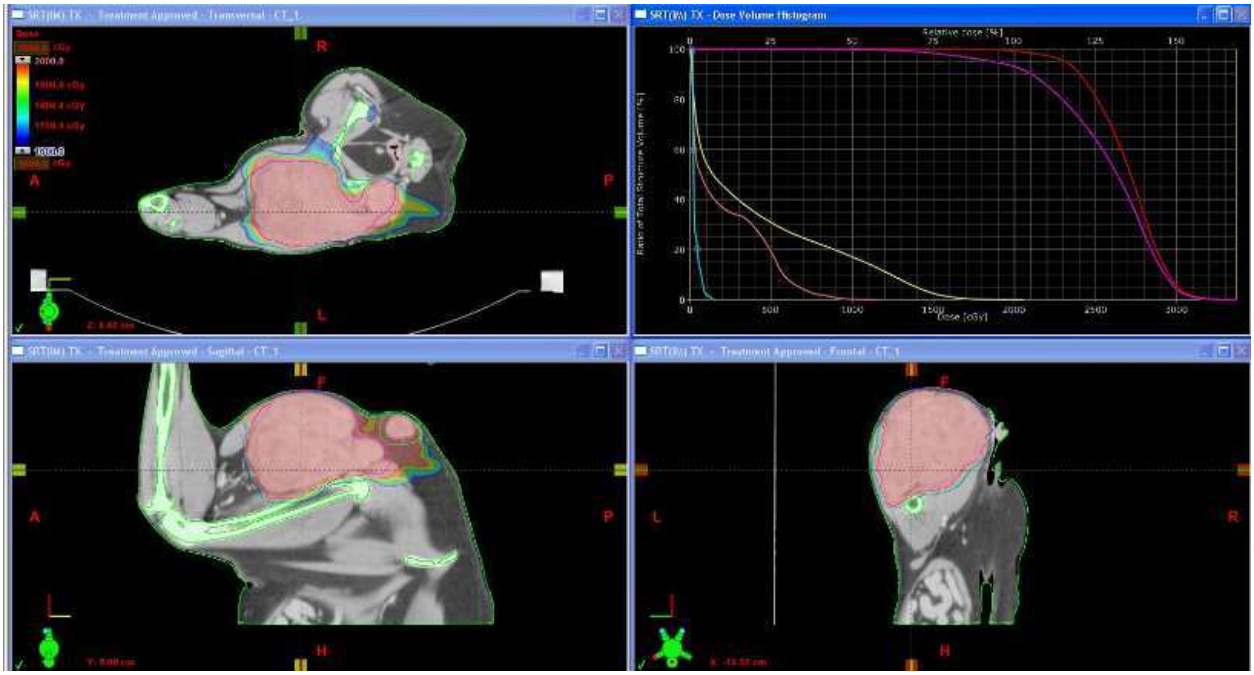

Figure 3.2: The treatment plan used to deliver 20 Gy in one fraction to a soft tissue sarcoma located on the caudal thigh of "Maggie" the dog. A dose color wash is shown over the gross tumor volume to note the steep dose drop off in tissues outside the demarcated tumor volume (top left and bottom images). The dose volume histogram (top right) illustrates percent of prescribed dose that would be delivered to volumes of tumor (GTV in red and CTV in pink) and to normal structures (skin in yellow, rectum in orange, and cauda equine in turquoise) in this plan.

Figure 3.3: Notable regression of the soft tissue sarcoma in “Maggie” the dog several months after SRT treatment with a single fraction of 20 Gy.

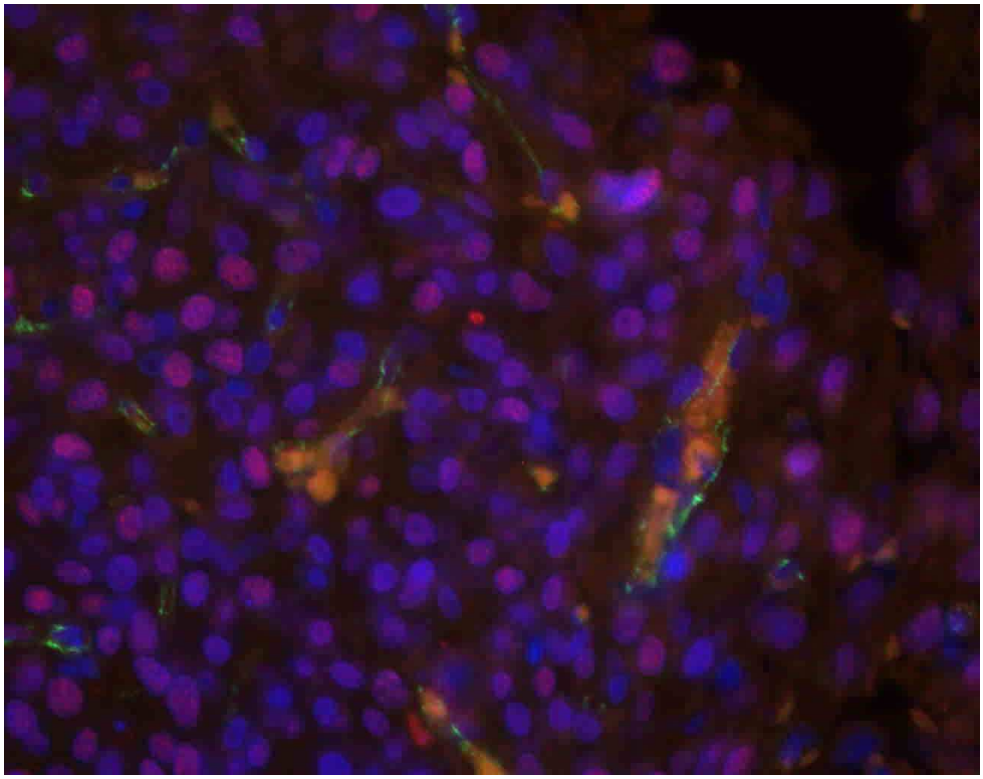

Figure 3.4: Immunofluorescence staining of CD-31 (green) for endothelial cells and TUNEL (red) for apoptotic cells with a DAPI nuclear stain (blue) in a paraffin embedded biopsy taken from a canine soft tissue sarcoma 5 hours after treatment with 20 Gy in one fraction in SRT. Overlapping green and red produces yellow colored regions of endothelial cell apoptosis.

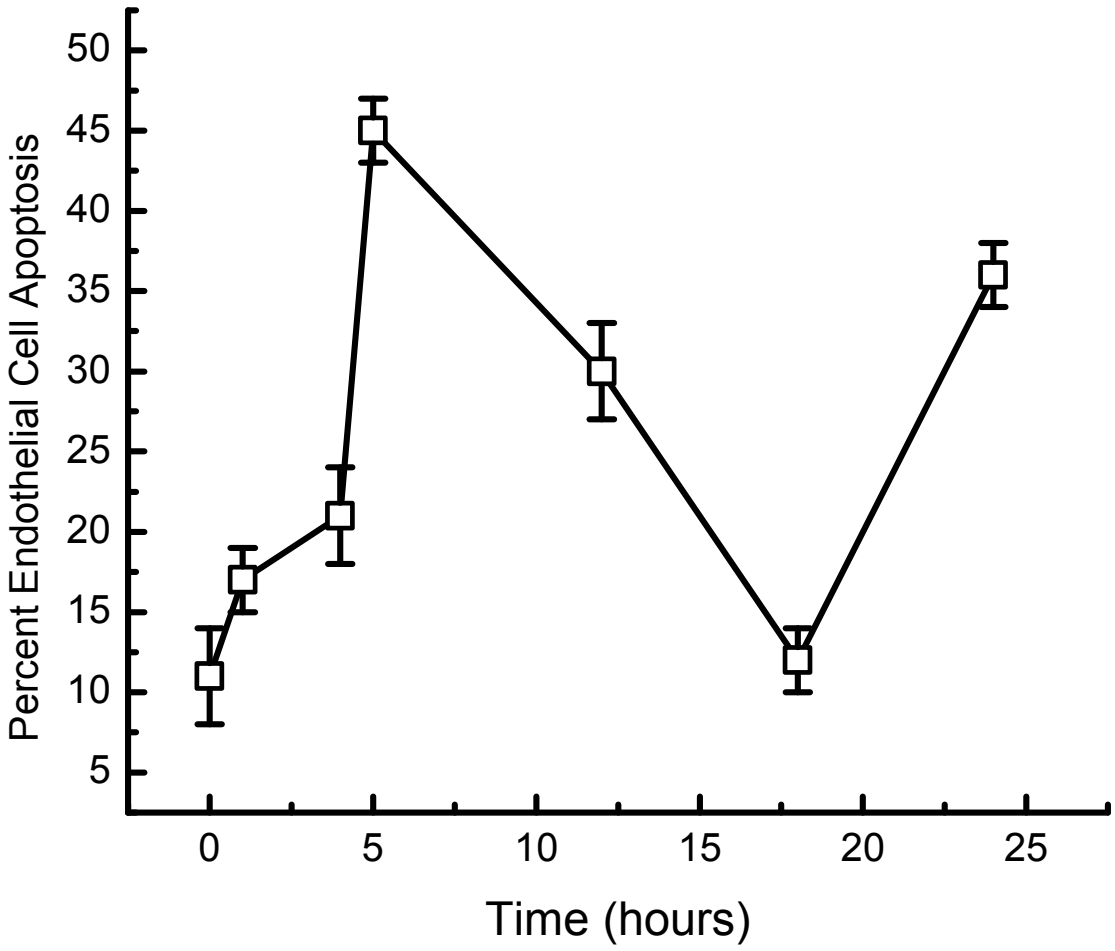

Figure 3.5: Percent of endothelial cells undergoing apoptosis as a function of time (zero time indicates pre-irradiation, or baseline endothelial cell apoptosis values) determined from immunofluorescence staining of vascular endothelium and TUNEL staining for apoptosis in biopsies taken from a canine soft tissue sarcoma treated with a single fraction of 20 Gy via SRT.

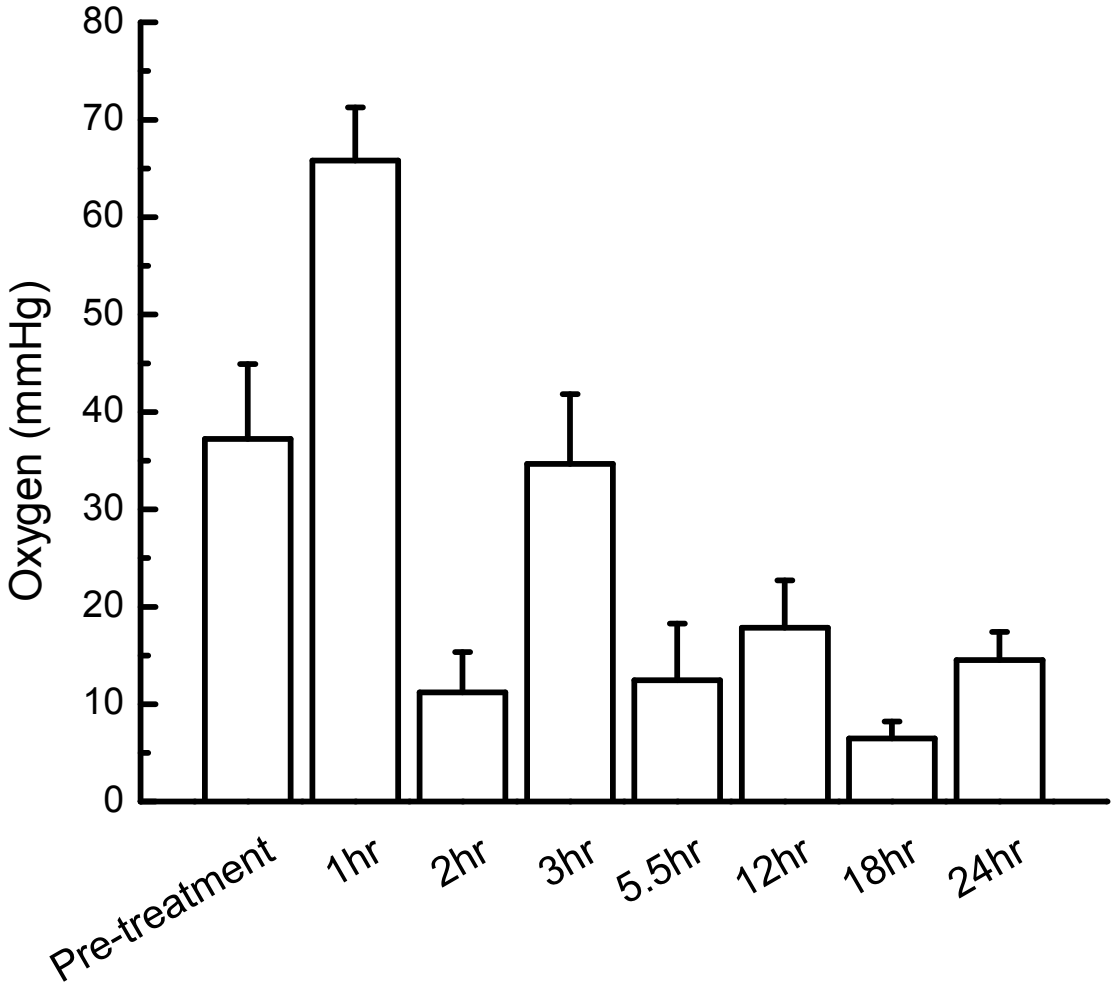

Figure 3.6: Preliminary results of oxygen measurements using an Oxylite™ probe inserted into a soft tissue sarcoma in one dog, "Maggie," at multiple time points before and after SRT with one fraction of 20 Gy. Oxygen decreased transiently around two hours after irradiation.

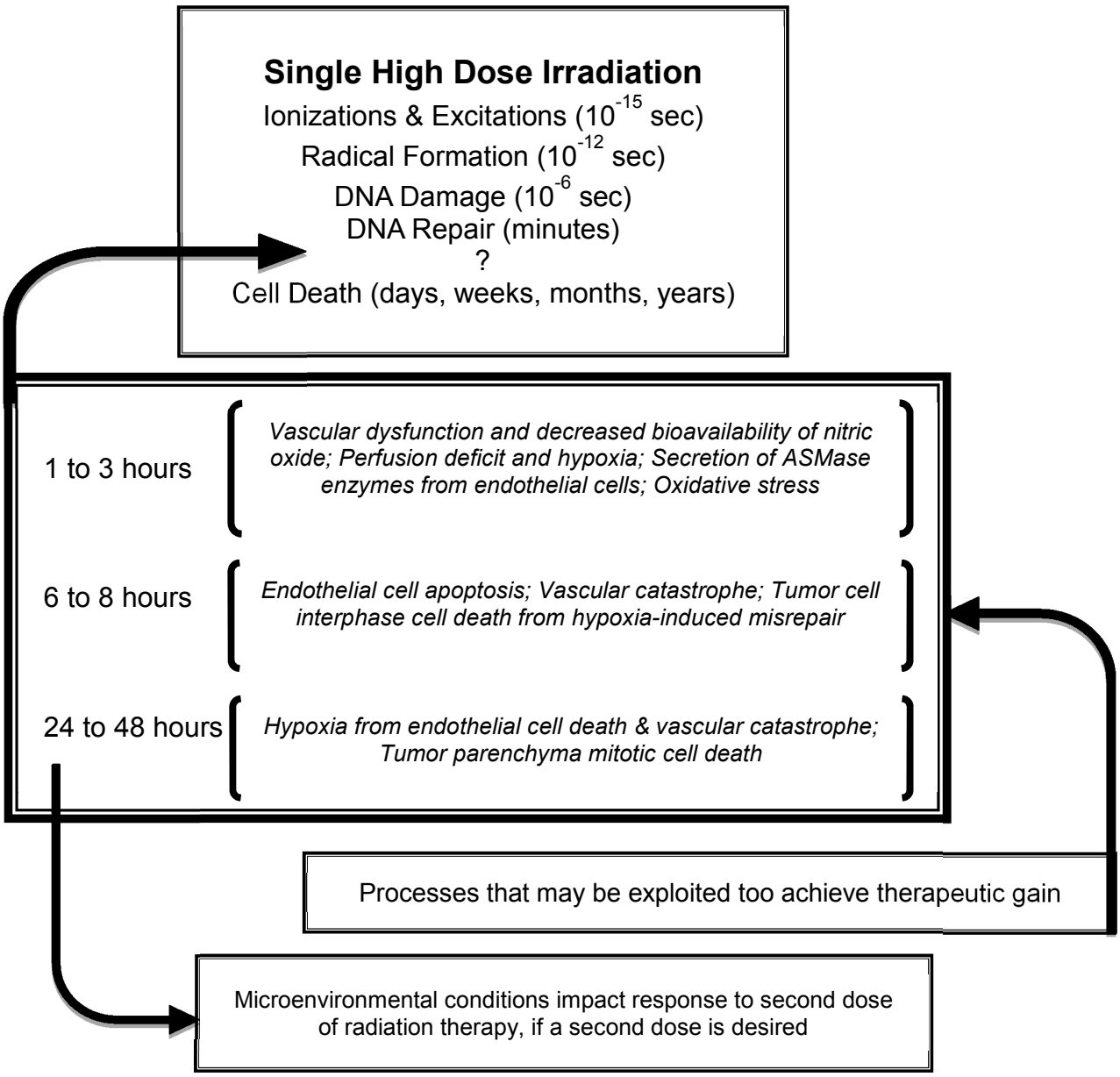

Figure 3.7: Biologic events following single high dose irradiation. Top box: Known physical and biologic events in all irradiated cells over the course of time. Bottom box: Hypothesized biologic events in tumors at certain times after single high dose irradiation. Of particular emphasis are the two phases of hypoxia: the 1 to 3 hour phase that could be caused by tumor microvascular dysfunction, and the 24 to 48 hour phase that could be due to endothelial cell death.

Table 3.1: Treatment plans for each dog were designed to deliver a prescribed dose of 24 Gy in one fraction. After randomization into 2, 8, or 24 Gy treatment groups, the dose delivered was adjusted for each individual. Doses delivered to 99% of the gross tumor volume (GTV) and to 95% of the planning treatment volume (PTV) before randomization are listed for each dog.

Dog (Treatment Group)	**Dose to 99% GTV (Gy)**	**Dose to 95% PTV (Gy)**
Sidney (2 Gy)	18.8763	19.9729
Sassy (2 Gy)	13.5501	16.7451
Tuli (2 Gy)	19.013	21.8961
Simon (8 Gy)	23.976	22.9871
Grunt (8 Gy)	16.9895	18.9729
Piper (8 Gy)	17.3293	17.8084
Wilkes (24 Gy)	18.7341	21.0969
Hoss (24 Gy)	18.3798	20.6389
Zena (24 Gy)	21.6022	23.2422

Table 3.2: Characteristics of SRT clinical trial participants: nine dogs with spontaneously occurring soft tissue sarcomas.

Dog	Dose (Gy)	Sex	Breed	Weight (kg)	Tumor Volume (cm^3)	Tumor Grade
Sidney	2	Female	Golden Retriever	28.6	2057.28	III
Tuli	2	Female	Mix	21.8	353.63	III
Sassy	2	Female	Mix	16.7	36.44	II
Simon	8	Male	Golden Retriever	29.0	909.31	II
Piper	8	Female	Mix	30.0	1772.94	II
Grunt	8	Female	Mix	27.0	103.15	I
Zena	24	Female	Mix	25.6	88.61	I
Hoss	24	Male	Boston Terrier	10.1	63.84	II
Wilkes	24	Male	Standard Poodle	33.7	2196.63	II

Table 2.3: Hounsfield units from planning CT scans before administration of contrast agent, in the arterial phase of contrast influx, in the venous phase of contrast efflux, and at three minutes after contrast enhancement at the location in soft tissue sarcomas where probes would later be placed. Contrast enhancement was not performed for Hoss and the Hounsfield units of Simon reflect probe placement within a fat layer rather than in tumor tissues.

Dog Name (Treatment Group)	**Pre-Contrast (HU)**	**Arterial Phase (HU)**	**Venous Phase (HU)**	**3 min Post-Contrast (HU)**
Sidney (2 Gy)	32.33	42.29	47.24	60.9
Tuli (2 Gy)	31.07	29.04	28.7	31.54
Sassy (2 Gy)	42.76	64.11	90.46	116.05
Simon (8 Gy)	-76.49	-71.95	-94.36	-92.79
Piper (8 Gy)	34.37	44.17	57.99	67
Grunt (8 Gy)	18.78	21.17	41.8	64.57
Zena (24 Gy)	30.62	56.67	91.14	104.88
Hoss (24 Gy)	53.04	---	---	69.64
Wilkes (24 Gy)	40.27	52.22	62.81	67.87

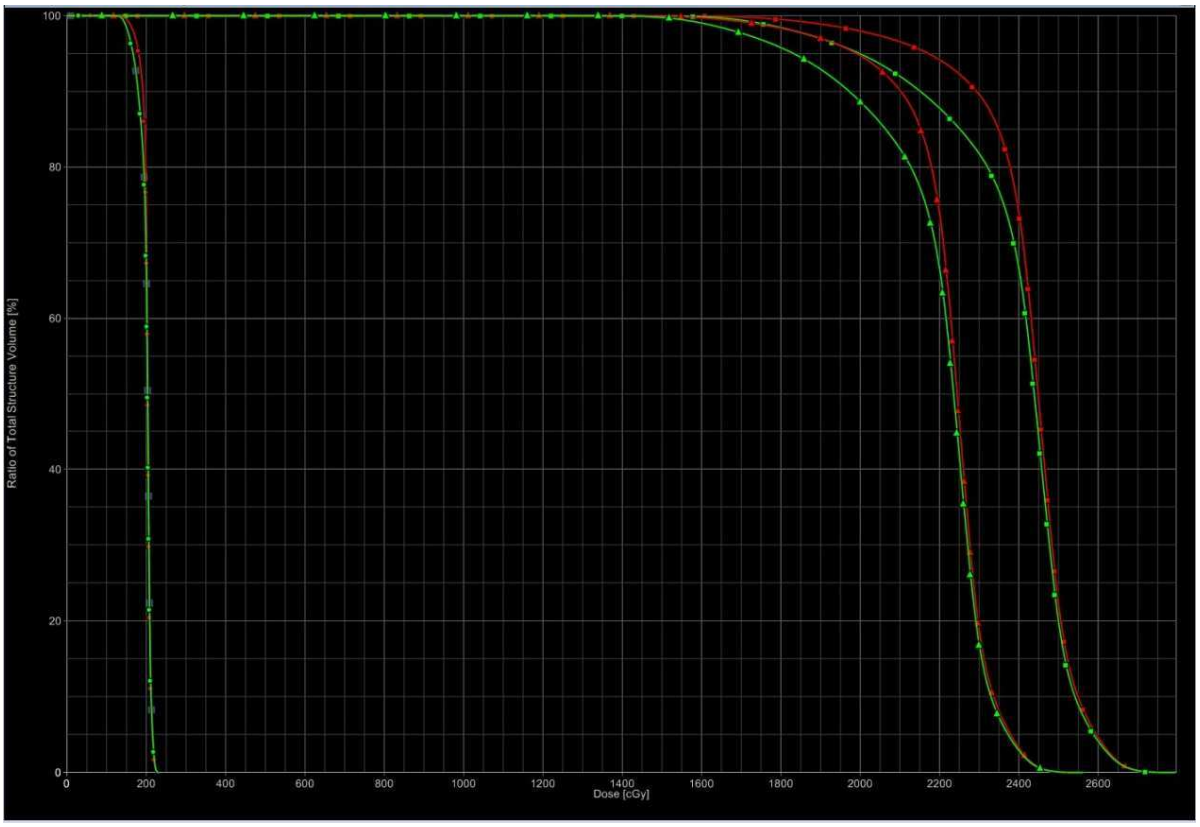

Figure 3.8: Dose volume histograms representing the treatment plan of soft tissue sarcoma-bearing dogs treated with 2 Gy for vascular response evaluation and followed up with 22 Gy after measurements were taken. Red lines represent dose to the gross tumor volume (GTV) and green lines represent dose to the planning target volume (PTV). All treatment plans were developed with the ability of delivering 24 Gy and scaled down appropriately for each case depending on the treatment group into which they were randomized.

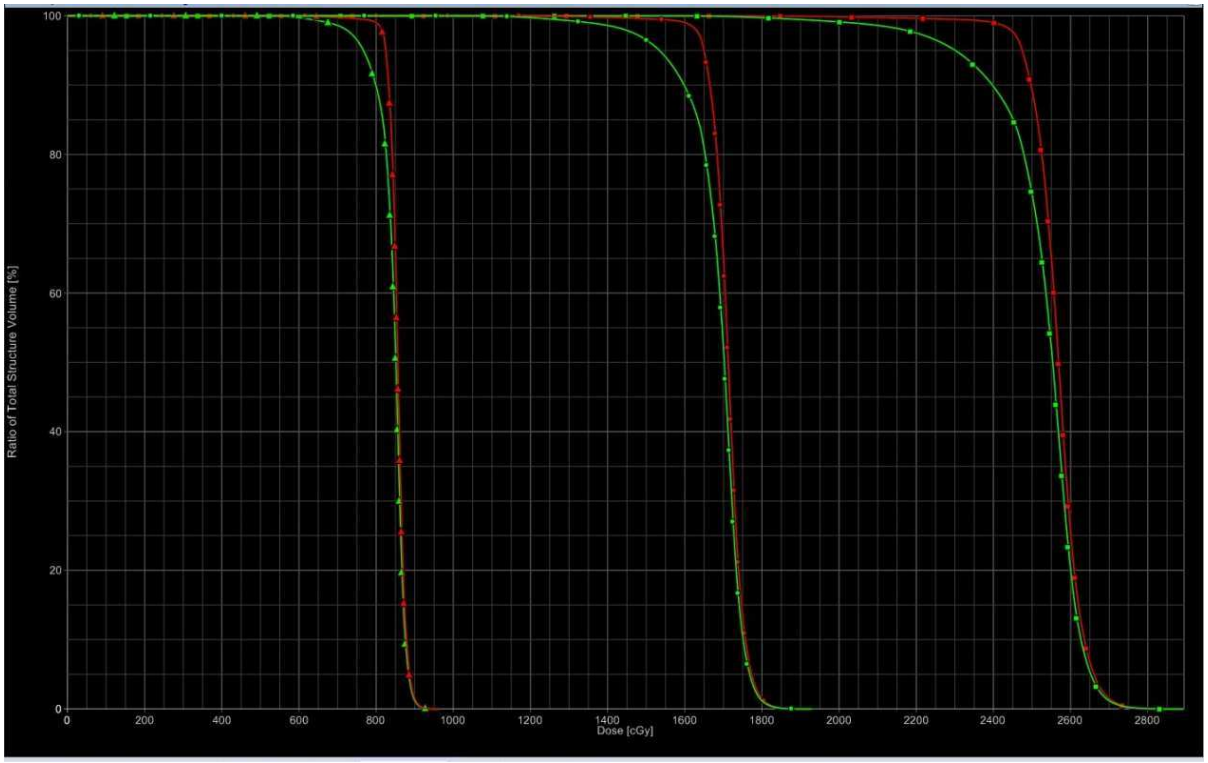

Figure 3.9: Dose volume histograms representing the treatment plan of soft tissue sarcoma-bearing dogs treated with 8 Gy for vascular response evaluation and followed up with 16 Gy after measurements were taken. Red lines represent dose to the gross tumor volume (GTV) and green lines represent dose to the planning target volume (PTV). All treatment plans were developed with the ability of delivering 24 Gy and scaled down appropriately for each case depending on the treatment group into which they were randomized.

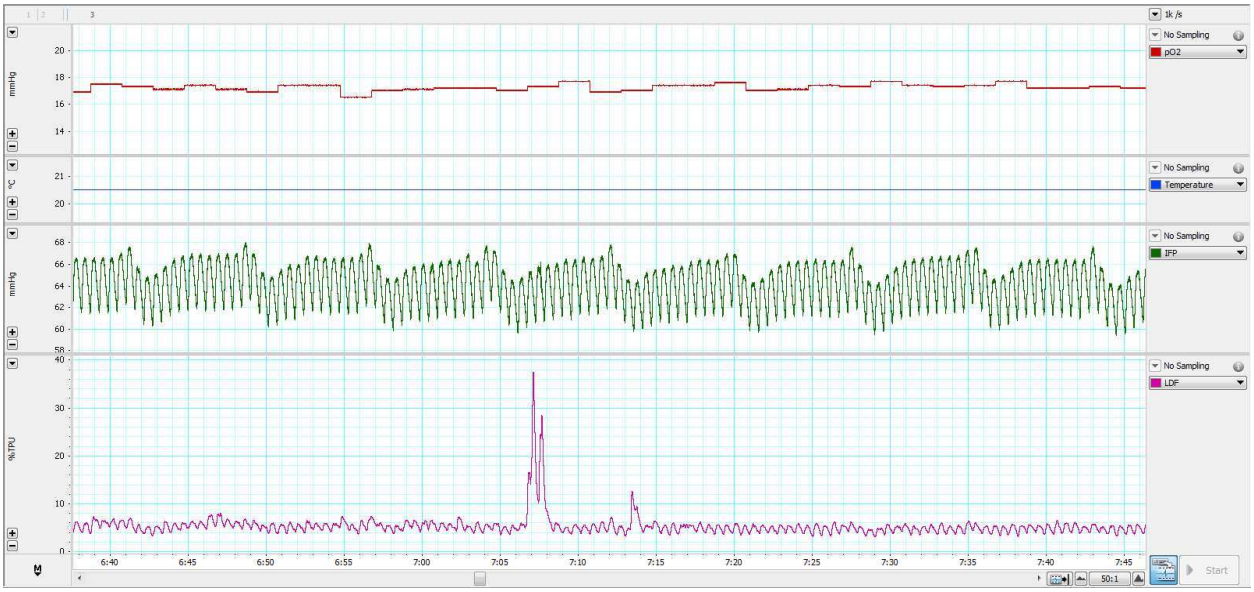

Figure 3.10: Typical data for about one minute of data collection for partial pressure of oxygen (top, in red), interstitial fluid pressure (green), and blood flow (bottom, in pink) in a canine soft tissue sarcoma. Note the large motion artifacts in laser Doppler measurements of blood flow.

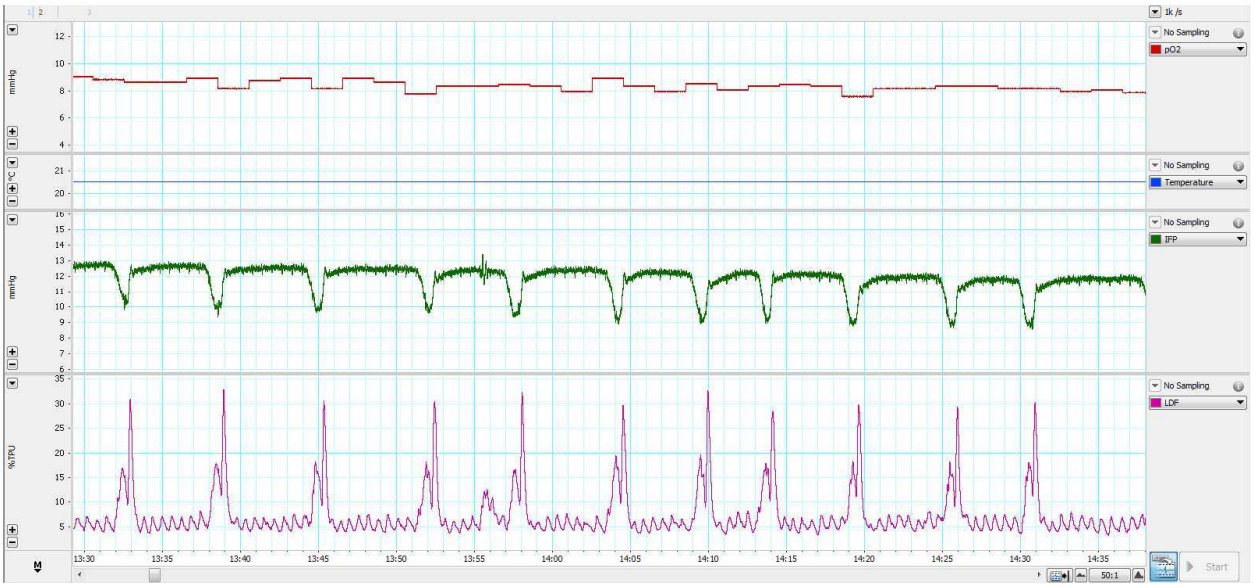

Figure 3.11: Typical data for about one minute of data collection for partial pressure of oxygen (top, in red), interstitial fluid pressure (green), and blood flow (bottom, in pink) in a canine soft tissue sarcoma. Note that different tumors may show different waveforms, which may be dependent on the proximity of the probes to larger vessels, clots, or capillary beds.

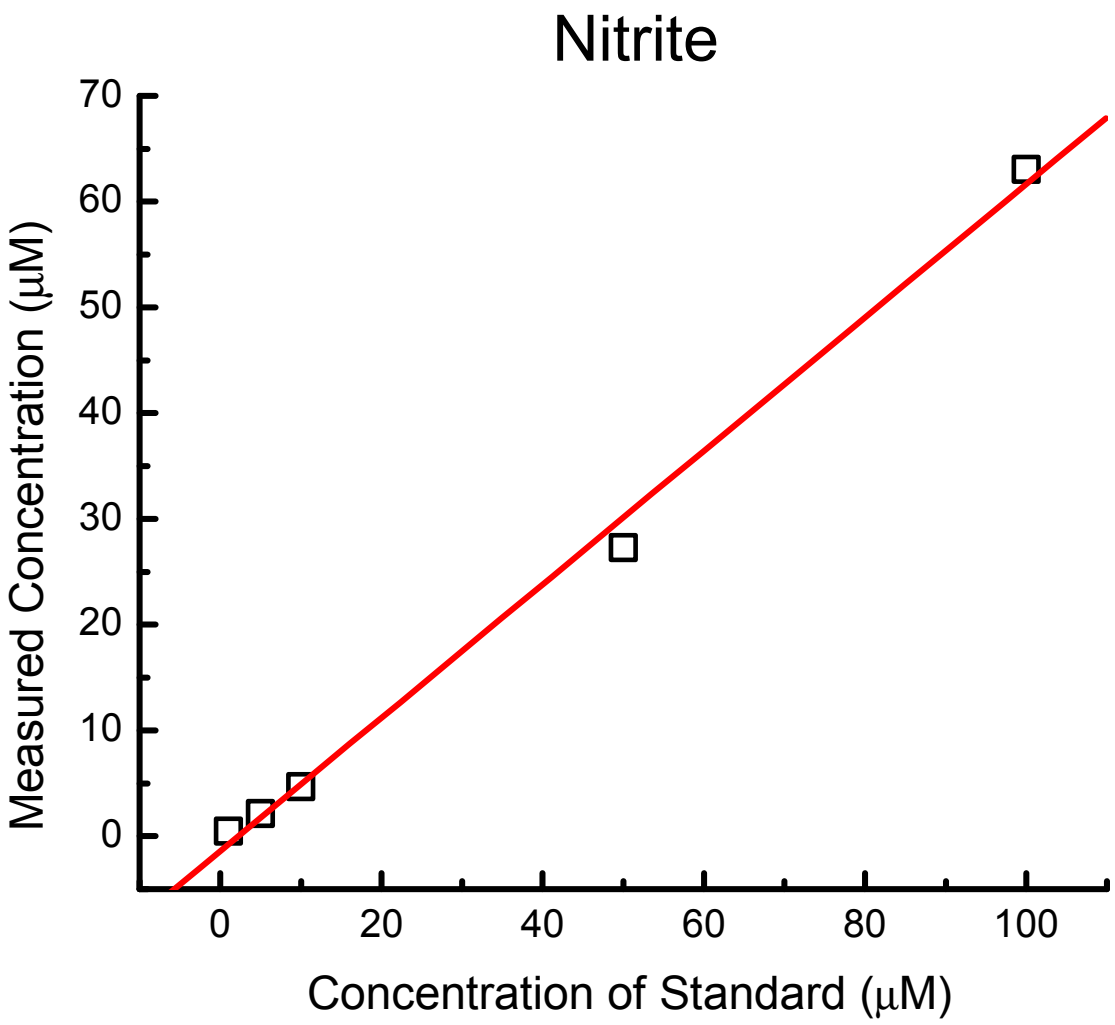

Figure 3.12: Standard curve for nitrite measurements in plasma using ion chromatography. Fitted linear regression analysis produced an R^2 value of 0.9959.

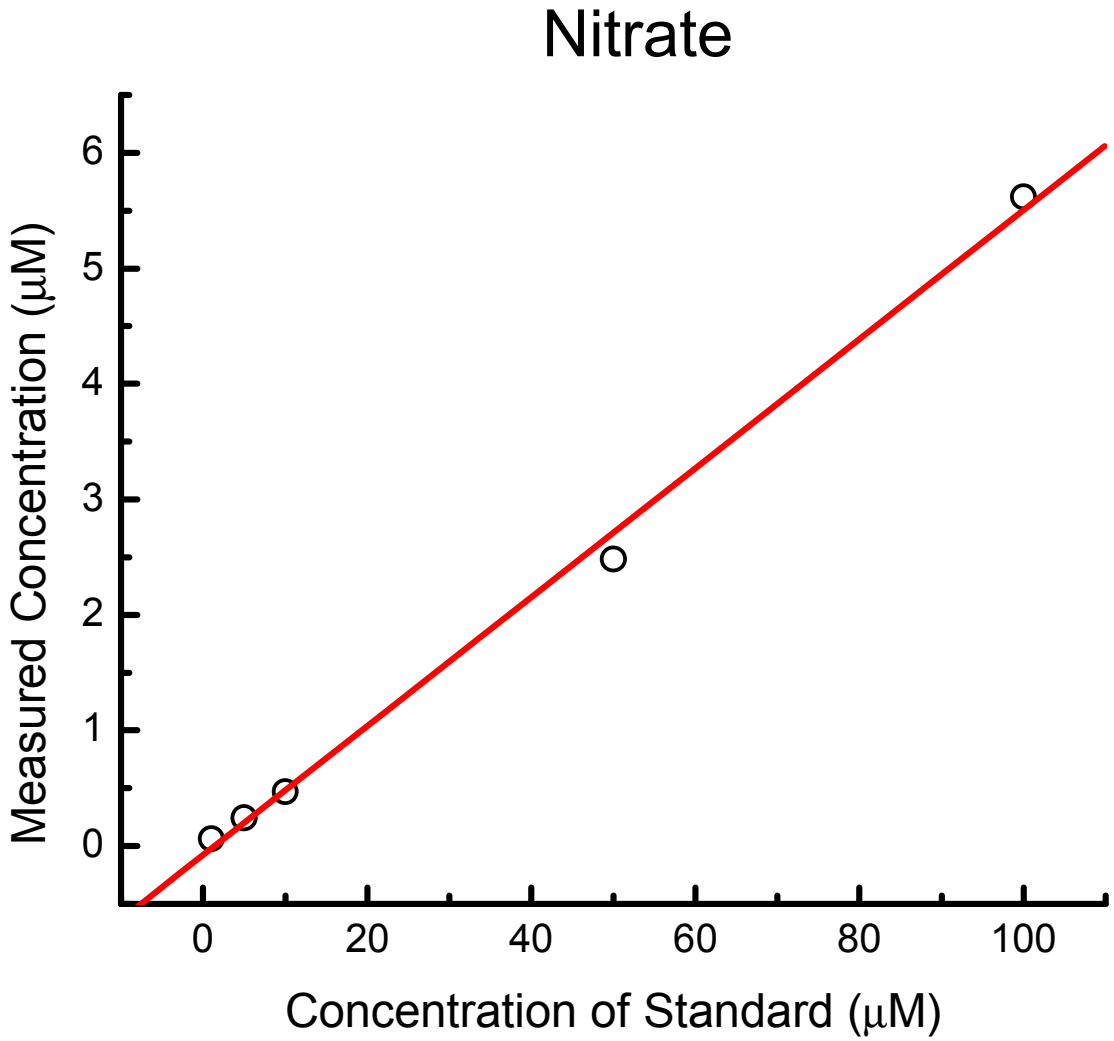

Figure 3.13: Standard curve for nitrate measurements in plasma using ion chromatography. Fitted linear regression analysis produced an R^2 value of 0.9966.

	1	2	3	4	5	6	7	8	9	10	11	12
A	0.083	0.138										
B	0.062	0.052	0.053	0.085	0.083	0.068	0.075	0.063	0.069			
C	0.062	0.051	0.052	0.115	0.055	0.058	0.109	0.061	0.061	2.200	1.407	2.028
D	0.093	0.053	0.050	0.113	0.064	0.054	0.072	0.067	0.075	1.487	1.827	1.554
E	0.059	0.076	0.056	0.080	0.058	0.054	0.092	0.065	0.064	1.281	1.108	1.288
F	0.096	0.053	0.058	0.108	0.105	0.090	0.068	0.064	0.056	1.353	0.754	0.802
G	0.065	0.058	0.051	0.104	0.077	0.057	0.096	0.082	0.064	1.203	0.482	0.445
H	0.062	0.064	0.058	0.102	0.094	0.090	0.077	0.080	0.085	0.048	0.052	0.347

Figure 3.14: Preliminary results of ASMase enzyme activity in dog serum. The colormetric assay was found to lack active enzyme in their proprietary mixtures, as evidenced by a failure of the positive controls in wells A1 and A2 to produce expected absorbances of 0.1 to 0.5. Wells in columns 10, 11 and 12 were standard curves and wells in columns 1 through 9 (excluding the positive controls in row A) were samples run in triplicate for three different dogs at pre-irradiatoin, post-irradiation, 1 hour, 2 hours, 3 hours, 24 and 48 hour time points.

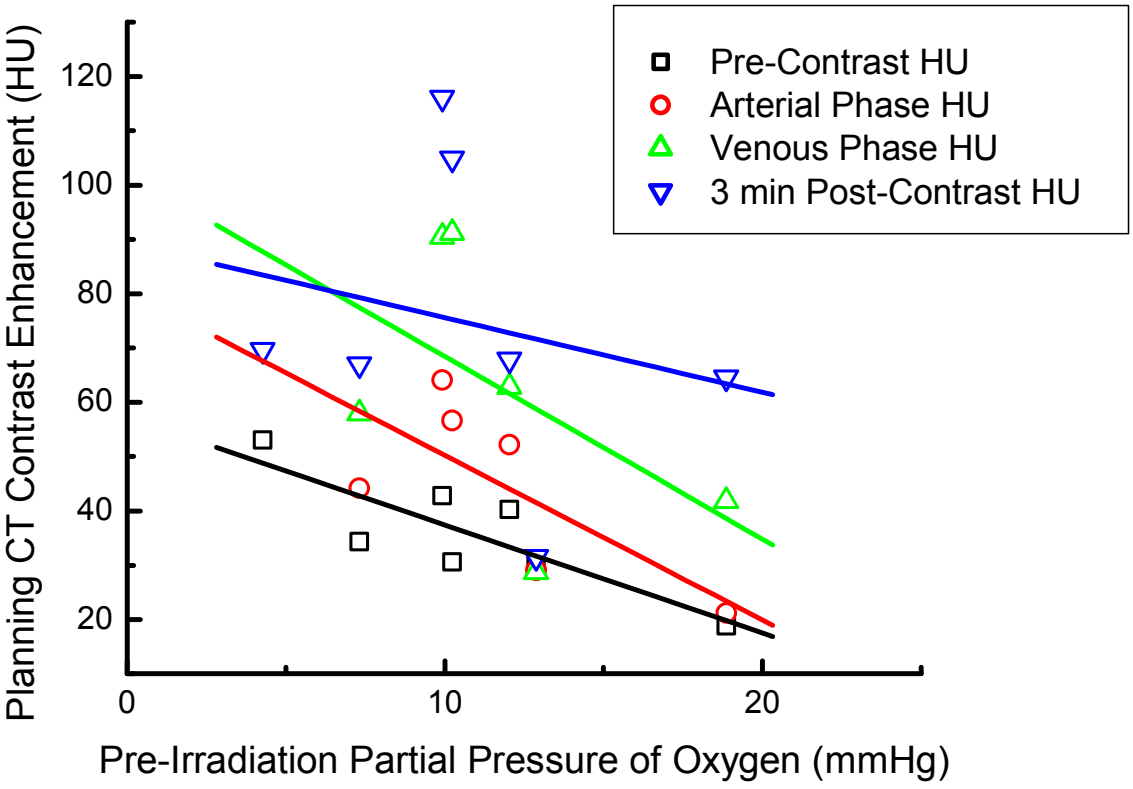

Figure 3.15: Planning CT values at the point of probe placement versus pre-irradiation oxygen measurements. There was a somewhat strong, negative correlation ($R^2 = 0.7108$) between pre-contrast HU and pre-irradiation partial pressure of oxygen, as measured by Oxylite probes, and weaker correlations with other phases of contrast enhancement.

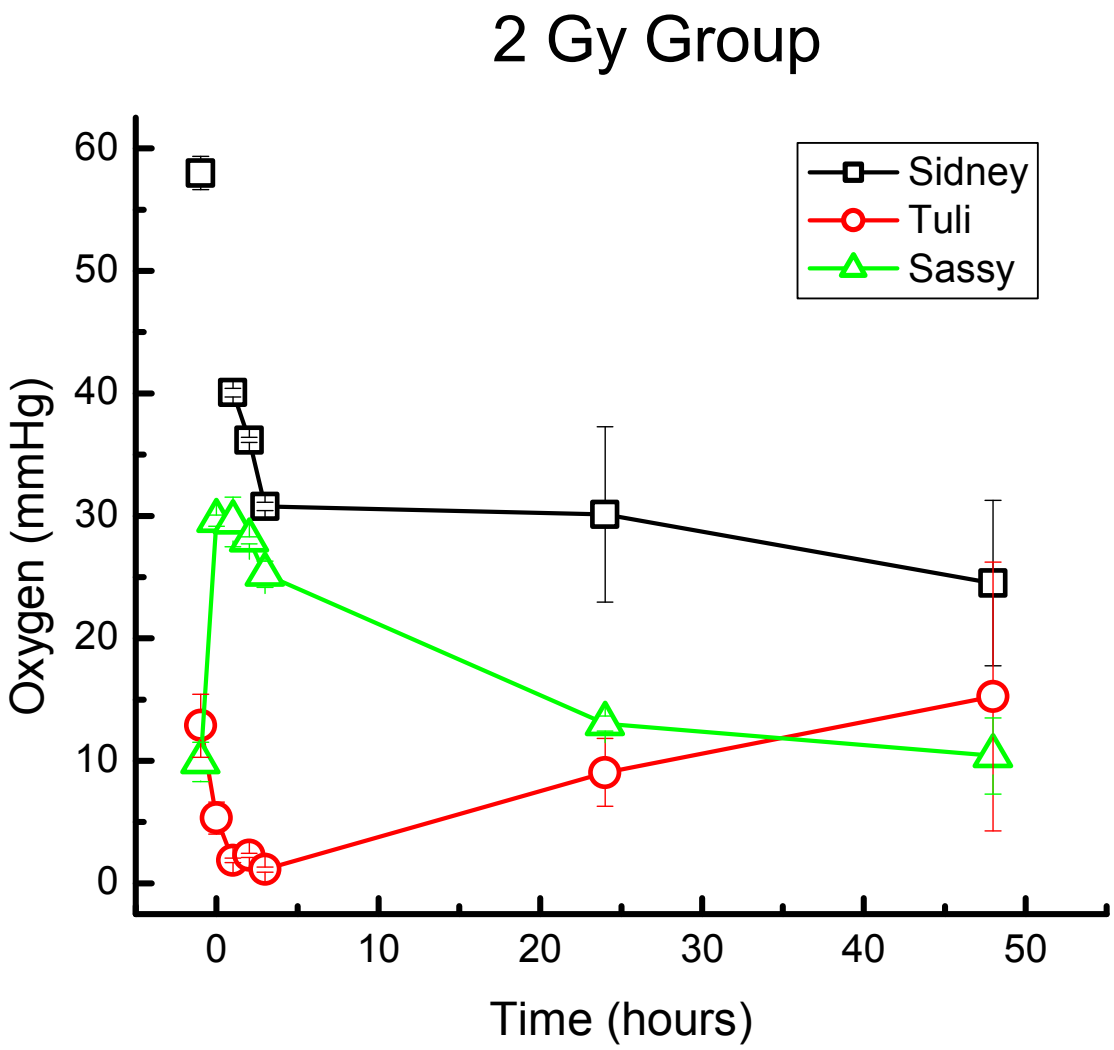

Figure 3.16: Oxygen measurements versus time in three canine soft tissue sarcomas treated with a single fraction of 2 Gy. Pre-irradiation measurements were designated a time of -1 hours and measurements at 0 hours were taken immediately after dose delivery was completed.

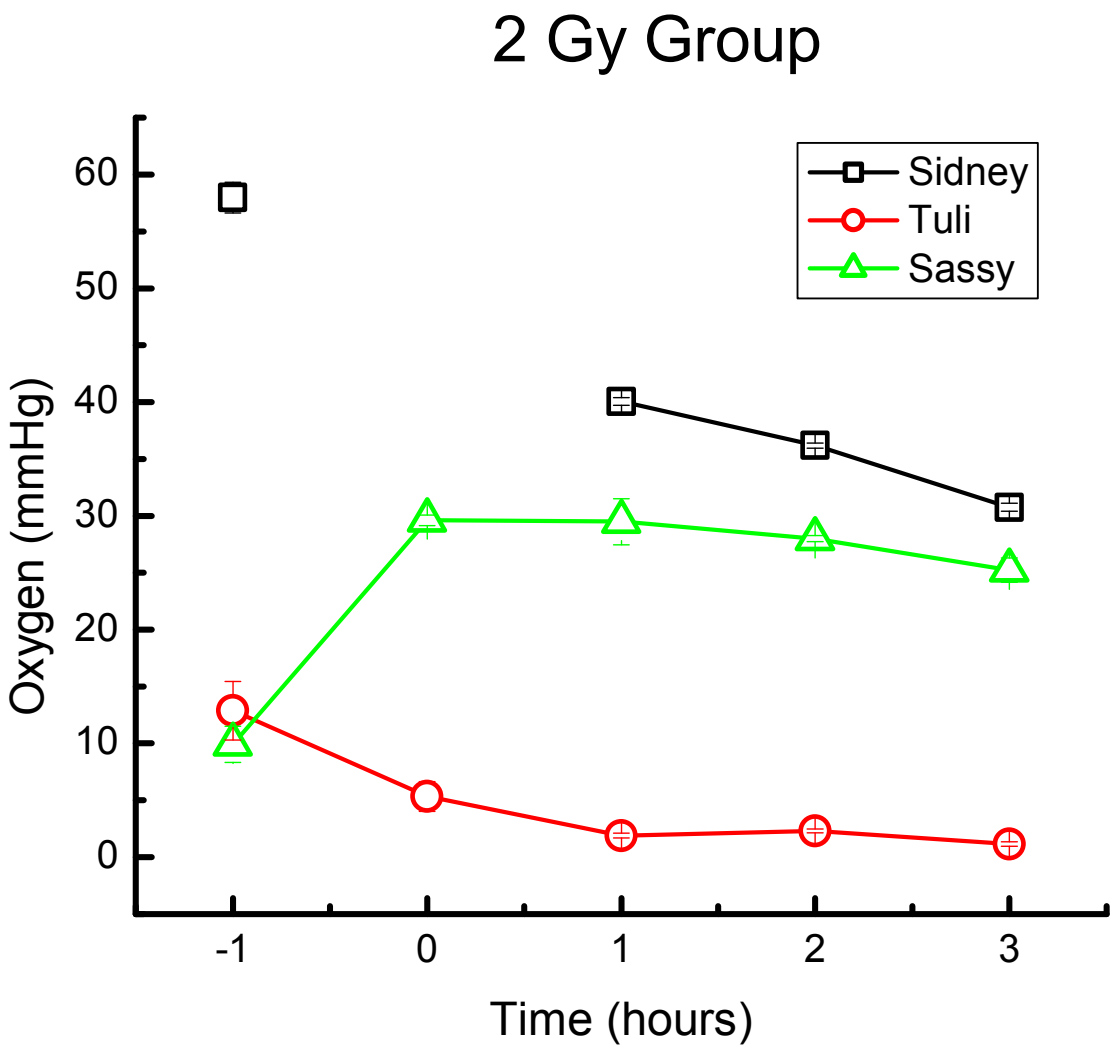

Figure 3.17: Oxygen measurements versus time in three canine soft tissue sarcomas treated with a single fraction of 2 Gy, with a focus on the first three hours post-irradiation (during which time probes were not repositioned).

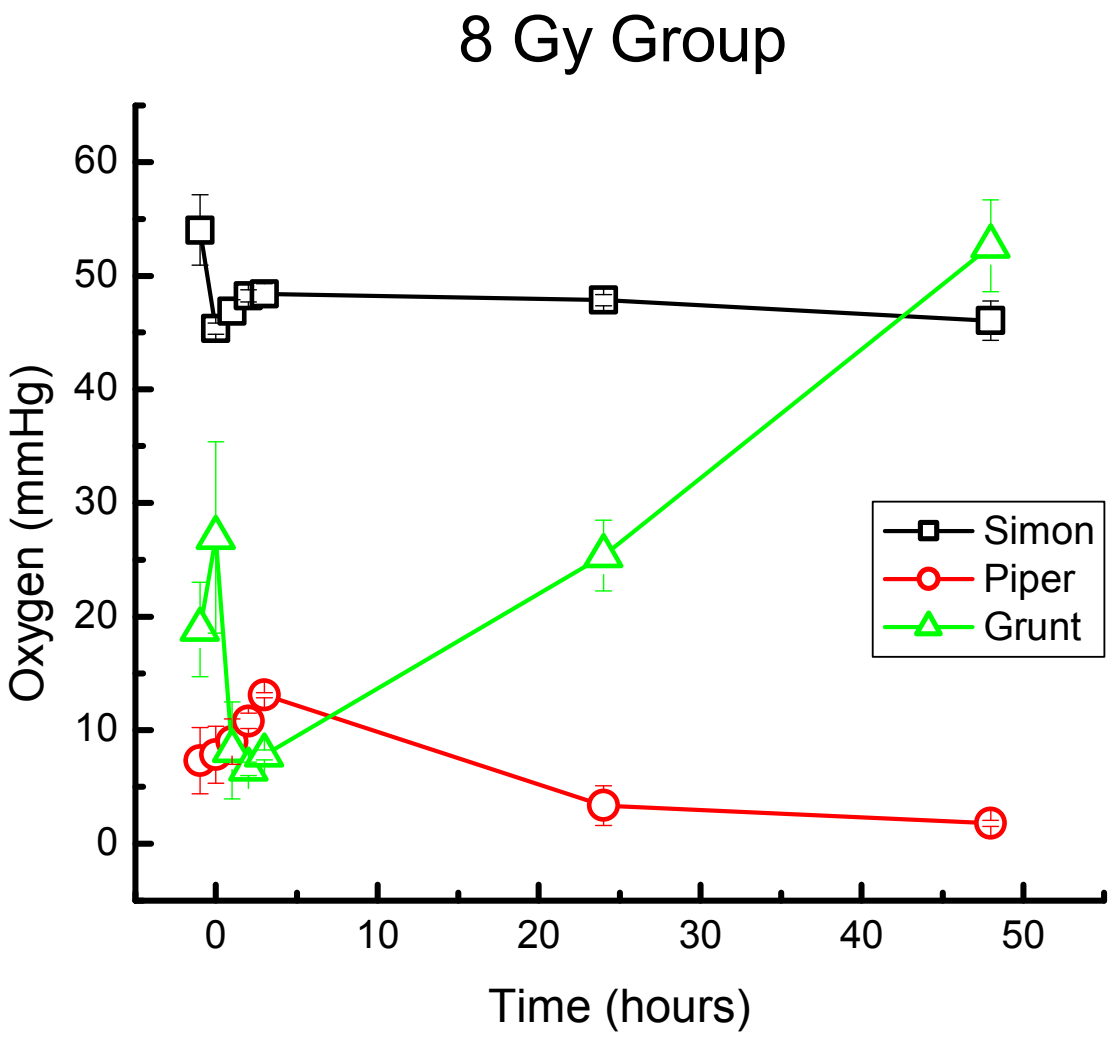

Figure 3.18: Oxygen measurements versus time in three canine soft tissue sarcomas treated with a single fraction of 8 Gy. Pre-irradiation measurements were designated a time of -1 hours and measurements at 0 hours were taken immediately after dose delivery was completed.

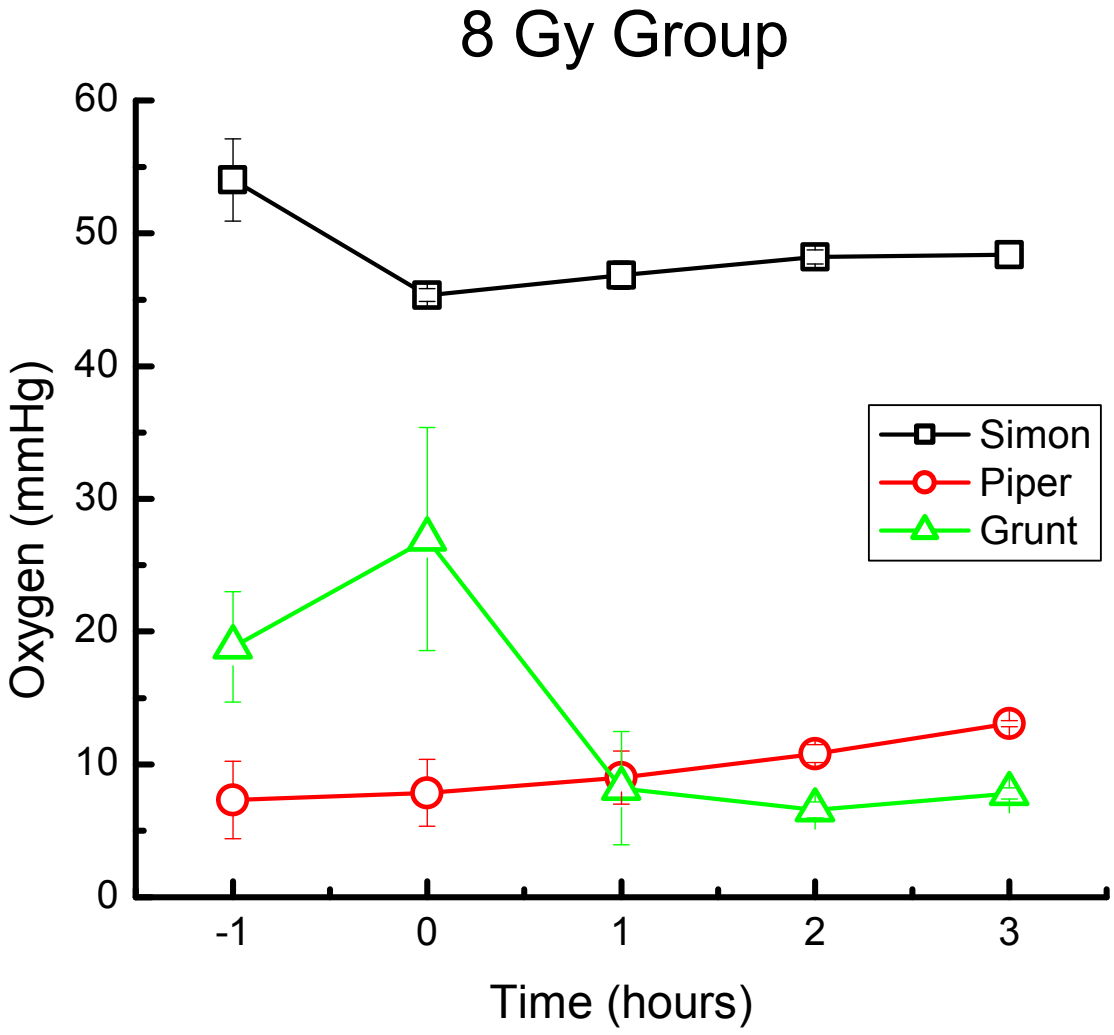

Figure 3.19: Oxygen measurements versus time in three canine soft tissue sarcomas treated with a single fraction of 8 Gy, with a focus on the first three hours post-irradiation (during which time probes were not repositioned).

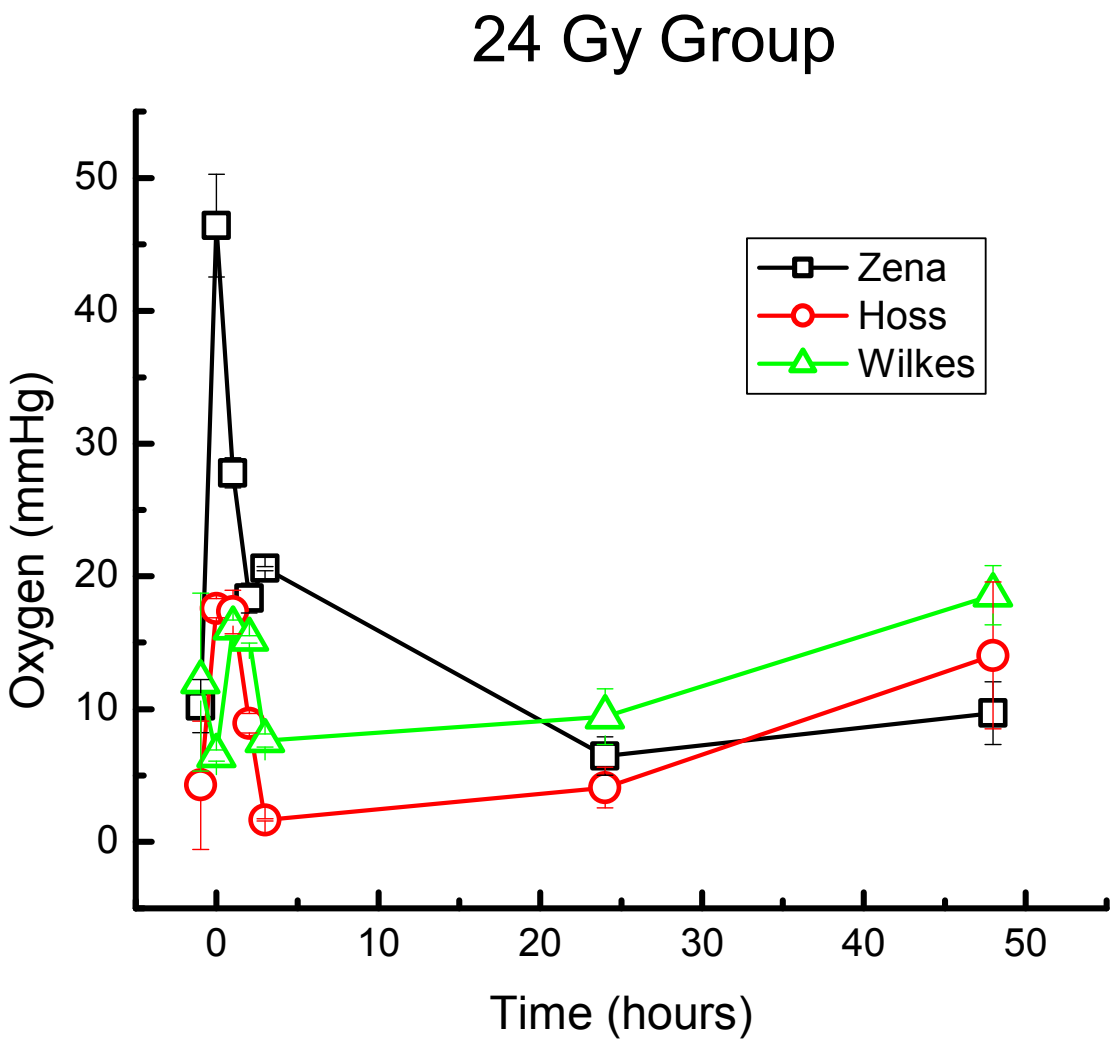

Figure 3.20: Oxygen measurements versus time in three canine soft tissue sarcomas treated with a single fraction of 24 Gy. Pre-irradiation measurements were designated a time of -1 hours and measurements at 0 hours were taken immediately after dose delivery was completed.

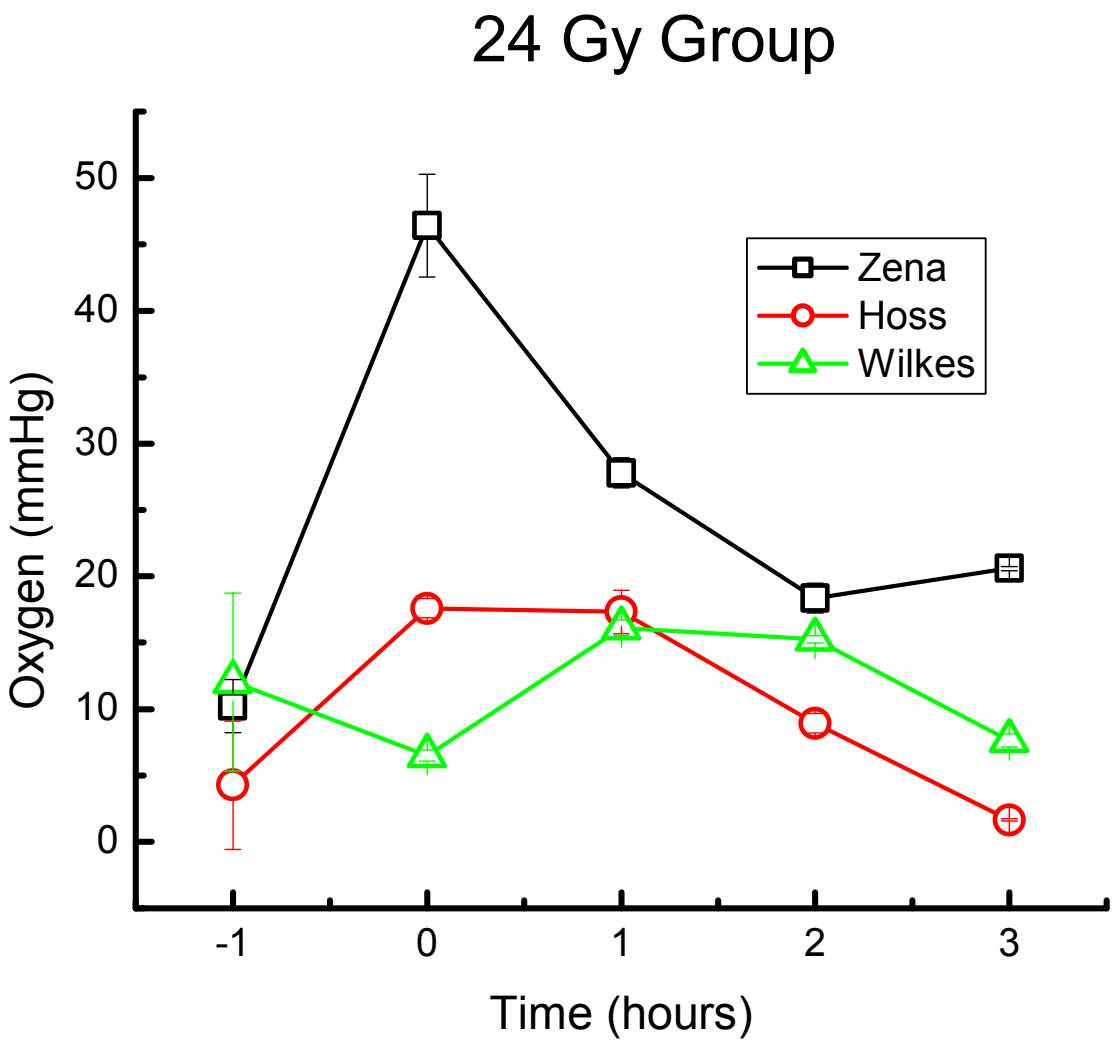

Figure 3.21: Oxygen measurements versus time in three canine soft tissue sarcomas treated with a single fraction of 24 Gy, with a focus on the first three hours post-irradiation (during which time probes were not repositioned).

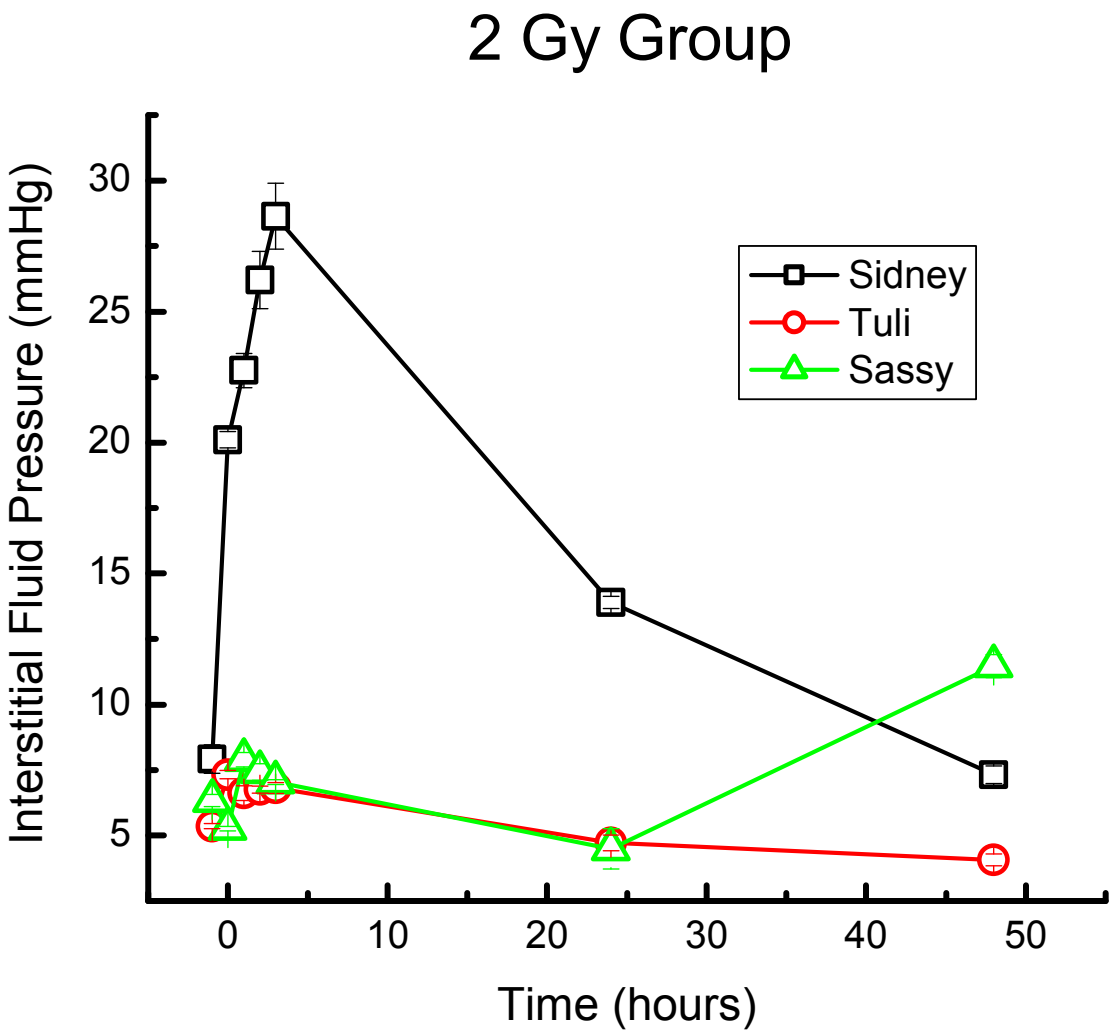

Figure 3.22: Interstitial fluid pressure measurements versus time in three canine soft tissue sarcomas treated with a single fraction of 2 Gy.

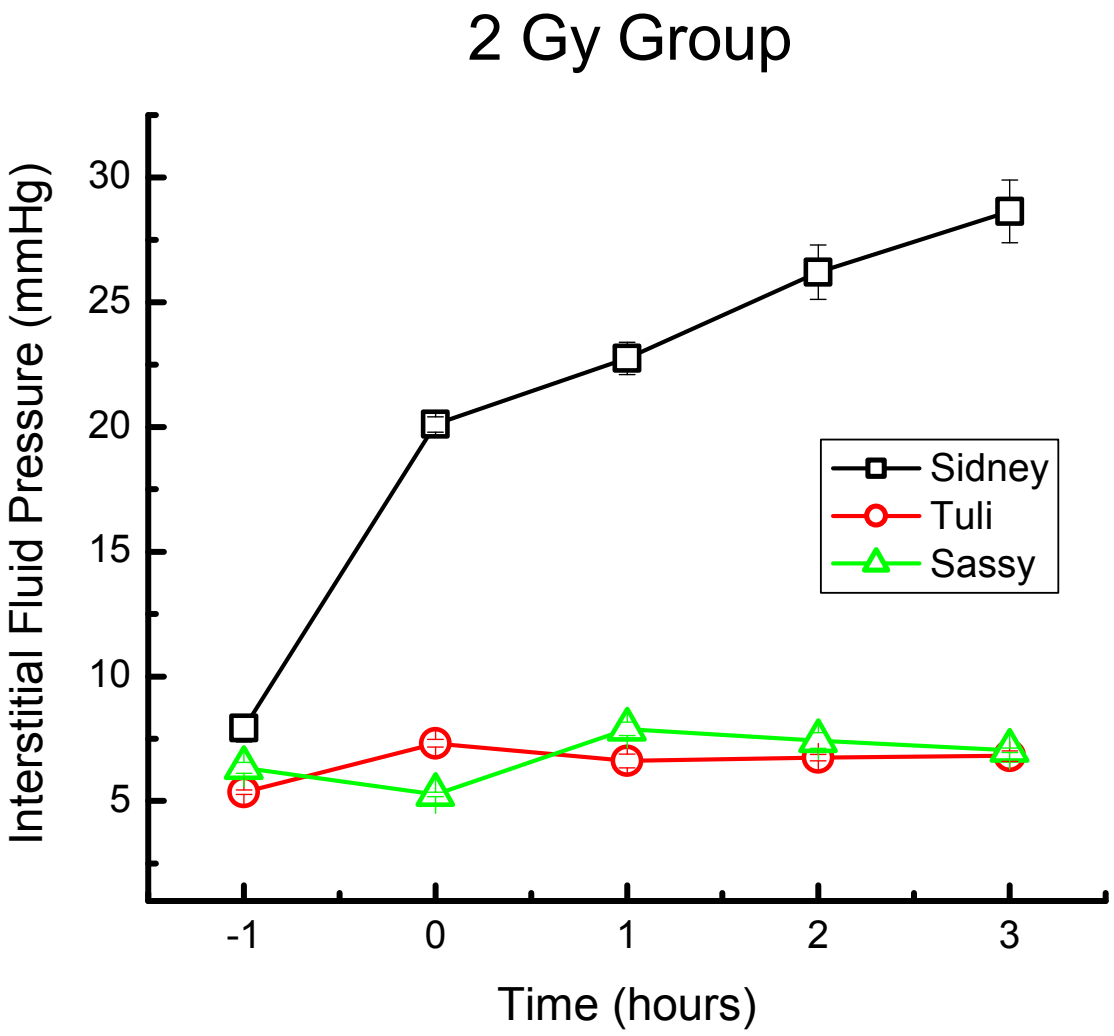

Figure 3.23: Interstitial fluid pressure measurements versus time in three canine soft tissue sarcomas treated with a single fraction of 2 Gy in the first three hours post-irradiation.

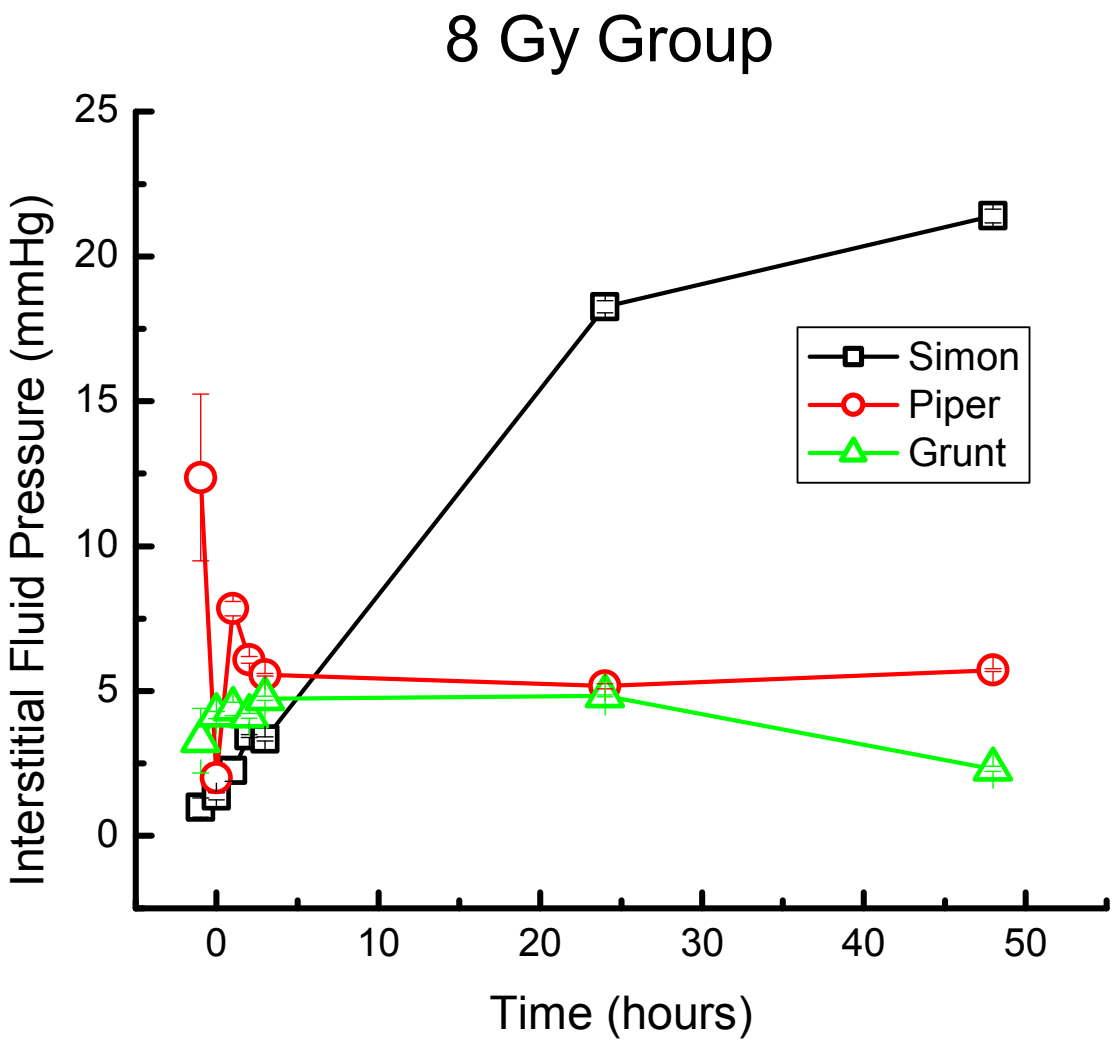

Figure 3.24: Interstitial fluid pressure measurements versus time in three canine soft tissue sarcomas treated with a single fraction of 8 Gy.

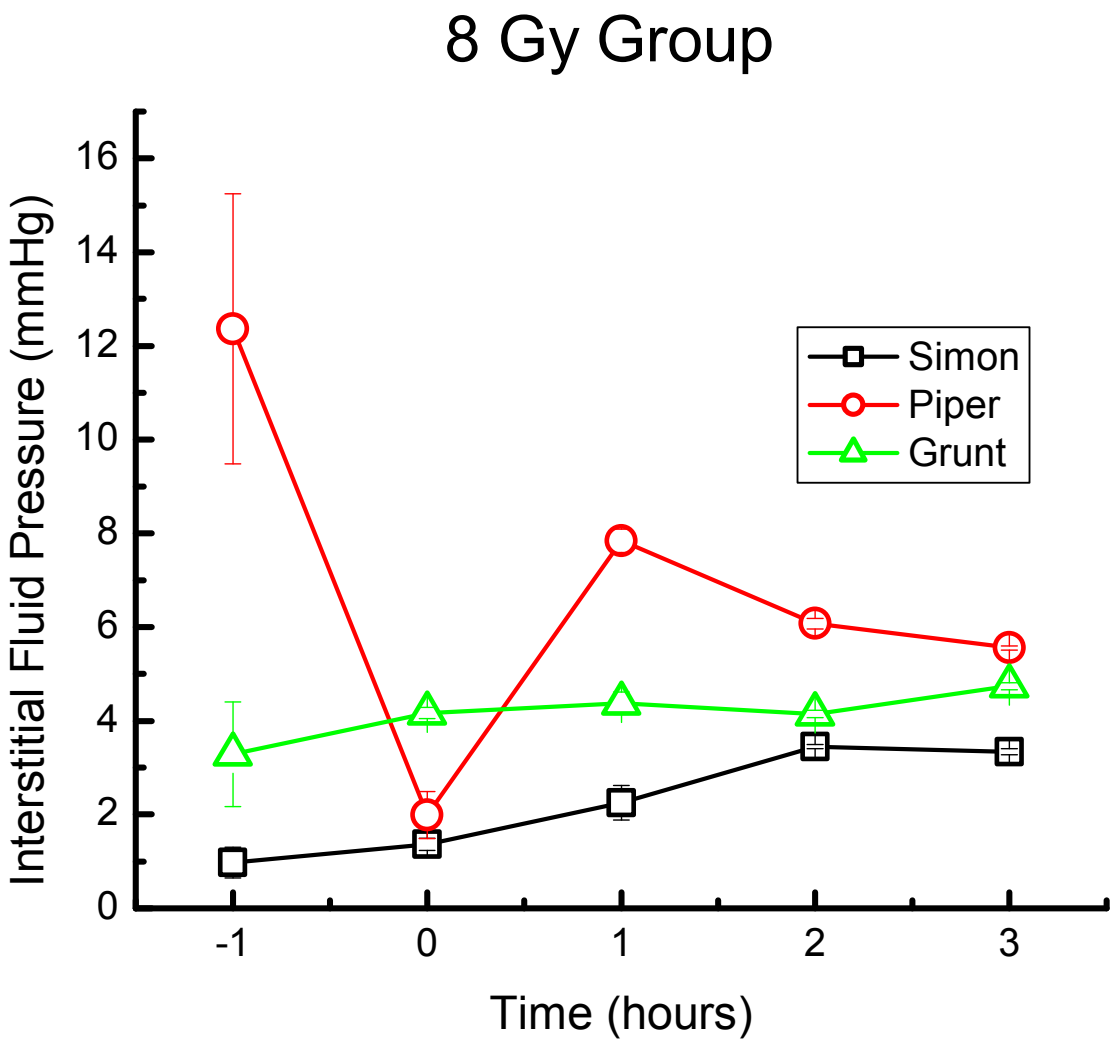

Figure 3.25: Interstitial fluid pressure measurements versus time in three canine soft tissue sarcomas treated with a single fraction of 8 Gy in the first three hours post-irradiation.

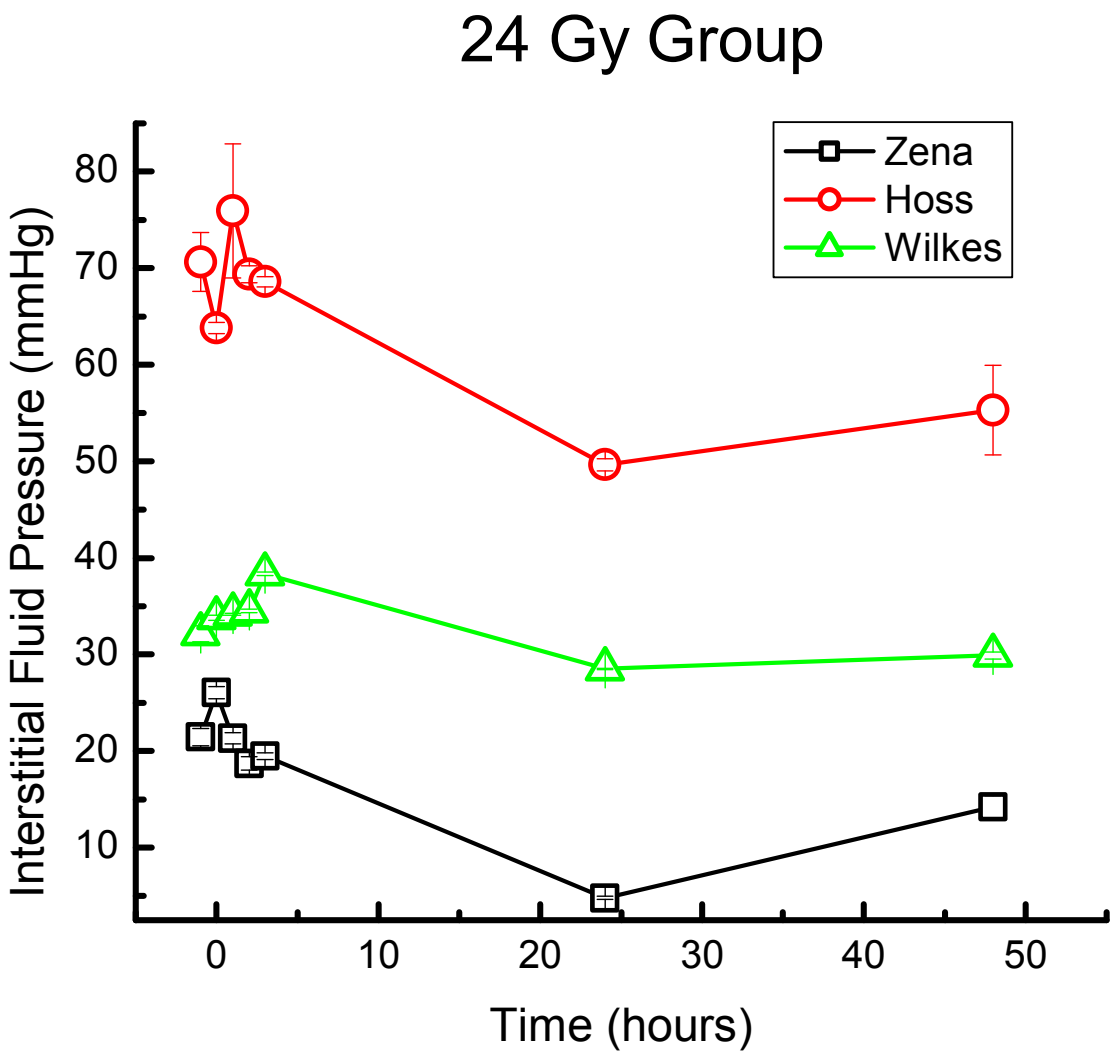

Figure 3.26: Interstitial fluid pressure measurements versus time in three canine soft tissue sarcomas treated with a single fraction of 24 Gy.

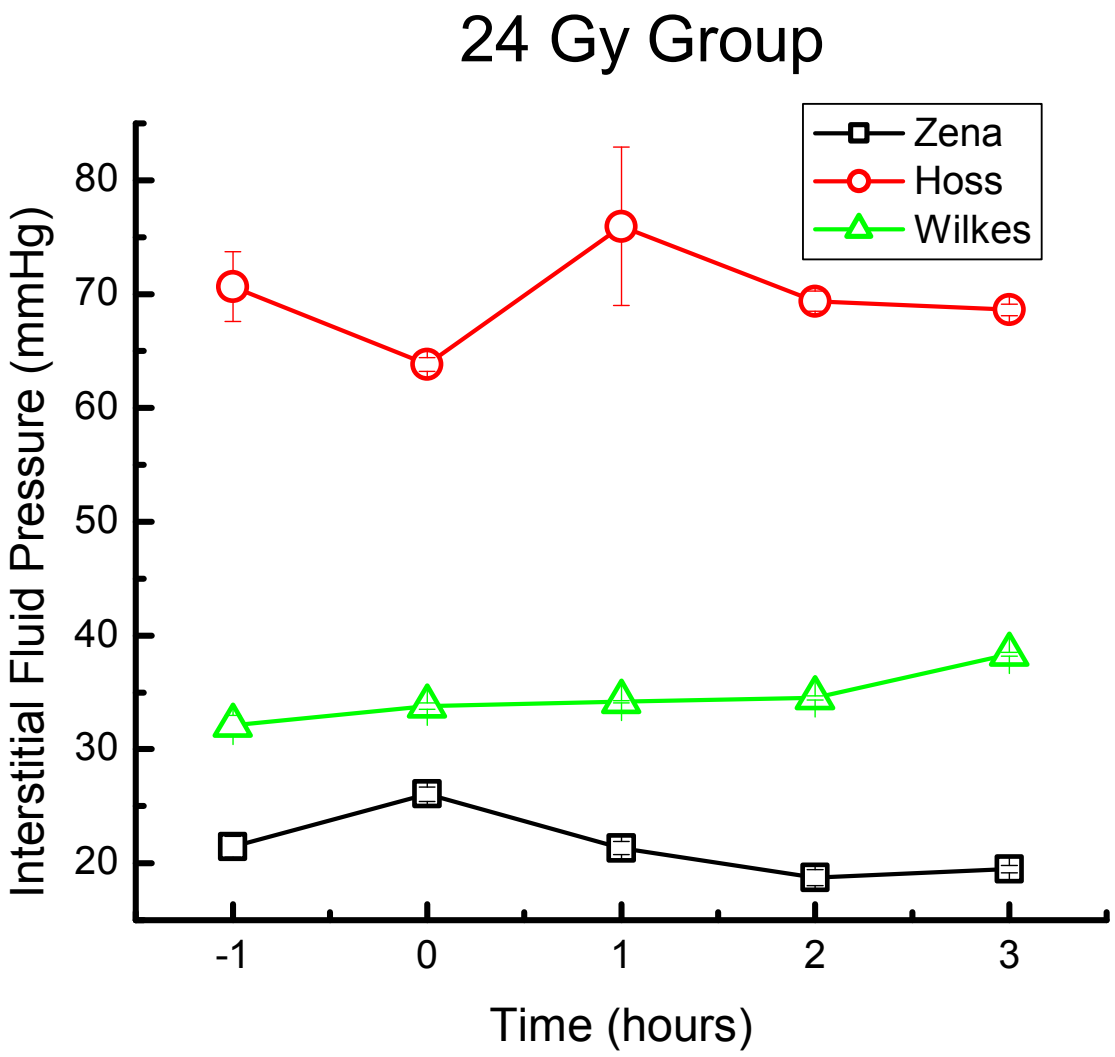

Figure 3.27: Interstitial fluid pressure measurements versus time in three canine soft tissue sarcomas treated with a single fraction of 24 Gy in the first three hours post-irradiation.

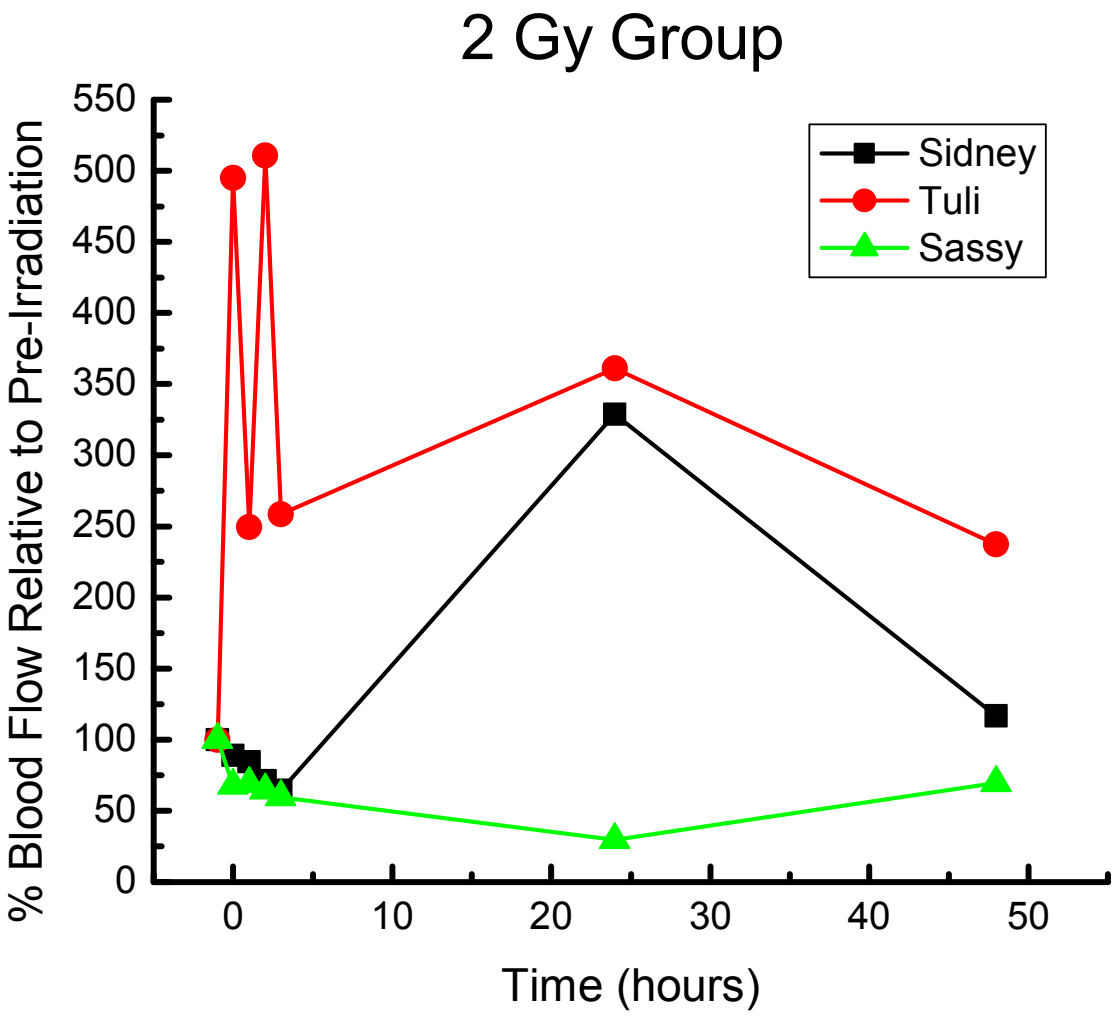

Figure 3.28: Perfusion measurements in terms of percent blood flow relative to pre-irradiation values versus time in three canine soft tissue sarcomas treated with a single fraction of 2 Gy.

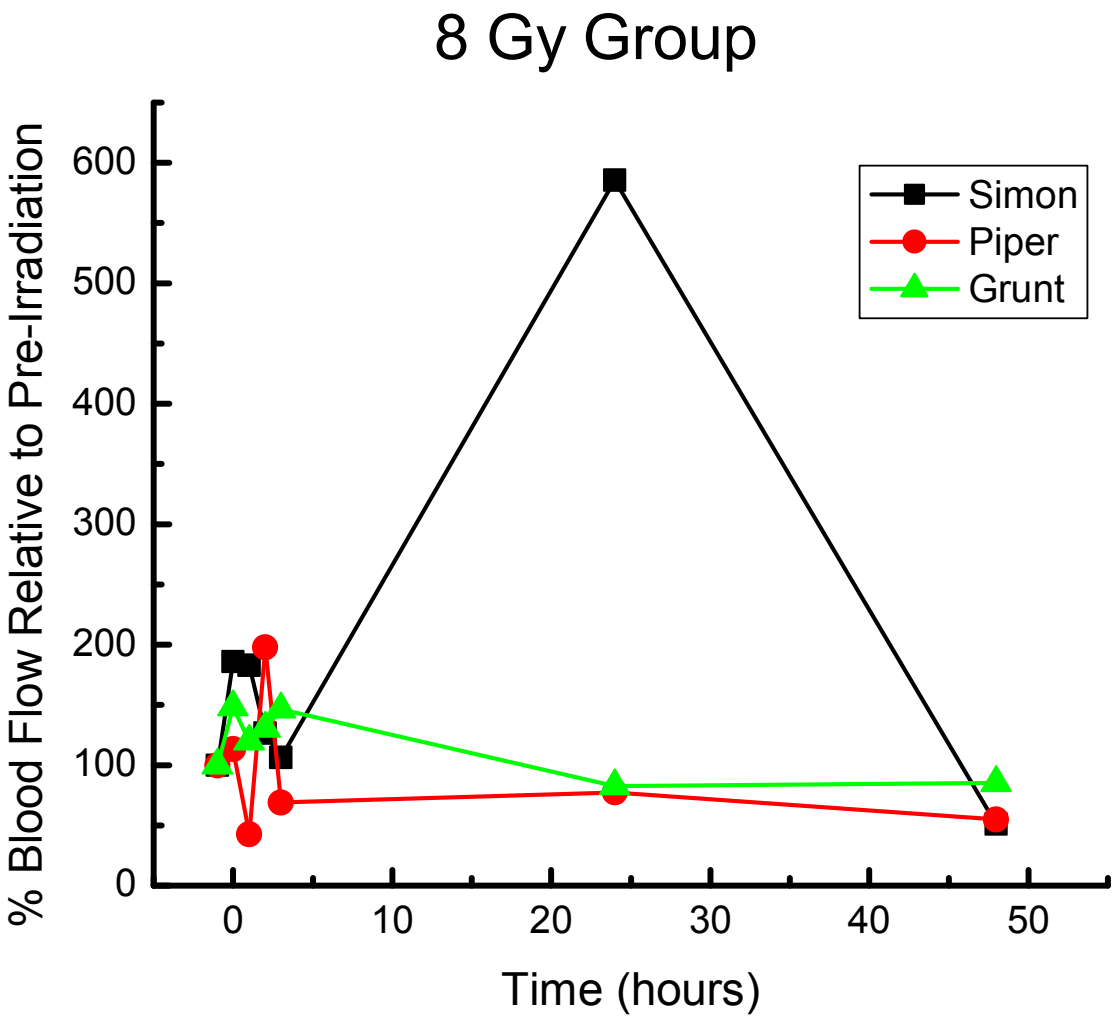

Figure 3.29: Perfusion measurements in terms of percent blood flow relative to pre-irradiation values versus time in three canine soft tissue sarcomas treated with a single fraction of 8 Gy.

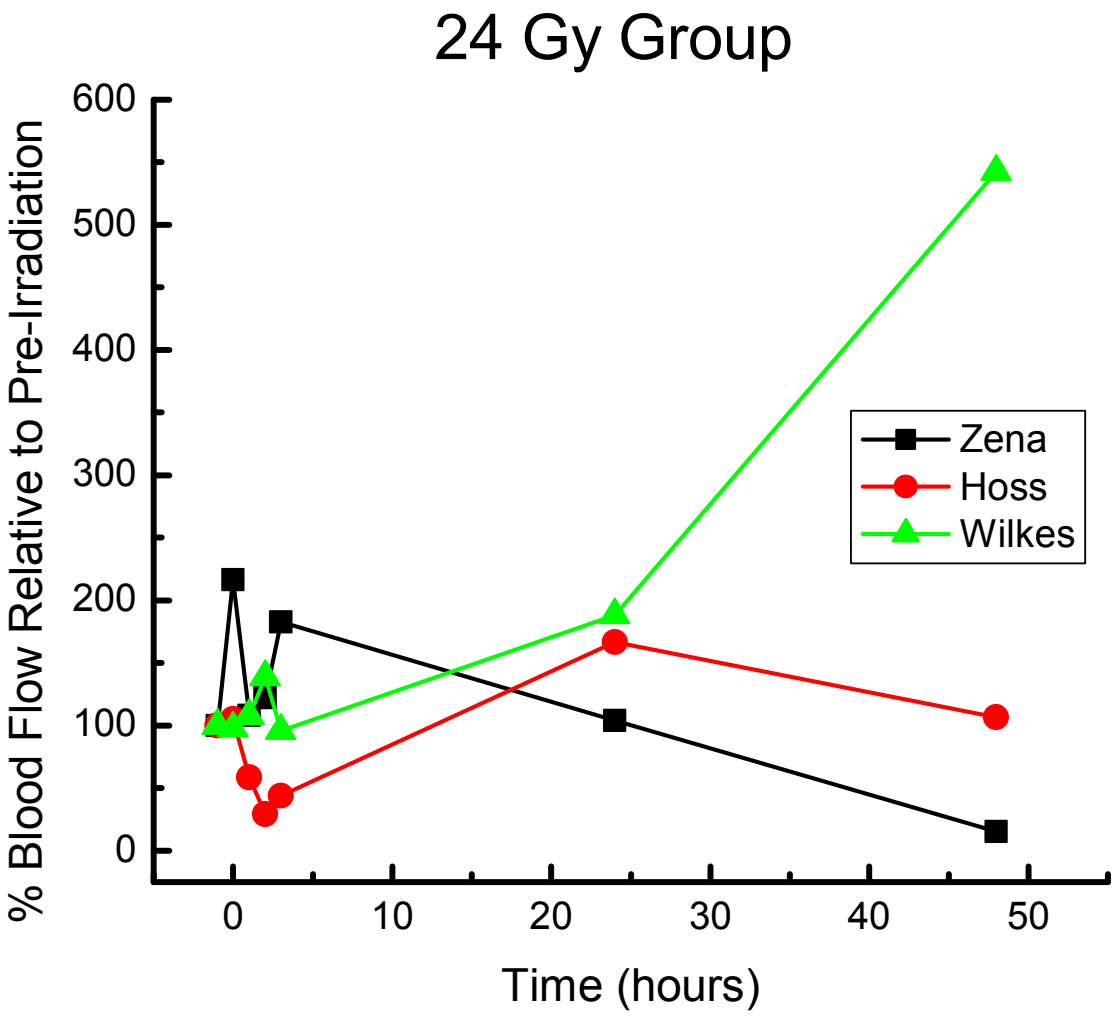

Figure 3.30: Perfusion measurements in terms of percent blood flow relative to pre-irradiation values versus time in three canine soft tissue sarcomas treated with a single fraction of 24 Gy.

REFERENCES

1. Vail DM, MacEwen EG. Spontaneously occurring tumors of companion animals as models for human cancer. *Cancer Investig* 2000; 18: 781-792.
2. Paoloni M, Khanna C. Translation of new cancer treatments from pet dogs to humans. *Nature Rev Cancer* 2008; 8: 147-156.
3. Gordon I, Paoloni M, Mazcko C, *et al.* The comparative oncology trials consortium: Using spontaneously occurring cancers in dogs to inform the cancer drug development pathway. *PLoS Med* 2009; 6: 1-5.
4. Withrow SJ, Gillette EL, Hoopes PJ, *et al.* Intraoperative irradiation of 16 spontaneously occurring canine neoplasms. *Vet Surgery* 1989; 18: 7-11.
5. Sindelar WF, Tepper JE, Kinsella TJ, *et al.* Late effects of intraoperative radiation therapy on retroperitoneal tissues, intestine, and bile duct in a large animal model. *Int J Radiat Oncol Biol Phys.* 1994; 29: 781-788.
6. Vujaskociv Z, Gillette SM, Powers BE, *et al.* Ultrastructural morphometric analysis of peripheral nerves after intraoperative irradiation. *Int J Radiat Biol* 1995; 68: 71-76.
7. Powers BE, Thames HD, Gillette EL. Long-term adverse effects of radiation inhibition of restenosis: Radiation injury to the aorta and branch arteries in a canine model. *Int J Radiat Oncol Biol Phys* 1998; 45: 753-759.
8. LaRue SM, Custis JT. Advances in veterinary radiation therapy: Targeting tumors and improving patient comfort. *Vet Clin Small Anim* 2014; 44: 909-923.
9. Straw RC, Withrow SJ, Powers BE. Management of canine appendicular osteosarcoma. *Vet Clin North Am Small Anim Pract* 1990; 20: 1141-1161.

10. Withrow SJ, Powers BE, Straw RC, *et al.* Comparative aspects of osteosarcoma- Dog versus man. *Clin Ortho Relat Res* 1991; 270: 159-168.
11. Heidner GL, Page RL, McEntee MC, *et al.* Treatment of canine appendicular osteosarcoma using cobalt 60 radiation and intraarterial cisplatin. *J Vet Intern Med* 1991; 5: 313-316.
12. Walter CU, Dernell WS, LaRue SE, *et al.* Curative-intent radiation therapy as a treatment modality for appendicular and axial osteosarcoma: A preliminary retrospective evaluation of 14 dogs with the disease. *Vet Comp Oncol* 2005; 3: 1-7.
13. LaRue SM, Withrow SJ, Powers BE, *et al.* Limb-sparing treatment for osteo-sarcoma in dogs. *J Am Vet Med Assoc* 1989; 195: 1734-1744.
14. McEntee MC, Page RL, Novotney CA, *et al.* Palliative radiotherapy for canine appendicular osteosarcoma. *Vet Radiol Ultrasound* 1993; 34: 367-370.
15. Ramirez O, Dodge RK, Page RL, *et al.* Palliative radiotherapy of appendicular osteosarcoma in 95 dogs. *Vet Rad Ultrasound* 1999; 40: 517-522.
16. Mueller F, Poirier V, Melzer K, *et al.* Palliative radiotherapy with electrons of appendicular osteosarcoma in 54 dogs. *In Vivo* 2005; 19: 713-716.
17. Mayer MN, Grier CK. Palliative radiation therapy for canine osteosarcoma. *Can Vet J* 2006; 47: 707-709.
18. Farese JP, Milner R, Thompson MS, *et al.* Stereotactic radiosurgery for treatment of osteosarcomas involving the distal portions of the limbs in dogs. *J Am Vet Med Assoc* 2004; 225: 1567-1572.
19. Coomer A, Farese J, Milner R, *et al.* Radiation therapy for canine appendicular osteosarcoma. *Vet Comp Oncol* 2009; 7: 15-27.

20. Ryan SD, Ehrhart NE, Worley D, *et al*. Clinical experience with stereotactic radiosurgery for extremity osteosarcoma. Annual Scientific Meeting of the American College of Veterinary Surgeons, Washington DC, October 8, 2009.
21. LaRue SM, Ryan SD, Custis JT, *et al*. Stereotactic radiation therapy for spontaneously occurring canine osteosarcoma. 56th Annual Scientific Meeting of the Radiation Research Society, Maui, HI, September 25, 2010.
22. Garcia-Barros M, Paris F, Cordon-Cardo C, *et al.* Tumor response to radiotherapy regulated by endothelial cell apoptosis. *Science* 2003; 300: 1155-1159.
23. Fuks Z, Kolesnick R. Engaging the vascular component of the tumor response. *Cancer Cell* 2005; 8: 89-91.
24. LaRue SM, Trncic N, Ehrhart EJ, *et al.* Stereotactic radiation therapy (SRT) alters tumor microenvironment. Gordon Research Conference in Radiation Oncology: Understanding the DNA Damage Response to Optimize Radiation Therapy, Ventura Beach, CA, January 27, 2008.
25. Trncic N. Tumor microenvironment in spontaneously occurring tumors and *in vitro* evaluation of hypoxia associated mutagenesis. Doctoral Dissertation. Colorado State University, Fort Collins, CO, 2008.
26. Mauldin GN. Soft tissue sarcomas. *Vet Clin North Am Small Anim Pract* 1997; 27: 139-148.
27. McKnight JA, Mauldin GN, McEntee MC, *et al.* Radiation treatment for incompletely resected soft-tissue sarcomas in dogs. *J Am Vet Med Assoc* 2000; 217: 205-210.
28. Stephens LC, Hunter NR, Ang KK, *et al.* Development of apoptosis in irradiated murine tumors as a function of time and dose. *Radiat Res* 1993; 135: 75-80.

29. Haimovitz-Friedman A, Kan CC, Ehleiter D, *et al.* Ionizing radiation acts on cellular membranes to generate ceramide and initiate apoptosis. *J Exp Med* 1994; 180: 525-535.

30. Kolesnick R, Fuks Z. Radiation and ceramide-induced apoptosis. *Oncogene* 2003; 22: 5897-5906.

31. Feletou M, Vanhoutte PM. Endothelial dysfunction: A multifaceted disorder. *Am J Physiol Heart Circ Physiol* 2006; 291: 985-1002.

32. Deanfield JE, Halcox JP, Rabelink TJ. Endothelial function and dysfunction: Testing and clinical relevance. *Circulation* 2007; 115: 1285-1295.

33. Symons JD, Abel ED. Lipotoxicity contributes to endothelial dysfunction: A focus on the contribution from ceramide. *Rev Endocr Metab Disord* 2013; 14: 59-68.

34. Evans NTS, Naylor PFD. The effect of oxygen breathing and radiotherapy upon the tissue oxygen tension of some human tumours. *Br J Radiol* 1963; 36: 418-425.

35. Gold R, Schmied M, Rothe G, *et al.* Detection of DNA fragmentation in apoptosis: Application of *in situ* nick translation to cell culture systems and tissue sections. *J Histochem Cytochem* 1993; 41: 1023-1030.

36. Miettinen M, Lindenmayer AE, Chaubal A. Endothelial cell markers CD31, CD34, and BNH9 antibody to H- and Y-antigens: Evaluation of their specificity and sensitivity in the diagnosis of vascular tumors and comparison with von Willebrand factor. *Mod Pathol* 1994; 7: 82-90.

37. Kallman RF. The phenomenon of reoxygenation and its implications for fractionated radiotherapy. *Radiol* 1972; 105: 135-142.

38. Dorie MJ, Kallman RF. Reoxygenation of the RIF-1 tumor after fractionated radiotherapy. *Int J Radiat Oncol Biol Phys* 1986; 12: 1853-1859.

39. Zywietz F, Reeker W, Kochs E. Tumor oxygenation in a transplanted rat rhabdomyosarcoma during fractionated irradiation. *Int J Radiat Oncol Biol Phys* 1995; 32: 1391-1400.

40. Fenton BM, Lord EM, Paoni SF. Effects of radiation on tumor intravascular oxygenation, vascular configuration, development of hypoxia, and clonogenic survival. *Radiat Res* 2001; 155: 360-368.

41. Paris F, Fuks Z, Kang A, *et al.* Endothelial apoptosis as the primary lesion initiating intestinal radiation damage in mice. *Science* 2001; 293: 293-297.

42. Garcia-Barros M, Paris F, Cordon-Cardo C, *et al.* Tumor response to radiotherapy regulated by endothelial cell apoptosis. *Science* 2003; 300: 1155-1159.

43. Brurberg KG, Skogmo HK, Graff BA, *et al.* Fluctuations in pO_2 in poorly and well-oxygenated spontaneous canine tumors before and during fractionated radiation therapy. *Radiother Oncol* 2005; 77: 220-226.

44. Fukumura D, Jain RK. Tumor microenvironment abnormalities: Causes, consequences, and strategies to normalize. *J Cell Biochem* 2007; 101: 927-949.

45. Stephens LC, Hunter NR, Ang KK, *et al.* Development of apoptosis in irradiated murine tumors as a function of time and dose. *Radiat Res* 1993; 135: 75-80.

46. Rofstad EK, Gaustad JV, Brurberg KG, *et al.* Radiocurability is associated with interstitial fluid pressure in human tumor xenografts. *Neoplasia* 2009; 11: 1243-1251.

47. Pigott KH, Hill SA, Chaplin DJ, *et al.* Microregional fluctuations in perfusion within human tumours detected using laser Doppler flowmetry. *Radiother Oncol* 1996; 40: 45-50.

48. Matsuo M, Matsumoto S, Mitchel JB, *et al.* Magnetic resonance imaging of the tumor microenvironment in radiotherapy: Perfusion, hypoxia, and metabolism. *Semin Radiat Oncol* 2014; 24: 210-217.

49. Xu J, Yan X, Gao R, *et al.* Effects of irradiation on microvascular endothelial cells of parotid glands in the miniature pig. *Int J Radiat Oncol Biol Phys* 2010; 78: 897-903.

CHAPTER 4

CONCLUSIONS AND FUTURE WORK

While treatment of tumors in a single dose of radiation occurred early in experimental, clinical work done shortly after the discovery of X-rays and at the origin of radiation oncology, the field quickly adopted fractionated radiation therapy as standard practice and made dogma of schedules of 2 Gy per day, delivered every day for several weeks to a large total dose. Technology has been a major factor driving increased use of modern, stereotactic radiation therapy (SRT),[1,2] in which large total doses are delivered in one to five fractions. When stereotactic radiosurgery (SRS), the first modern single fraction, high-dose technology, was contemplated for use in extracranial tumors, it was suggested that the high doses used in one fraction of SRS should be broken down into at least five fractions considering the involvement of normal tissues, which may not be as redundant in structure or parallel in nature as brain tissue, and in many cases the increased size of extracranial masses.[3] Early clinical trials of SRT for extracranial tumors used dose fractionation schemes using one fraction, three fractions, or five fractions of ionizing radiation to high total doses, but such protocols were derived from linear quadratic formalism, a tool that has proven most accurate and useful at 2 Gy and with questionable ability to translate to very high dose irradiation, or (admittedly) from clinically informed guesswork. By far the best way to develop clinical radiation therapy protocols is to use existing mechanistic knowledge of known biologic effects. However, a great emphasis on the effects of exposure to 2 Gy and similar low doses has predominated research in the field for the past several decades. A majority of knowledge of high dose effects comes from the study of intraoperative radiation therapy (IORT), which does not directly translate to biologic effects of

SRT due to differences in radiation quality (i.e. electron beams versus photons), complication of results from IROT studies that used additional fractionated radiation therapy for subsequent treatment, or differences generated by the process of surgery such as wound healing and inflammation. Research on cellular and tissue responses to high doses specifically relevant to SRT is greatly needed, as it is unlikely that the first clinical trials discovered the optimal SRT dose delivery protocol by sheer luck on their first attempts.

Due to successful clinical results achieved beyond expectations or predictions based on linear quadratic formalism from the first studies using SRT to treat extracranial masses, it seems as though the biologic response to high doses differs from the known mechanistic responses of cells and tissues to low doses. The studies described herein detailed investigations of high dose effects *in vitro* using canine cell lines and also *in vivo* using spontaneously occurring soft tissue sarcomas in dogs as a model. Results from both collections of studies suggest that cellular and tumor tissue behaviors following high-dose irradiation are different than the known responses to low dose irradiation.

Firstly, survival at high doses (10 Gy or above) was shown to be decreased relative to predictions from linear quadratic curve fitting in a majority of cell lines. Only two cell lines, K9TCC and Dennys (and marginally good fitting in CTAC cells) were well-described in the high dose region by the linear quadratic expression. The linear quadratic and other three models, the single-hit multitarget model, Kavanagh-Newman universal survival curve, and a modified linear quadratic "γD^3" equation, generally succeeded in fitting low dose data in all cell types; however, no single model could consistently describe high dose data across different cell types. The theoretical basis for these models (in cases where dual radiation action or target theories are applied) may very well apply to low dose effects, but they do not seem to explain effects at high

doses. Furthermore, when listed in rank order of smallest surviving fraction at a given dose to largest surviving fraction (i.e. most radiosensitive to most radioresistant), low dose rankings were generally consistent, with few changes in rank order comparing measured SF_2 values to measured SF_8. On the other hand, rankings of measured SF_8 values differed greatly in order from theoretical SF_{24} values calculated by extrapolating high dose data in a simple exponential fashion. In several cases, cell lines radiosensitive at SF8 were ranked with greater radioresistance at SF_{24}, and vice versa. At some point with increasing dose, the survival curves must cross over each other. If all cell lines decreased consistently relative to other cell lines in terms of dose-dependent survival, then the extrapolated SF_{24} data would be equal to predicted SF_{24} values calculated from the cubed SF_8 measurements. Our results showed that the extrapolated SF_{24} values were several orders of magnitude lower than predicted by $(SF_8)^3$. The high dose data of these survival curves indicate that the cellular response to high dose irradiation is not a simple and proportional increase in the number of events known to cause cell death at low doses. Additional mechanisms may come into play at doses where the formulae begin to fail in their attempts to explain data using supposedly biologically-based mechanisms. Since survival data at high doses is extremely difficult to acquire, the conclusion that novel events may occur at high doses, independent of other cell types or any sort of stromal response, is a radical departure from existing radiation biology dogma and requires further study to establish acceptance.

Secondly, our preliminary *in vivo* study suggested that canine soft tissue sarcomas treated with a single dose of 24 Gy in SRT experienced an increase in tumor oxygenation at one hour after radiation therapy before declining sharply by three hours and decreasing more gradually up to twenty four hours after irradiation before a similarly gradual increase to nearly pre-irradiation

values. The oxygenation response to 24 Gy seemed to have an acute phase (showing an increase at one hour post-treatment) and a second phase on the order of days rather than hours (observed as a transient decrease in partial pressure of oxygen) in all three dogs studied. This pattern was different from oxygen measurements taken in three canine soft tissue sarcomas treated with a single dose of 2 Gy, which (once the highly well oxygenated tumor was excluded) showed signs of classic reoxygenation by twenty four or forty eight hours following dose delivery. Tumors in dogs treated with 24 Gy also experienced a transient decrease in interstitial fluid pressure between three hour post-irradiation and forty eight hour measurements, with a high degree of variability among individuals for measurements in the pre-irradiation to three hours post-irradiation time frame. In all three dogs in the 24 Gy group, interstitial fluid pressure showed no sign of approaching normal values (-3 to 3 mmHg) and all three were trending toward increasing interstitial fluid pressures by forty eight hours. In two of the three dog tumors treated with 2 Gy, interstitial fluid pressure seemed to be decreasing toward the normal range by forty eight hours. While results for the three dogs in the 8 Gy treatment group varied for all parameters, some resembling results from the 2 Gy group while others mimicked findings in the 24 Gy group, the differences between the 2 and 24 Gy treatment groups with respect to oxygenation and interstitial fluid pressure changes were notable and may resolve with greater clarity if a larger sample size was studied. The take home message of this preliminary study is that the behaviors of tumor oxygenation and interstitial fluid pressure are not the same when treated with 24 Gy as with 2 Gy, which suggests that the tumor microvascular response to a large dose of ionizing radiation is mechanistically distinct from the tumor microvascular response to a small dose.

Because the parameters measured in our *in vivo* study (partial pressure of oxygen, interstitial fluid pressure, etc.) showed discrepancy between tumor behaviors following

irradiation with 2 versus 24 Gy, we suspect that the mechanism(s) behind such differences between dose groups are related to the tumor microvascular response to ionizing radiation. In order to further determine how tumor microvasculature behaves following single fraction irradiation with 2 versus 24 Gy (as well as 8 Gy), blood samples and tumor biopsies were taken from each of the nine dogs enrolled in this preliminary study. Blood samples and biopsies were taken at pre-irradiation, immediately after dose-delivery, and at one, two, three, twenty four, and forty eight hours after radiation therapy treatment in an effort to elucidate mechanistic responses involving tumor vasculature on two time scales: the very acute time scale within three hours of irradiation, and the longer (but still considered acute) time scale on the order of days. The biopsies will be useful in determining percent endothelial cell apoptosis using immunohistologic staining. We expect endothelial cell apoptosis to peak at three hours in these samples because the peak percent endothelial cell apoptosis was seen at six hours post-irradiation in one canine soft tissue sarcoma treated with a single fraction of 20 Gy in preparation for this study ("Maggie"). Other studies have shown that the highest levels of tumor parenchymal cell apoptosis occurs around six hours after irradiation, but this occurs at low and high doses (with apoptotic events increasing with dose).[4] Studies specifically examining tumor endothelial cells in fibrosarcomas implanted onto wild-type mice also observed the highest numbers of apoptotic cells per field (at x400 magnification) at six hours after exposure to 15 Gy.[5] Due to IACUC concerns and the increasing difficulty of collecting samples with increasing numbers of collection times, our preliminary study in dogs did not include a six-hour time point. Future studies should consider adding six or eight hour post-irradiation tumor biopsy and blood sampling, if possible.

According to previous studies of endothelial cell apoptosis, irradiated endothelial cells recruit ASMase enzymes to the cell surface where they can catalyze the hydrolysis of sphingomyelin membrane lipids into ceramide, which then triggers secondary messenger molecules to start the highly regulated, step-wise process of apoptotic cell death.[6,7] Once on the surface of the endothelial cell, it is anticipated that ASMase may be swept up in the blood and circulate before eventual loss of enzymatic activity and degradation. We took blood samples at multiple time points pre- and post-irradiation in all nine soft tissue sarcoma-bearing dogs in the hopes of isolating serum from these samples to study soluble proteins. Commercial assays are available for both ASMase quantification and evaluation of ASMase enzymatic activity. Trends in ASMase activity should mirror trends in percent endothelial cell apoptosis, but ASMase release would occur at a much earlier time point in response to radiation exposure.

Along with radiation-induced ASMase release, potential mechanistic events impacting tumor microvasculature on an even faster time frame than endothelial cell apoptosis may include endothelial cell dysfunction. Endothelial cell dysfunction is specifically defined in terms of an endothelial cell's ability to respond to vasodilatory stimuli. It is characterized by decreased bioavailability of nitric oxide and lack of vasodilatory response to endothelium-dependent vasodilatory drugs such as acetylcholine.[8] The gold standard method for assessment of endothelium-dependent vascular dysfunction would be to dissect arteries and suspend segments in a physiological tissue bath to monitor changes in vasodilation or vasoconstriction via isometric force transducers upon application of acetylcholine or other vasoactive drugs. This is not recommended for clinical trial purposes, as arterial or arteriole segments within a tumor would be rare, fragile, and impossible to dissect, not to mention said dissection would be inappropriate for the canine patient. An alternative method of assessing vascular function could

be to monitor plasma nitrite and nitrate concentrations at various time points before and after irradiation. Nitric oxide radicals react rapidly and are degraded to nitrite and nitrate ions before being released in the blood, meaning that plasma or serum nitrite and nitrate are good indicators of the original trends in nitric oxide production and availability.[9-11] While this was originally attempted using gas chromatography mass spectrometry according to published protocols,[12-14] attempts at derivatizing the nitrogenous ions into a volatile compound were inefficient. Ion chromatography for detection of plasma nitrite and nitrate seems to be more promising;[15,16] to date, we have constructed a standard curve for nitrite and nitrate using ion chromatography from which nitrite and nitrate may be quantified in frozen plasma samples from our nine clinical trial dogs. Nitrite and nitrate preserve well in frozen samples for up to a year.[9]

A contributing factor to endothelial cell dysfunction is ambient oxidative stress. Oxidative stress is generated in terms of high concentrations of free radicals during the irradiation of cells and tissues. Cells may deal with such oxidative stress by scavenging with antioxidant molecules or they may be overwhelmed. We would anticipate significantly high levels of oxidative stress following irradiation, but also at baseline as cancer-bearing dogs have been shown to have higher serum MDA (an oxidized lipid byproduct generated in the presence of reactive oxygen species) levels than dogs without cancer.[17] If high oxidative stress is indicated after the initial wave of radiation-induced free radical production, and persists above pre-irradiation values in dogs with soft-tissue sarcomas, then some connection to vascular dysfunction may be made.

In conclusion, the *in vitro* and *in vivo* experiments described herein lend credibility to the idea that single fraction high dose irradiation induces a distinct biologic mechanism from the known mechanistic response of low doses used in traditional, fractionated radiation therapy. Our

clinical trial treating canine soft tissue sarcomas suggest (by means of tumor oxygenation and interstitial fluid pressure observations) that the unique biologic mechanism following high dose irradiation involves tumor microvascular damage. Whether this microvascular damage is led by endothelial cell apoptosis and driven by subsequent events, or if endothelial cell dysfunction precedes endothelial cell apoptosis is uncertain. Further investigation is required to determine the order of events and the impact of each event on the tumor microenvironment.

It is our hope that additional studies will help to elucidate the biologic mechanism underlying responses to single fraction high dose irradiation, and allow for the development of new models to better describe cellular response to high doses. The linear quadratic model should remain in use for low dose responses; however, a model for high dose responses would be useful, in understanding that "all models are wrong, but some are useful."[18] Enrolling more dogs into the clinical trial comparing 2, 8, and 24 Gy delivered in a single fraction to treat soft tissue sarcomas may allow trends in vascular response to become more clear and allow for improved statistical analysis that could lead us to an understanding of how SRT achieves tumor control.

REFERENCES

1. Glatstein E. Assessment of technological advances in radiation oncology: From whence comes the funding? *Int J Radiat Oncol Biol Phys* 2008; 72: 11-12.
2. Brown JM, Adler JR. Is equipment development stifling innovation in radiation oncology? *Int J Radiat Oncol Biol Phys* 2015; 92: 713-714.
3. Hall EJ, Brenner DJ. The radiobiology of radiosurgery: Rationale for different treatment regimes for AVMs and malignancies. *Int J Radiat Oncol Biol Phys* 1993; 25: 381-385.
4. Stephens LC, Hunter NR, Ang KK, *et al.* Development of apoptosis in irradiated murine tumors as a function of time and dose. *Radiat Res* 1993; 135: 75-80.
5. Garcia-Barros M, Paris F, Cordon-Cardo C, *et al.* Tumor response to radiotherapy regulated by endothelial cell apoptosis. *Science* 2003; 300: 1155-1159.
6. Haimovitz-Friedman A, Kan CC, Ehleiter D, *et al.* Ionizing radiation acts on cellular membranes to generate ceramide and initiate apoptosis. *J Exp Med* 1994; 180: 525-535.
7. Kolesnick R, Fuks Z. Radiation and ceramide-induced apoptosis. *Oncogene* 2003; 22: 5897-5906.
8. Fujioka H, Ayajiki K, Shinozaki K, *et al.* Mechanisms underlying endothelium-dependent, nitric oxide- and prostanoid-independent relaxation in monkey and dog coronary arteries. *Arch Pharmacol* 2002; 366: 488-495.
9. Moshage H, Kok B, Huizenga JR, *et al.* Nitrite and nitrate determinations in plasma: A critical evaluation. *Clin Chem* 1995; 41: 892-896.
10. Kelm M, Preik-Steinhoff H, Preik M, *et al.* Serum nitrite sensitively reflects endothelial NO formation in human forearm vasculature: Evidence for biochemical assessment of the endothelial l-arginine-NO pathway. *Cardiovas Res* 1999; 41: 765-772.

11. Tsikas D, Gutzki FM, Stichtenoth DO. Circulating and excretory nitrite and nitrate as indicators of nitric oxide synthesis in humans: Methods of analysis. *Eur J Clin Pharmacol* 2006; 62: 51-59.
12. Tsikas D, Boger RH, Bodeboger SM, *et al.* Quantification of nitrite and nitrate in human urine and plasma as pentafluorobenzyl derivatives by gas-chormatography mass-spectrometry using their N-15-labeled analogs. *J Chromatog B- Biomed App* 1994; 661: 185-191.
13. Tsikas D, Gutzki FM, Rossa S, *et al.* Measurement of nitrite and nitrate in biological fluids by gas chromatography-mas spectrometry and by the Griess assay: Problems with the Griess assay- Solutions by gas chromatography-mass spectrometry. *Analyt Biochem* 1997; 244: 208-220.
14. Tsikas D. Simultaneous derivitization and quantification of the nitric oxide metabolites nitrite and nitrate in biological fluids by gas chromatography/mass spectrometry. *Analyt Chem* 2000; 72: 4064-4072.
15. Michigami Y, Yamamoto Y, Ueda K. Determination of nitrite, sulfate, bromide and nitrate in human-serum by ion chromatography. *Analyst* 1989; 114: 1201-1205.
16. Crowther D, Monaghan JM, Cook K, *et al.* Nitrate and nitrite determination in complex matrices by gradient ion chromatography. *Analyt Commun* 1996; 33: 51-52.
17. Macotpet A, Suksawat F, Sukon P, *et al.* Oxidative stress in cancer-bearing dogs assessed by measuring serum malondialdehyde. *BMC Vet Res* 2013; 9: 1-6.
18. Box GEB, Draper NR. *Empirical model-building and response surfaces*. Wiley, New York, NY, 1987.

APPENDIX A

INTERIM STATISTICAL ANALYSIS

Descriptive Statistics for Tumor Oxygenation

Dose (Gy)	Time Point	N	Mean	Std Dev	95% confidence limits of mean		Median	Minimum	Maximum
2	**Pre-IR**	38	28.33	23.05	20.75	35.90	13.15	8.36	60.33
	Post-IR	22	17.47	12.47	11.95	23.00	18.26	3.47	30.63
	1 hr	34	24.29	16.37	18.57	30.00	30.49	1.59	40.98
	2 hr	34	22.57	14.64	17.46	27.68	28.08	2.09	36.62
	3 hr	34	19.39	13.03	14.84	23.94	24.64	0.87	31.42
	24 hr	25	15.02	8.60	11.48	18.57	12.57	5.09	37.71
	48 hr	25	16.29	9.55	12.35	20.23	15.10	2.90	34.86
8	**Pre-IR**	43	30.90	21.50	24.28	37.52	21.78	4.29	59.30
	Post-IR	26	27.45	16.21	20.90	34.00	29.30	6.02	46.29
	1 hr	30	22.67	18.88	15.62	29.72	11.32	1.13	48.02
	2 hr	33	21.87	19.01	15.13	28.61	10.99	6.08	49.41
	3 hr	33	23.09	18.30	16.60	29.58	12.99	7.46	49.92
	24 hr	26	25.53	18.98	17.86	33.19	24.35	1.03	48.79
	48 hr	30	33.49	23.08	24.87	42.11	46.27	1.32	60.01
24	**Pre-IR**	33	8.72	6.06	6.57	10.87	8.49	0.06	18.66
	Post-IR	33	23.50	17.22	17.39	29.61	17.36	5.80	52.70
	1 hr	33	20.41	5.45	18.48	22.34	17.36	14.72	29.32
	2 hr	33	14.18	4.06	12.74	15.62	15.12	7.81	21.45
	3 hr	33	9.96	8.03	7.12	12.81	7.61	1.56	20.85
	24 hr	32	6.58	2.74	5.59	7.56	6.94	2.85	14.60
	48 hr	31	14.39	5.15	12.50	16.28	15.72	5.33	20.42

Linear Regression Analysis on Ranked Data Relative to Pre-Irradiation Values for Tumor Oxygenation.

Comparison of Timepoints to Pre-IR Values			Estimate	95% Confidence Limits		P-value
2 Gy	1 hr	2 Gy	-40.7291	-304.927	223.4685	0.7625
2 Gy	2 hr	2 Gy	-46.2585	-296.859	204.3422	0.7175
2 Gy	24 hr	2 Gy	-100.413	-264.737	63.9114	0.231
2 Gy	3 hr	2 Gy	-77.1703	-334.809	180.4681	0.5572
2 Gy	48 hr	2 Gy	-87.8126	-229.91	54.2844	0.2258
2 Gy	Post-IR	2 Gy	-104.871	-491.841	282.0998	0.5953
8 Gy	1 hr	8 Gy	-89.8698	-174.338	-5.4019	0.037
8 Gy	2 hr	8 Gy	-97.0395	-248.847	54.7682	0.2103
8 Gy	24 hr	8 Gy	-60.7813	-152.164	30.6011	0.1924
8 Gy	3 hr	8 Gy	-67.3879	-221.235	86.4593	0.3906
8 Gy	48 hr	8 Gy	-15.4031	-215.413	184.6066	0.88
8 Gy	Post-IR	8 Gy	-24.4544	-119.147	70.2382	0.6127
24 Gy	1 hr	24 Gy	201.2424	105.709	296.7759	<.0001
24 Gy	2 hr	24 Gy	117.8788	78.1152	157.6423	<.0001
24 Gy	24 hr	24 Gy	-45.9574	-92.6749	0.7601	0.0538
24 Gy	3 hr	24 Gy	13.697	-123.948	151.3415	0.845
24 Gy	48 hr	24 Gy	116.7977	16.7006	216.8947	0.0222
24 Gy	Post-IR	24 Gy	168.9697	-71.4362	409.3756	0.1683

Linear Regression Analysis on Ranked Data for Tumor Oxygenation to Compare Values at Different Time Points

Comparison of Treatments				Estimate	95% Confidence Limits		P-value
8 Gy	Pre-IR	2 Gy	Pre-IR	25.0171	-305.61	355.644	0.8821
24 Gy	Pre-IR	2 Gy	Pre-IR	-209.689	-453.124	33.746	0.0914
24 Gy	Pre-IR	8 Gy	Pre-IR	-234.706	-491.44	22.028	0.0732
8 Gy	1 hr	2 Gy	1 hr	-49.1407	-326.513	228.2313	0.7284
8 Gy	2 hr	2 Gy	2 hr	-50.781	-343.776	242.2145	0.7341
8 Gy	24 hr	2 Gy	24 hr	39.6313	-148.393	227.6556	0.6795
8 Gy	3 hr	2 Gy	3 hr	9.7823	-290.295	309.8599	0.9491
8 Gy	48 hr	2 Gy	48 hr	72.4095	-172.938	317.7571	0.563
8 Gy	Post-IR	2 Gy	Post-IR	80.4164	-317.972	478.8044	0.6924
24 Gy	1 hr	2 Gy	1 hr	241.9715	-38.968	522.911	0.0914
24 Gy	2 hr	2 Gy	2 hr	164.1373	-89.5985	417.8731	0.2048
24 Gy	24 hr	2 Gy	24 hr	54.4552	-116.381	225.2911	0.5321
24 Gy	3 hr	2 Gy	3 hr	90.8672	-201.235	382.9692	0.5421
24 Gy	48 hr	2 Gy	48 hr	204.6103	30.7972	378.4233	0.021
24 Gy	Post-IR	2 Gy	Post-IR	273.8405	-181.726	729.4075	0.2387
24 Gy	1 hr	8 Gy	1 hr	291.1122	163.5917	418.6327	<.0001
24 Gy	2 hr	8 Gy	2 hr	214.9183	57.9892	371.8473	0.0073
24 Gy	24 hr	8 Gy	24 hr	14.8239	-87.8078	117.4556	0.7771
24 Gy	3 hr	8 Gy	3 hr	81.0849	-125.349	287.5189	0.4414
24 Gy	48 hr	8 Gy	48 hr	132.2008	-91.4581	355.8596	0.2467
24 Gy	Post-IR	8 Gy	Post-IR	193.4241	-64.9587	451.8069	0.1423

Descriptive Statistics for Tumor Interstitial Fluid Pressure

Dose (Gy)	Time Point	N	Mean	Std Dev	95% confidence limits of mean		Median	Minimum	Maximum
2	**Pre-IR**	42	6.56	1.11	6.21	6.90	6.26	5.24	8.96
	Post-IR	33	10.90	6.67	8.53	13.26	7.31	5.12	20.55
	1 hr	28	11.73	7.13	8.96	14.49	7.78	6.30	23.23
	2 hr	32	13.06	9.03	9.81	16.32	7.26	6.40	28.18
	3 hr	34	14.59	10.56	10.90	18.27	7.08	6.64	31.27
	24 hr	34	7.88	4.54	6.30	9.46	5.04	3.49	14.21
	48 hr	33	7.20	3.18	6.07	8.33	7.11	3.76	12.06
8	**Pre-IR**	45	5.34	5.39	3.72	6.96	2.49	0.56	19.53
	Post-IR	34	2.46	1.26	2.02	2.90	1.76	1.06	4.35
	1 hr	32	4.90	2.35	4.06	5.75	4.50	1.93	8.24
	2 hr	33	4.56	1.13	4.16	4.96	4.17	3.39	6.33
	3 hr	33	4.55	0.93	4.22	4.88	4.73	3.23	5.65
	24 hr	31	8.85	6.12	6.61	11.10	5.18	4.79	18.45
	48 hr	31	9.57	8.42	6.48	12.66	5.72	2.05	21.84
24	**Pre-IR**	35	42.89	20.85	35.73	50.06	32.80	20.44	74.53
	Post-IR	33	41.23	16.55	35.36	47.10	33.78	25.45	64.76
	1 hr	33	43.81	24.00	35.30	52.32	34.21	20.80	88.81
	2 hr	33	40.87	21.50	33.25	48.49	34.49	17.81	70.51
	3 hr	33	42.14	20.56	34.85	49.43	38.40	18.92	69.38
	24 hr	33	27.64	18.61	21.04	34.24	28.53	4.52	50.36
	48 hr	30	35.02	17.13	28.63	41.42	30.17	13.20	61.80

Linear Regression Analysis on Ranked Data Relative to Pre-Irradiation Values for Tumor Interstitial Fluid Pressure

Comparison of Timepoints to Pre-IR Values			Estimate	95% Confidence Limits		P-value
24 Gy	1 hr	24 Gy	0.7372	-28.9008	30.3752	0.9611
24 Gy	2 hr	24 Gy	-14.8537	-69.3596	39.6523	0.5933
24 Gy	24 hr	24 Gy	-142.687	-311.474	26.0996	0.0975
24 Gy	3 hr	24 Gy	-9.6416	-64.1984	44.9153	0.7291
24 Gy	48 hr	24 Gy	-40.4476	-72.3833	-8.512	0.0131
24 Gy	Post-IR	24 Gy	-4.2022	-28.4146	20.0103	0.7337
8 Gy	1 hr	8 Gy	23.941	-32.9397	80.8217	0.4094
8 Gy	2 hr	8 Gy	-9.6566	-131.174	111.8606	0.8762
8 Gy	24 hr	8 Gy	99.2061	-206.011	404.4227	0.5241
8 Gy	3 hr	8 Gy	-5.202	-140.055	129.6514	0.9397
8 Gy	48 hr	8 Gy	93.0125	-246.352	432.3773	0.5911
8 Gy	Post-IR	8 Gy	-105.16	-312.702	102.3813	0.3207
2 Gy	1 hr	2 Gy	93.3333	66.7658	119.9008	<.0001
2 Gy	2 hr	2 Gy	95.5476	52.1403	138.955	<.0001
2 Gy	24 hr	2 Gy	-38.5553	-125.964	48.8531	0.3873
2 Gy	3 hr	2 Gy	102.2535	31.9496	172.5574	0.0044
2 Gy	48 hr	2 Gy	-27.6039	-152.273	97.065	0.6643
2 Gy	Post-IR	2 Gy	51.8961	-38.6657	142.4579	0.2614

Linear Regression Analysis on Ranked Data for Tumor Interstitial Fluid Pressure to Compare Values at Different Time Points

Comparison of Treatments				Estimate	95% Confidence Limits		P-value
8 Gy	Pre-IR	2 Gy	Pre-IR	-124.175	-339.948	91.5986	0.2593
24 Gy	Pre-IR	2 Gy	Pre-IR	304.4619	203.005	405.9188	<.0001
24 Gy	Pre-IR	8 Gy	Pre-IR	428.6365	208.9317	648.3414	0.0001
8	1 hr	2 Gy	1 hr	-69.3924	-132.172	-6.613	0.0303
8	2 hr	2 Gy	2 hr	-105.204	-234.241	23.8331	0.1101
8	24 hr	2 Gy	24 hr	137.7614	-179.725	455.2475	0.3951
8	3 hr	2 Gy	3 hr	-107.456	-259.535	44.6237	0.1661
8	48 hr	2 Gy	48 hr	120.6164	-240.923	482.1559	0.5132
8	Post-IR	2 Gy	Post-IR	-157.056	-383.496	69.3833	0.174
24	1 hr	2 Gy	1 hr	-92.5961	-132.399	-52.7936	<.0001
24	2 hr	2 Gy	2 hr	-110.401	-180.08	-40.7228	0.0019
24	24 hr	2 Gy	24 hr	-104.132	-294.208	85.945	0.2829
24	3 hr	2 Gy	3 hr	-111.895	-200.884	-22.9058	0.0137
24	48 hr	2 Gy	48 hr	-12.8437	-141.538	115.8506	0.8449
24	Post-IR	2 Gy	Post-IR	-56.0983	-149.841	37.6444	0.2408
24 Gy	1 hr	8 Gy	1 hr	-23.2037	-87.3429	40.9354	0.4783
24 Gy	2 hr	8 Gy	2 hr	-5.1971	-138.379	127.9844	0.939
24 Gy	24 hr	8 Gy	24 hr	-241.893	-590.671	106.8849	0.174
24 Gy	3 hr	8 Gy	3 hr	-4.4395	-149.911	141.0318	0.9523
24 Gy	48 hr	8 Gy	48 hr	-133.46	-474.324	207.4039	0.4428
24 Gy	Post-IR	8 Gy	Post-IR	100.958	-107.991	309.9069	0.3436

Descriptive Statistics for Tumor Perfusion

Dose (Gy)	Time Point	N	Mean	Std Dev	95% confidence limits of mean		Median	Minimum	Maximum
2	**Pre-IR**	40	5.13	1.43	4.68	5.59	5.41	2.87	7.01
	Post-IR	33	8.11	4.98	6.34	9.87	5.79	3.48	16.17
	1 hr	29	5.58	1.70	4.94	6.23	5.46	3.37	7.61
	2 hr	27	7.73	5.51	5.55	9.91	4.70	2.95	15.49
	3 hr	30	4.68	1.79	4.01	5.35	4.17	3.15	7.83
	24 hr	31	10.65	8.10	7.68	13.62	10.74	1.32	22.88
	48 hr	34	6.27	1.73	5.66	6.87	7.08	2.57	8.01
8	**Pre-IR**	44	5.64	2.91	4.76	6.53	4.33	2.70	14.19
	Post-IR	34	7.61	2.30	6.81	8.41	7.56	4.58	13.85
	1 hr	29	4.88	1.64	4.26	5.50	4.13	3.68	8.73
	2 hr	33	9.26	6.53	6.94	11.57	4.87	4.02	21.27
	3 hr	33	5.28	0.97	4.94	5.62	5.33	2.83	6.79
	24 hr	30	9.91	8.60	6.70	13.12	6.95	2.53	27.01
	48 hr	30	3.41	1.23	2.95	3.87	3.14	1.84	5.20
24	**Pre-IR**	26	5.82	1.70	5.13	6.50	6.24	2.46	7.83
	Post-IR	33	5.86	1.04	5.49	6.23	5.46	4.67	7.98
	1 hr	26	4.85	2.39	3.88	5.81	3.27	2.22	7.88
	2 hr	33	4.80	3.75	3.47	6.13	4.19	1.25	10.21
	3 hr	33	4.56	1.97	3.87	5.26	4.84	1.99	7.26
	24 hr	30	8.30	4.37	6.67	9.93	7.83	2.53	13.64
	48 hr	28	16.73	17.69	9.87	23.59	4.87	0.34	39.72

Linear Regression Analysis on Ranked Data Relative to Pre-Irradiation Values for Tumor Perfusion

Comparison of Timepoints			Estimate	95% Confidence Limits		P-value
2 Gy	1 hr	2 Gy	31.9164	-255.722	319.555	0.8278
2 Gy	2 hr	2 Gy	28.2306	-342.244	398.7052	0.8813
2 Gy	24 hr	2 Gy	96.9169	-287.541	481.3754	0.6212
2 Gy	3 hr	2 Gy	-48.9917	-341.578	243.5945	0.7428
2 Gy	48 hr	2 Gy	86.8809	-152.297	326.0583	0.4765
2 Gy	Post-IR	2 Gy	81.1598	-248.349	410.6689	0.6293
8 Gy	1 hr	8 Gy	-32.2053	-321.056	256.6458	0.827
8 Gy	2 hr	8 Gy	95.9545	67.7435	124.1655	<.0001
8 Gy	24 hr	8 Gy	73.097	-206.495	352.6894	0.6084
8 Gy	3 hr	8 Gy	20.2576	-111.928	152.4436	0.7639
8 Gy	48 hr	8 Gy	-147.703	-220.828	-74.5778	<.0001
8 Gy	Post-IR	8 Gy	162.1578	19.4332	304.8823	0.026
24 Gy	1 hr	24 Gy	-95.6154	-209.898	18.6671	0.101
24 Gy	2 hr	24 Gy	-113.797	-250.071	22.4766	0.1017
24 Gy	24 hr	24 Gy	54.0846	-122.373	230.5423	0.548
24 Gy	3 hr	24 Gy	-103.206	-224.536	18.1233	0.0955
24 Gy	48 hr	24 Gy	-4.4725	-181.149	172.2044	0.9604
24 Gy	Post-IR	24 Gy	14.7028	-75.211	104.6166	0.7486

Linear Regression Analysis on Ranked Data for Tumor Perfusion to Compare Values at Different Time Points

Comparison of Treatments				Estimate	95% Confidence Limits		P-value
8 Gy	Pre-IR	2 Gy	Pre-IR	-2.1886	-241.423	237.0461	0.9857
24 Gy	Pre-IR	2 Gy	Pre-IR	53.7904	-148.59	256.1711	0.6024
24 Gy	Pre-IR	8 Gy	Pre-IR	55.979	-184.253	296.211	0.6479
8	1 hr	2 Gy	1 hr	-64.1217	-471.762	343.519	0.7579
8	2 hr	2 Gy	2 hr	67.724	-303.823	439.2712	0.7209
8	24 hr	2 Gy	24 hr	-23.82	-499.194	451.5538	0.9218
8	3 hr	2 Gy	3 hr	69.2492	-251.811	390.3096	0.6725
8	48 hr	2 Gy	48 hr	-234.584	-484.69	15.5223	0.066
8	Post-IR	2 Gy	Post-IR	80.9979	-278.093	440.0891	0.6584
24	1 hr	2 Gy	1 hr	-127.532	-437.042	181.9783	0.4193
24	2 hr	2 Gy	2 hr	-142.028	-536.771	252.7153	0.4807
24	24 hr	2 Gy	24 hr	-42.8323	-465.852	380.1873	0.8427
24	3 hr	2 Gy	3 hr	-54.2146	-370.96	262.5306	0.7373
24	48 hr	2 Gy	48 hr	-91.3534	-388.709	206.0026	0.5471
24	Post-IR	2 Gy	Post-IR	-66.4571	-408.013	275.0992	0.7029
24 Gy	1 hr	8 Gy	1 hr	-63.4101	-374.047	247.2272	0.6891
24 Gy	2 hr	8 Gy	2 hr	-209.752	-348.915	-70.5885	0.0031
24 Gy	24 hr	8 Gy	24 hr	-19.0124	-349.632	311.6071	0.9103
24 Gy	3 hr	8 Gy	3 hr	-123.464	-302.891	55.963	0.1774
24 Gy	48 hr	8 Gy	48 hr	143.2305	-47.9815	334.4425	0.1421
24 Gy	Post-IR	8 Gy	Post-IR	-147.455	-316.14	21.2305	0.0867